MITOCHONDRIA AND MICRODOMAINS IN VASCULAR SMOOTH MUSCLE CELL Ca^{2+} SIGNALING

By

DAMON TODD POBURKO

B.Sc., The University of British Columbia, 2001

A THESIS SUBMITTED IN PARTIAL FULFILMENT OF
THE REQUIREMENTS FOR THE DEGREE OF

DOCTOR OF PHILOSOPHY

in

THE FACULTY OF GRADUATE STUDIES

(Pharmacology and Therapeutics)

THE UNIVERSITY OF BRITISH COLUMBIA

November 2005

ABSTRACT

Contraction of vascular smooth muscle (VSM) is regulated by fluctuations in the intracellular concentration of free ionic calcium ($[Ca^{2+}]_i$). The spatio-temporal regulation of $[Ca^{2+}]_i$ relies on the sub-cellular architecture of the smooth muscle cell and the juxtaposition of opposing plasmalemma (PM), sarcoplasmic reticulum (SR) and mitochondria. This thesis addresses two related aspects of Ca^{2+}-signaling in VSM: 1) basal Ca^{2+}-entry across the PM and 2) mitochondrial Ca^{2+}-uptake during agonist mediated stimulation in cultured rat aorta smooth muscle cells.

Basal Ca^{2+}-entry into resting cells, measured with radio-labeled $^{45}Ca^{2+}$, was blocked (~80%) by organic inhibitors of L-type voltage-gated Ca^{2+}-channels (nifedipine), store-/receptor-operated Ca^{2+}-channels (SKF-96365) and inositol-1,4,5-trisphosphate receptors (IP_3R) (2-APB). At increasing concentrations, gadolium (Gd^{3+}) biphasically inhibited Ca^{2+}-uptake. The maximal effect of the first phase (100μM Gd^{3+}) was equally as effective as combined treatment with 2-APB and SKF-96365. At 0.2-10mM, Gd^{3+} inhibited Ca^{2+} influx to a greater extent than the organic inhibitors. We concluded that basal Ca^{2+} entry primarily occurred via basal activity of excitable channels, and PCR analysis suggests this influx to involve L-type voltage-gated Ca^{2+}-channels, and TRPC1, TRPC4 and TRPC6.

Next, we used Ca^{2+}-sensitive proteins (aequorins and pericams) and dyes (fura-2) to measure parallel $[Ca^{2+}]$ changes in the mitochondrial matrix, subplasmalemmal cytosol and bulk cytosol. Replacing extracellular Na^+ with n-methyl-d-glucamine (NMDG) caused Ca^{2+}-entry by reversal of the Na^+/Ca^{2+}-exchanger (NCX), which was selectively blocked by KB-R7943. NCX-reversal increased mitochondrial and subplasmalemmal but not bulk cytosolic $[Ca^{2+}]$ revealing a local interaction of the SR, NCX and mitochondria. Furthermore, NCX-reversal and mitochondrial Ca^{2+}-uptake appear to occur during the $[Ca^{2+}]_i$ plateau phase of the response to purinergic stimulation (ATP). However, this mitochondrial Ca^{2+}-uptake does not increase $[Ca^{2+}]_{MT}$ because of a compensatory stimulation of mitochondrial Ca^{2+}-extrusion (blocked by CGP-37157).

Finally, we dissected the $[Ca^{2+}]_{MT}$ response to SR Ca^{2+}-release in response to agonist-mediated stimulation. ATP and $[ARG^8]$-vasopressin transiently increased $[Ca^{2+}]_{MT}$ by activating

both IP_3R and ryanodine receptors (RyR) (selectively inhibited by 2-APB and procaine). Image analysis of fluorescently labeled mitochondria, IP_3R and RyR corroborated functional evidence that IP_3R and RyR release Ca^{2+} from separate sub-compartments of the SR and that physiological $[Ca^{2+}]_{MT}$ elevations rely on IP_3R-RyR cross-talk.

TABLE OF CONTENTS:

LIST OF TABLES

LIST OF FIGURES

LIST OF SYMBOLS & ABBREVIATIONS

$[Ca^{2+}]$	free ionic Ca2+ concentration
$[Ca^{2+}]_{cyto}$	[Ca2+] in the bulk cytosol
$[Ca^{2+}]_{MT}$	[Ca2+] in the mitochondrial matrix
$[Ca^{2+}]_{SR}$	[Ca2+] in the sarcoplasmic reticulum
$[Ca2+]_{subPM}$	[Ca2+] in the subplasmalemmal domain
2-APB	2-aminoethyl diphenylborate
ADP	adenosine diphosphate
ANT	adenine nucleotide translocase
ATP	adenosine 5'-trisphosphate
AVP	$[ARG^8]$-vasopressin
BAPTA-AM	1,2-Bis(2-amino-5-bromophenoxy)ethane-*N,N,N',N'*-tetraacetic acid acetoxy methyl ester. A calcium chelator
Cam-KII	Ca2+-calmodulin dependent kinase II
CCE	capacitative Ca^{2+} entry
CPA	cyclopiazonic acid (SERCA blocker)
CsA	cyclosporin A
cytoC	cytochrome C
DIDS	4,4'-diisothiocyanostilbene-2,2'-disulfonic Acid
$\Delta\psi_m$	mitochondrial membrane potenial
EGTA	Ethylene glycol-bis(2-aminoethyl)-N,N,N',N'-tetraacetic acid
E_m	membrane potential
ER	endoplasmic reticulum
ETC	electron transport chain
FCCP	carbonyl cyanide 4-(trifluoromethoxy)phenylhydrazone
GFP	green fluorescent protein
H_2O_2	hydrogen peroxide
HXC	H+/Ca2+ exchanger
IP_3	inositol 1,4,5-trisphosphate
IP_3R	inositol 1,4,5-trisphosphate receptor
L	vasopressor receptor ligand
mito-aeq	mitochondrial targeted aequorin
mito-GFP	mitochondria targeted GFP
mitoNCX	mitochondrial Na+/Ca2+ exchanger; mNCX
MLCK	myosin light chain kinase
MLCP	myosin light chain phosphatase
MT	mitochondria(l)
mUni	mitochondrial Ca2+ uniporter
NA	numerical aperture
NKA	Na^+/K^+-ATPase
NCX	Na+/Ca2+ exchanger
P_i	phosphate
PKC	protein kinase C
PM-aeq	See SNAP-aeq
PM	plasmalemma
PTP	mitochondrial permeability transition pore
ROK	Rho kinase
RyR	ryanodine receptor Ca2+ channel
R	membrane bound agonist receptor
SERCA	sarco/endoplasmic reticulum ATPase
SMC	smooth muscle cell
SNAP-aeq	SNAP-25 tagged, sub-plasmalemmal targeted aequorin
SOC	store-operated channel
SR	sarcoplasmic reticulum
SSR	superficial SR
TrpC	transient receptor potential gene
TRPC	canonical transient receptor potential channe
U	mitochondrial Ca2+ uniporter
VDAC	voltage-dependant anion channel (aka -porin)
VSMC	vascular smooth muscle cells
VSM	vascular smooth muscle

LIST PUBLICATIONS & ABSTRACTS

Material from this dissertation has been published in:

- **Poburko D,** Lhote P, Szado T, Behra T, Rahimian R, McManus B, van Breemen C, Ruëgg UT. Basal Calcium entry in vascular smooth muscle. **European Journal of Pharmacology.** 2004; 505(1-3): 19-29.
- **Poburko D,** Lee C-H, van Breemen. Vascular smooth muscle mitochondria at the cross roads of Ca^{2+} regulation. **Cell Calcium.** 2004; 35(6): 509-21. (Invited Review)
- **Poburko D,** Kuo K-H, Dai J, Lee C-H, van Breemen C. Organellar junctions promote targeted Ca^{2+} signaling in smooth muscle: Why two membranes are better than one. **Trends in Pharmacological Sciences.** 2004 Jan; 25(1): 8-15. (Invited Review)

Material from this dissertation has been submitted for publication in:

- Damon **Poburko,** Kathryn Potter, Edo van Breemen, Nicola Fameli, Olivier Basset, Urs T Ruegg, and Cornelis van Breemen. Mitochondria buffer NCX-mediated Ca^{2+}-entry and limit its diffusion into vascular smooth muscle cells. *Cell Calcium*

Material from this dissertation has been presented in poster format at the following international meetings:

- Damon **Poburko,** Megan McLarnon, Eric Lin, Hubert Walinski, Edo van Breemen, Cornelis van Breemen. Activation of different G-protein linked receptors leads to convergent mitochondrial Ca^{2+} signaling in aortic smooth muscle cells. FASEB Experimental Biology Congress, April, 2005, San Diego, California. FASEB JOURNAL 19 (5): A1084-A1084 Part 2 Suppl. S MAR 7 2005
- Damon **Poburko,** Nicola Fameli, Aaron Wong, Cornelis van Breemen. Impairing mitochondrial Ca2+ uptake mechanisms and collapsing of the $\Psi\Delta m$ differentially affect subplasmalemmal Ca^{2+} signaling. Biophysical Society Annual Meeting, February 12-16, 2005, Long Beach, California. BIOPHYSICAL JOURNAL 88 (1): 90A-91A Part 2 Suppl. S JAN 2005
- Damon **Poburko,** Kate Potte, Edo van Breemen, Megan McLarnon, Cornelis van Breemen. Linked Ca^{2+} transport between smooth muscle mitochondria and the Na^{+}/Ca^{2+}-exchanger. FASEB Experimental Biology Congress, April, 2004, Washington, DC. FASEB JOURNAL 18 (4): A703-A703 Suppl. S MAR 23 2004
- Damon **Poburko,** Kathryn Potter, Edo van Breemen, Enrique Gallego, Urs Ruegg, Cornelis van Breemen. Privileged Ca^{2+} communication between smooth muscle mitochondria and the Na^{+}/Ca^{2+}-exchanger. CIHR-ICRH Young Investigator's Forum, May 6-9, 2004, Winnipeg, Canada.
- **Poburko D,** Gallego E, van Breemen C. Altered mitochondrial Ca^{2+} transport could underlie cyclosporin A-induced hypertension. Canadian Society for Clinical Pharmacology 25th anniversary meeting. Sept. 19-21. Ottawa, Canada.
- **Poburko DT,** Ruegg UT, van Breemen C. Mitochondrial calcium transport in resting & stimulated smooth muscle. FASEB JOURNAL 17 (4): A46-A46 Part 1 Suppl. S MAR 14 2003 (resulted in invitation to publish both a primary paper and scholarly review)

- **Damon Poburko**, A. Mike Keep, Amrit Mahil, Megan McLarnon, Cornelis van Breemen. Vascular Smooth Muscle Heterogeneity of Calcium Recycling & Junctional Composition. IUPHAR World Congress, July 12-15, 2002, San Fransisco, Ca.
- **Poburko D**, van Breemen C. Mitochondrial calcium transport in resting & stimulated vascular smooth muscle. Frontiers in Cardiovascular Science. February 02-03, Vancouver, British Columbia
- **Damon Poburko**, Tania Szado, Tasneim Behra, Roshanak Rahimian, Bruce McManus, Cornelis van Breemen, Urs T. Ruegg. Ca^{2+} influx pathways mediating basal calcium entry in vascular smooth muscle: The calcium leak and excitable channels. IUPHAR satellite meeting: Vascular Neuroeffectors Meeting, July12-15, 2002, Grenlibakken Resort, Lake Tahoe, California.

Material from this dissertation has also been presented orally for the Graduate Student Seminars Series in the Department of Pharmacology and Therapeutics at UBC

ACKNOWLEDGEMENTS

My time as a graduate student has been incredibly enjoyable and educational and has taught me many lessons. For this my deepest thanks go to Dr. Casey van Breemen, who embodies everything good that one could ask for in a scientist, a supervisor, and friend. To him I owe an immense debt of gratitude for the knowledge and experience that he shared, for his trust and encouragement, and his fathomless patience. Above all, he opened my eyes to the wonder of research and the value of a balanced life. Thank you.

Over the last few years, I have had the opportunity to learn from the experiences of fellow trainees and to work with many students and technicians. I would especially like to thank Mike Keep, Megan McLarnon, Edo van Breemen, and Kate Potter for your hard work and dedication and for keeping everyone smiling. To Tania Szado, I owe a special thanks for establishing the aequorin technique in the lab. Thanks to Eric Lin for his patient lessons and assistance with deconvolution and confocal microscopy. To the rest of the gang at the BC Research Institute for Children's and Women's Health and at St. Paul's Hospital, thank you for your technical support, laughs and insightful discussions.

I must also recognize two special individuals, Dr. Urs Ruegg and Mr. Philippe Lhote in Geneva & Lausanne, Switzerland for all their supervision and excellent technical assistance. I will never forget my time in Lausanne, and it would not have been so productive without the commitment of these two to our common goals. Thank you.

To my most amazing family and friends, thank you for your encouragement, advice, love and support. Thank you for understanding when I couldn't be there, and thank you for being there when I needed you.

Finally, I would like to acknowledge the Natural Sciences and Engineering Research Council of Canada, the Michael Smith Foundation for Health Research and the Killam Foundation for their financial support during my training.

CHAPTER I
Introduction to calcium signaling in vascular smooth muscle

1.1 The basics of smooth muscle.

1.1.1 Physiological role of smooth muscle.

Blood vessels provide the primary route of transportation for nutrients, immune cells, and signaling molecules in the body. Like most hollow organs in the body, the function of blood vessels is highly dependent on the layer of smooth muscle, or tunica media, that surrounds them. The vessel wall is further composed of an outer layer of connective tissue (tunica adventitia) that provides structural integrity to the vessel, and the endothelial layer (tunica intima) that lines the lumen of the vessel (figure 1.1). In their contractile phenotype, the basic physiological role of the vascular smooth muscle (VSM) is to regulate the diameter of the vessel lumen in order to control perfusion pressure and direct regional blood flow. The physiological control of vascular tone is modulated by numerous factors, thus VSMC are responsive to changes in perfusion pressure, autonomic stimuli through the innervation of larger vessels, paracrine and autocrine receptor ligands, and oxygen tension. In damaged vessels however, VSM cells can differentiate to a secretary/ proliferative phenotype to assist with blood vessel repair. In both phenotypes, changes in the free ionic concentration of calcium in the cytosol ($[Ca^{2+}]_i$) play a central role in the regulation of multiple functions of the VSM. However, with increasing age, poor diet and a lack of exercise, the regulation of VSM becomes increasingly prone to failure. This failure can lead to hypertension, vasospasm and may contribute to the progression of atherosclerosis.

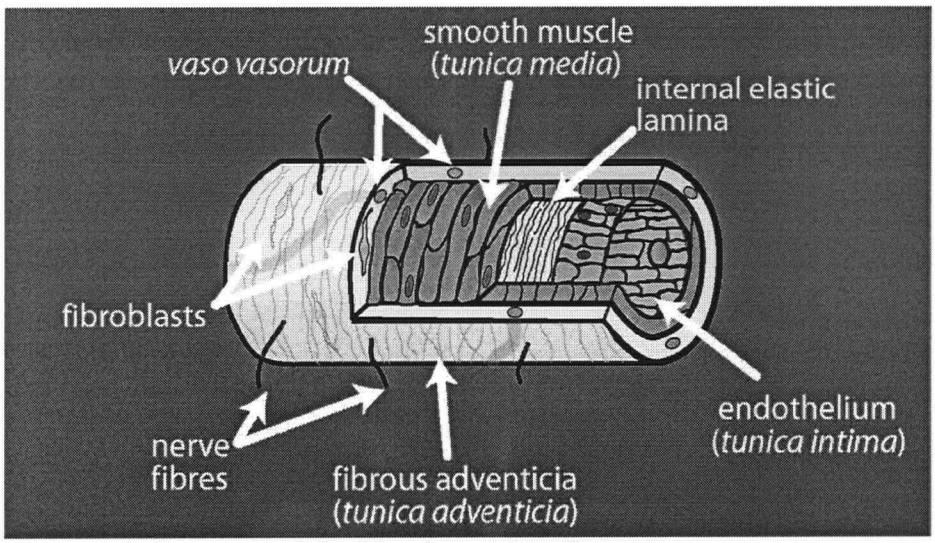

Figure 1.1. Structure of the blood vessel wall.

1.1.2 The mechanism of smooth muscle contraction.

Cytosolic free ionic Ca^{2+} is the primary second messenger linking membrane excitation or stimulation to the contraction of smooth muscle cells. Vascular smooth muscle cells can be described as tapering cylinders 3-10 μm in diameter depending on the state of contraction and 50-500 μm in length (33). In most vessels, the VSMC are wrapped around the blood vessels in a slightly helical manner, while in some vessels a layer of smooth muscle is also oriented along the longitudinal axis of the cell. Within the smooth muscle cell is a contractile apparatus consisting of thick myosin filaments surrounded by thin α-actin filaments that are anchored to dense bodies throughout the cytosol and dense bands (or plaques) at the plasma membrane (PM) (210). Elevation of $[Ca^{2+}]_i$ promotes the binding of 4 Ca^{2+} ions to calmodulin (CaM), which then binds to and activates the myosin light chain kinase (MLCK) (Figure 1.2). Activated MLCK then phosphorylates the myosin light chain and stimulates acto-myosin cross-bridge cycling (188). The activity of MLCK is opposed by myosin light chain phosphatase (MCLP). The opposing actions of MLCL and MCLP on myosin phosphorylation can also be modulated by Ca^{2+}-independent phosphorylation events, causing an apparent shift in the Ca^{2+}-sensitivity of the myofilaments. For example, Rho-kinase (ROK) can phosphorylate MLCP and impair its dephosphorylation of myosin thereby favouring contraction (Figure 1.2) (218). Phosphorylation of the actin-associated proteins, caldesmon and calponin, also regulate their inhibitory effect on cross-bridge cycling (6;69). Relative to cardiac or skeletal muscles, smooth muscle can maintain tension with much less energy expenditure by virtue of a prolonged association of actin and myosin upon myosin dephosphorylation known as the "latch-state" (97;171). This model has recently been expanded into an 8-state model, which further accounts for the phosphor-regulation of the thin actin filament (96), and future iterations may include regulatory influences of proteins such as ROK.

1.1.3 Mechanisms of Ca^{2+} Homeostasis and Signaling in VSM.

In order for $[Ca^{2+}]_i$ to increase and stimulate the contractile apparatus or other Ca^{2+}-dependent processes, Ca^{2+} must enter the cytosol from the extracellular space or be released into the cytosol from the sarcoplasmic reticulum (summarized in Figure 1.2).

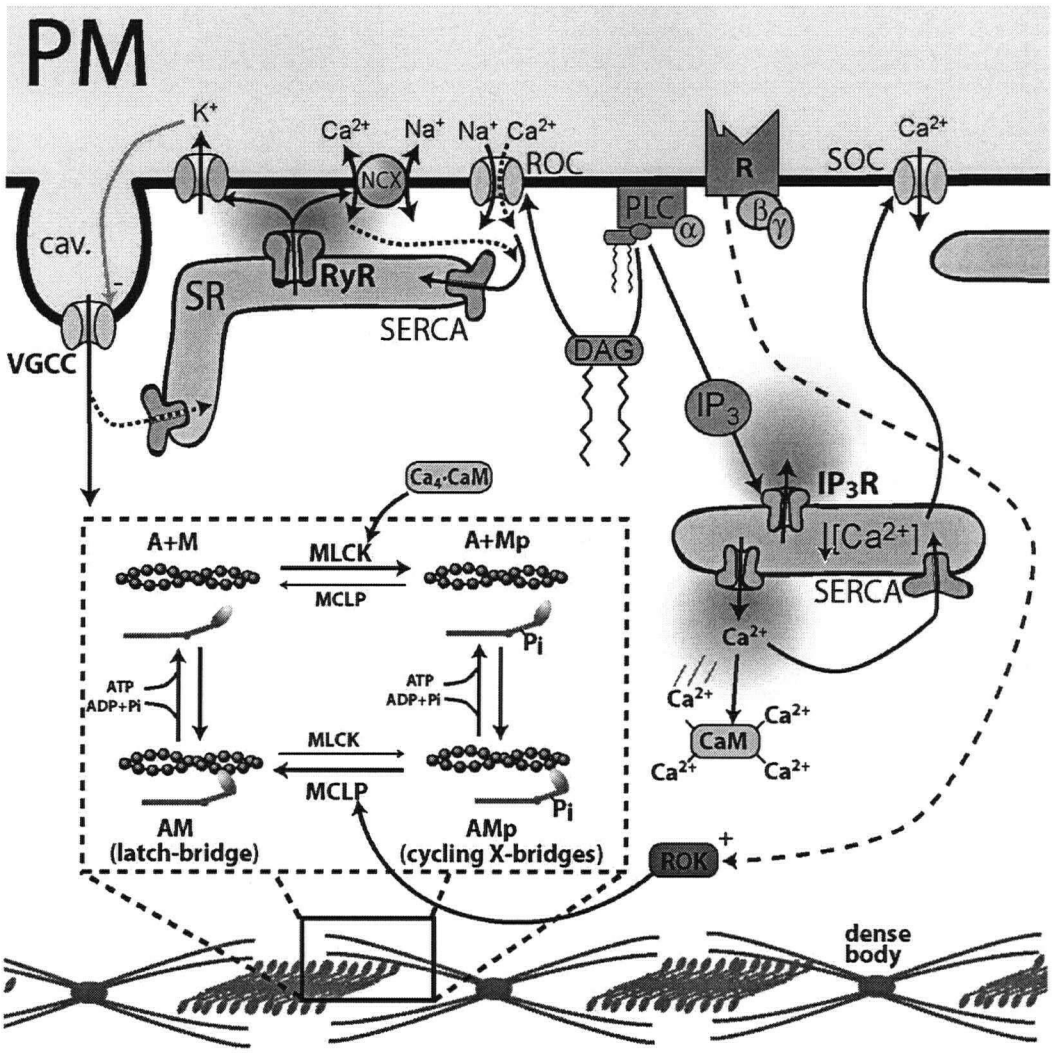

Figure 1.2 Calcium and Excitation-contraction coupling. A general scheme is depicted for the agonist dependent elevation of intracellular [Ca^{2+}] via activation of phospholipase C. Ca^{2+} release from the SR activates store-operated Ca^{2+}-channels, while DAG activates non-selective cation channels that mediate the Na^{+}-influx required for NCX reversal. Elevation of $[Ca^{2+}]_i$ causes Ca^{2+} to bind to calmodulin. $Ca^{2+}{}_4$·CaM then activates MCLK, which phosphorylates myosin and stimulates acto-myosin cross-bridge cycling. MLCP-dependent dephosphorylation of myosin is impaired by Rho-kinase that is stimulated by receptor activation. Abbreviations: A, actin; CaM, calmodulin; cav, caveolae; DAG, diacylglycerol; IP_3, inositol trisphosphate; IP_3R, IP_3 receptor; M, myosin; MLCK, myosin light chain kinase; MCLP, myosin light chain phosphatase; NCX, Na^{+}/Ca^{2+}-exchanger; PLC, phospholipase C; R, G-protein coupled receptor; ROC, receptor-operated channel; ROK, Rho kinase; RyR, ryanodine receptor; SERCA, sarco/endoplasmic reticulum Ca^{2+}-ATPase; SOC, store-operated channel; SR, sarcoplasmic reticulum; VGCC, voltage-gated Ca^{2+} channel.

The permeation of Ca^{2+} across the smooth muscle PM is mediated by several types of channels. Depolarization activates a family of voltage-gated Ca^{2+} channels, which are encoded by separate genes. It has also been known for at least 30 years that depletion of SR Ca^{2+} stores and activation of G-protein coupled receptors can activate Ca^{2+} influx through what have been termed store-operated channels (SOC) and receptor-operated channels (ROC). Only recently were the transient receptor potential proteins (TRPs) identified as molecular candidates for SOCs and ROCs (21). In smooth muscle it is currently debated whether SOCs are primarily Ca^{2+}-

selective or non-selective channels, but either way channels sensitive to SR Ca^{2+} depletion likely contain some combination of TRPC1, TRPC4, and TRPC5. In contrast, ROCs appear to be activated by diacylglycerol (DAG) that is generated with inositol-1,4,5-trisphosphate (IP_3) following hydrolysis of phosphatidyl inositol by phospholipase C (PLC) (225). These ROCs are non-selective cation channels (NSCC) and are likely composed of TRPC3 and TRPC6 (21;225). Since the extracellular concentration of Na^+ is ~100-fold higher than that of Ca^{2+}, these channels mediate substantial Na^+ influx, which in turn causes the Na^+/Ca^{2+}-exchanger (NCX) to reverse and bring Ca^{2+} into the cell (11).

Release of Ca^{2+} from the sarcoplasmic reticulum is mediated by two types of Ca^{2+}-channels, ryanodine receptors (RyR) and in IP_3 receptors (IP_3R) each of which is expressed in three isoforms. Both channels are essentially gated by local $[Ca^{2+}]$, such that cyclic-ADP-ribose (cADPr) and IP_3 alter the Ca^{2+}-affinity of the RyR and IP_3R, respectively. Release of SR Ca^{2+} induced by PLC-linked receptors, such as α-adrenergic receptors, is often associated with the production of IP_3 and the activation of IP_3R. In contrast, less is known about linkage between receptor activation and the production of cADPr by ADP ribose cyclase (aka CD38) (15). Rather the activation of RyR is most often attributed to Ca^{2+}-induced Ca^{2+}-release (CICR) in response to local elevation of $[Ca^{2+}]$ (254). Despite the fact that both receptors release Ca^{2+} into the cytosol, evidence suggests that they may be localized to separate elements of the SR (85;153), which may allow each receptor to regulate specific processes in the cell.

Calcium acts is a second messenger for numerous signaling cascades, and cells possess sophisticated and redundant mechanisms to clear Ca^{2+} from the cytosol. Both the sarcoplasmic reticulum and mitochondria serve as rapid cytosolic buffers of Ca^{2+}. However, for the intracellular Ca^{2+} content to be maintained at a steady-state level in the face of basal or stimulated Ca^{2+} entry, the Ca^{2+} that is taken up by these buffers must eventually be extruded from the cell. With a $[Ca^{2+}]_i$ of ~100nM at rest and an extracellular $[Ca^{2+}]$ of ~1.5mM, Ca extrusion is an energy dependent process that is mediated by the plasma membrane Ca^{2+}-ATPase (PMCA) and the NCX, which extrudes Ca^{2+} in exchange for Na^+ at an electrogenic ratio of $1Ca^{2+}:3Na^+$ (33).

Having introduced the major players in VSM Ca^{2+} signaling, the next two sections discuss in detail how the behaviour of individual smooth muscle cells requires precise choreography between these ion translocators, with special emphasis the role of mitochondria.

1.2 LINKED Ca^{2+} TRANSPORT IN VASCULAR SMOOTH MUSCLE[1]

Calcium (Ca^{2+}) regulates nearly all fast processes in the body, including contraction, chemotaxis, secretion, synaptic transmission, and several slower processes, including fertilization, proliferation, learning, memory and apoptosis. An important unresolved question is how the fluctuations of the concentration of a single inorganic ion, Ca^{2+}, can regulate such a multitude of cellular processes. On the one hand, cells have developed a plethora of Ca^{2+}-sensitive, signal-transducing proteins to tailor their cell-specific regulation of many diverse processes by Ca^{2+} (recently reviewed in (23)). Yet this cannot entirely explain how multiple processes, such as cross-bridge cycling and myosin filamentogenesis in smooth muscle or endothelial nitric oxide (NO) and epoxyeicosatrienoic acid production, can be regulated simultaneously. It has been proposed that the solution lies in the physical and temporal separation of numerous targets for Ca^{2+}, combined with the generation of localized cytoplasmic Ca^{2+} gradients (176). Clearly, mitochondrial dehydrogenases, voltage-gated Ca^{2+} channels (VGCCs), inositol (1,4,5)-trisphosphate (IP_3) receptors (IP_3R) and DNAses are localized in different sub-cellular regions and could be selectively activated by focal Ca^{2+} signals. Moreover, activation of certain target proteins by Ca^{2+}-calmodulin could be site-specific, despite the wide-spread intracellular distribution of calmodulin (CaM), since CaM can be tethered to effector complexes, such as smooth muscle myofilaments (256).

Analysis of the interaction of Ca^{2+}-transport molecules in the plasmalemma, the sarco/endoplasmic reticulum (SR/ER), the nuclear envelope and mitochondria suggests that these interactions provide structural basis for the spatially and temporally encoded fluctuations in cytosolic concentration of Ca^{2+} ($[Ca^{2+}]_i$) that are thought to mediate site-specific Ca^{2+} signaling. This interaction takes place in two fundamentally different ways: (i) directed Ca^{2+} supply to or removal from the Ca^{2+}-sensing domains of signal-transducing molecules and Ca^{2+} translocators; and (ii) Ca^{2+} delivery from a transport site located in one membrane to a second Ca^{2+} transport site located in an apposing membrane. An example of the first type of interaction is the delay of Ca^{2+}-mediated inhibition of VGCCs due to nearby mitochondria sequestering Ca^{2+} (156). The second type of interaction is exemplified by coupling of Ca^{2+} entry through the NCX to the sarco-endoplasmic reticulum Ca^{2+}-ATPase (SERCA) during store refilling (133). The concept of preferential Ca^{2+} delivery from one transporter to the next is referred to as "linked Ca^{2+}

[1] Aversion of section 1.2 has previously been published as: Poburko D, Kuo KH, Dai J, Lee CH, van Breemen C. Organellar junctions promote targeted Ca2+ signaling in smooth muscle: why two membranes are better than one. **Trends Pharmacol Sci**.. 25(1):8-15. Review.

transport." This process circumvents free diffusion throughout the cytoplasm and, typically, takes place at organellar junctions where physically restricted diffusion of Ca^{2+} within the narrow cytoplasmic domain is further slowed down by a high density of fixed, negatively charged Ca^{2+} binding sites (24). Table 1.1 lists both known and hypothesized junctions within smooth muscle.

Table 1.1. Intracellular linked Ca^{2+} and Na^+ transport [a-c].

Delivering Structures		*Acceptors*		*Event*	*Ref*
Membrane	*Translocator*	*Membrane*	*Translocator*		
		Ca^{2+}			
PM	VGCC	SSR	SERCA	Buffering	
PM	SOC	SSR	SERCA	Refilling	(133)
PM	NCX	SSR	SERCA	Refilling	(133)
SSR	RYR	PM	NCX	Unloading	(162)
SSR	IP3R	PM	NCX	Unloading	(162)
SR	IP_3R & RYR	SR	SERCA	Recycling	(162)
ER1	" "	ER2	SERCA	Redistribution	N/A
SR/ER	" "	MT	uniporter	Mito. Ca^{2+} sig.	(74;220)
MT	MNCX	SR/ER	SERCA	" buffering	(10)
MT	MHCX	SR/ER	SERCA	" "	N/A
MT	PTP depol	SR/ER	SERCA	" "	(36)
SR/ER	IP_3R & RYR	MT	PTP pol	" "	N/A
		Na^+			
PM	SOC	PM	NCX	NCX reversal	(133)
PM	SOC	PM	NKA α3	Na^+ extrusion	(12)
PM	NCX	PM	NKA α3	Na^+ extrusion	(12)

[a] The ion translocators delivering Ca^{2+} or Na^+ are listed under "Delivering Structures," and the transport molecules accepting the ions, thus completing the linked transport, are listed under "Acceptors."

[b] Although some of the above mechanisms remain hypothetical, various levels of supportive evidence has been presented for all cases (see main text).

[c] Abbreviations: ER & ER1, endoplasmic reticulum; ER2, adjacent but luminally distant endoplasmic reticulum; for standard abbreviations see main list of abbreviations

1.2.1 Structural considerations of PM-SR junctions.

The SR of smooth muscle is a continuous network of membranous tubules and sheets that can be divided into superficial and deep SR and the nuclear envelope (164). Electron microscopy of serial sections shows that the superficial SR forms a flattened pedestal as it approaches the PM. The junctional cytoplasmic space between the PM and SR pedestals has a consistent width of 15–20 nm and a diameter of up to 500 nm. In vascular smooth muscle (VSM) cells of the rabbit inferior *vena cava* (IVC), 14.2 ± 0.7% of the PM (including the necks of caveolae) is closely associated (within 30 nm) with the superficial SR, the junctional width averages 19 ± 1 nm (133), and the apices of the caveolae protrude through this thin fenestrated junctional SR (58;63). At present, it is unknown what causes a particular portion of the PM to form a junction, although such junctions are common in caveolae rich regions of the PM. The junctional PM might have specific chemical characteristics, such as those of cholesterol and sphingolipid-rich

lipid rafts, which form platforms for signaling and transport molecules (14), or plasmalemmal receptors may be physically linked to SR proteins such as the linkage of metabotropic glutamate receptors to SR release channels via Homer proteins (72). Interestingly, the $\alpha 1_D$-adrenoceptor contains a consensus sequence for Homer protein binding (266). The regularity of the width of the PM-SR junction both within a single junction and between junctions is similar to that seen in the triads and diads of skeletal and cardiac muscle. In these tissues junctophilins 1, 2 and 3 are candidates for the structural cement between the T-tubular and SR membranes. Junctophilins (JP) are SR/ER transmembrane proteins with a cytoplasmic region (MORN motifs) that bind to the plasma membrane, and JP-2 is critical to normal calcium signaling in cardiac myocytes (223). Unfortunately the difficulty in isolating smooth muscle PM-SR junctions has so far precluded identification of their chemical nature.

1.2.2 Function of PM-SR junctional complexes

1.2.2.1 Dynamic Ca^{2+} buffering and cycling in resting smooth muscle. The "superficial buffer barrier" function of the superficial SR (SSR) in smooth muscle provided the first example of linked Ca^{2+} transport (4;233). In this case a fraction of Ca^{2+} entering the cell through plasmalemmal Ca^{2+} channels is taken up by SERCA of the superficial-SR before it has time to diffuse to the deeper myoplasm (Table 1.1 and Figure 1.3). The concept of active Ca^{2+} uptake by an organellar network to limit diffusion into other regions of the cell was subsequently applied to the "nuclear Ca^{2+} buffer barrier" (249) in coronary smooth muscle and the "mitochondrial Ca^{2+} buffer barrier" in pancreatic acinar cells (170). To maintain the superficial buffer barrier, Ca^{2+} accumulating in the superficial-SR is recycled to the extracellular space as it is released by the superficial SR in a vectorial manner into the PM-SR junctional space coupled to the forward mode of the NCX in the PM (162). The superficial buffer barrier occurs in many types of smooth muscle including coronary artery, airway and uterine smooth muscle (115;214;222), and it provides a mechanism to generate peripheral Ca^{2+} gradients and protect cells from Ca^{2+} overload. This protective role appears to be compromised in diabetic vascular disease and up-regulated as a result of exercise (249). Based on the morphology described above, Figure 1.3 illustrates that the superficial buffer barrier involves two types of linked Ca^{2+} transport: (i) "loosely coupled" transport, where SERCA captures part of the Ca^{2+} entering the cell through the non-junctional PM, possibly including the caveolar apices; and (ii) "tightly coupled" transport within the PM-SR junction between SR release channels and the NCX. When the NCX is blocked, Ca^{2+} is conserved within the SR by SERCA mediated re-uptake, indicating

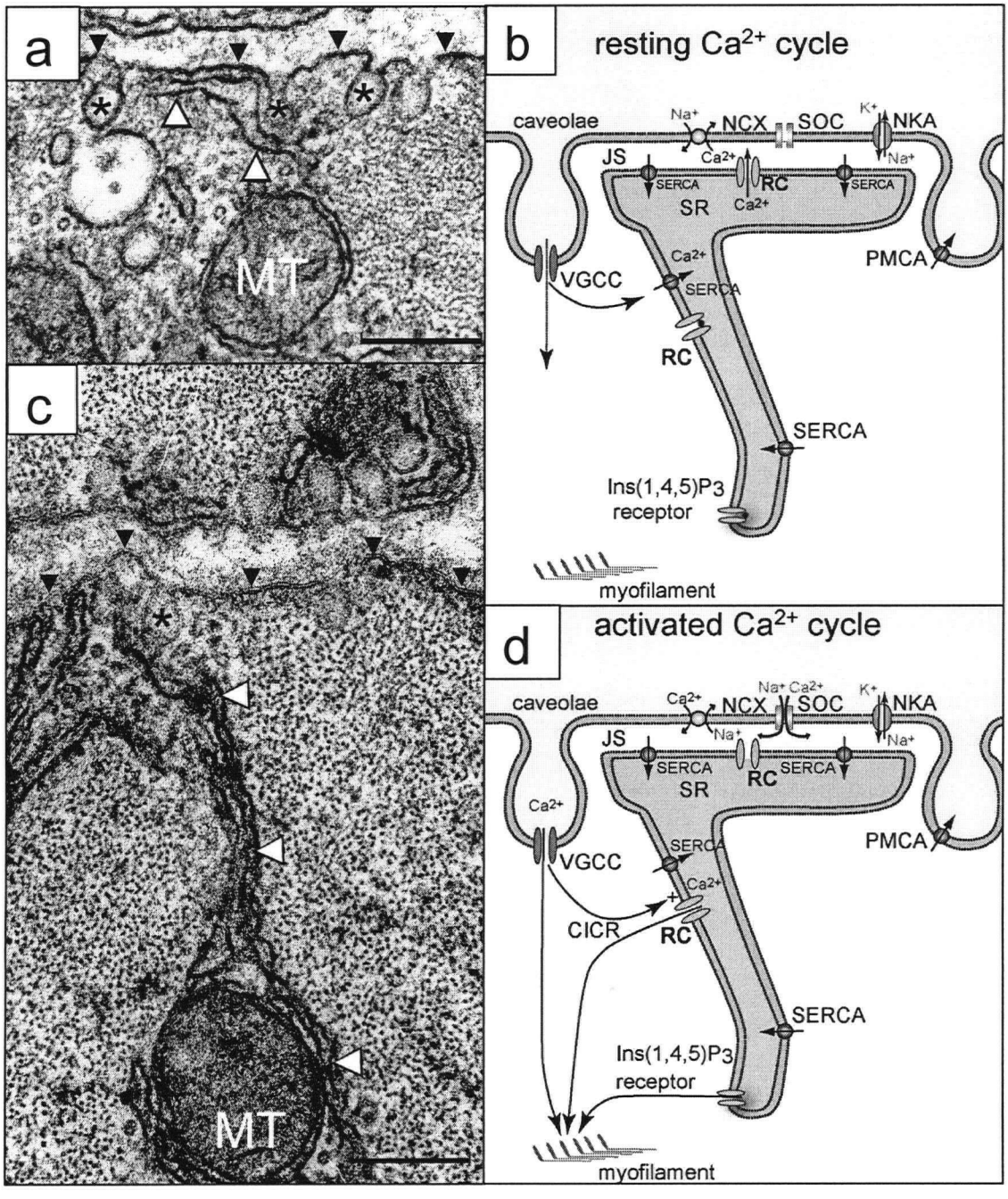

Figure 1.3. Ca^{2+} cycling at PM-SR junctions in smooth muscle. (a) This electron micrograph shows superficial-SR (white arrow heads) associated with the PM (black arrow heads) and caveole (asterisk). (b) *Ca^{2+} cycling in the superficial buffer barrier in non-stimulated VSM.* The superficial-SR buffers Ca^{2+} entry due to basal activity of excitable Ca^{2+} channels, and cycles it, via release channels (RC: IP_3R, RYR), to the NCX in the junctional space (JS) to be extruded. Ca^{2+} is also extruded by the PMCA in non-junctional PM. (c) This EM depicts superficial and radial SR (white arrow heads) associated with a mitochondrion (MT), caveolae (asterisk) and plasmalemma (black arrow heads). (d) *Ca^{2+} fluxes associated with agonist-mediated smooth muscle stimulation.* Ca^{2+} is release from IP_3R near the myofilaments, and SR depletions and receptor stimulation opens a Na^+ and Ca^{2+} permeable SOC. Na^+ influx depolarizates the cell and opens VGCC, while the $[Na^+]$ builds in the junction and reverses NCX to bring Ca^{2+} to SERCA for store refilling. *Other abbreviations*: IP_3 – inositol(1,4,5)-trisphosphate, RC – release channel, RY – ryanodine,. Scale bar = 400 nm. ** electron micrograph courtesy of Dr. Kuo-hsing Kuo.

that SERCA are located in or very near the PM-SR junctions (162). Only when both NCX and SERCA are blocked is Ca^{2+}-release from the SR extruded from the cell by the plasmalemmal Ca^{2+}-ATPase (PMCA), which, in this instance, is assumed to be located in non-junctional PM. Co-localization of calsequestrin within the superficial-SR and NCX in the PM (157) provides morphological support for the transport scheme of Figure 1.3, but more precise imaging is required to test the rank ordering of linkage between IP_3/ryanodine (RY) receptors and NCX, SERCA and PMCA.

Analogous to the superficial buffer barrier, Ca^{2+}-uptake by SERCA located in the nuclear envelope, which displays extensive inwardly directed cristae, can regulate the flow of Ca^{2+} between the cytoplasm and nucleus. This mechanism, termed the "nuclear buffer barrier" is postulated to exert control over gene expression (249). In this context, it is most interesting that experimental separation of the inner and the outer membranes of the nuclear envelope from hepatocytes revealed that SERCA was specifically localized to the outer membrane of the nuclear envelope (107), and that SERCA inhibition with thapsigargin abolishes the Ca^{2+} gradient between nuclear and cytosolic [Ca^{2+}] (103).

1.2.2.2 Wave-like $[Ca^{2+}]_i$ oscillations in activated smooth muscle. Ca^{2+} oscillations appear to be a common regulatory mechanism in several types of smooth muscle (2). In large veins and arteries, α-adrenergic-mediated force development is regulated by recruitment of cells and the frequency of asynchronous, agonist-induced Ca^{2+} oscillations that are primarily generated by the release of Ca^{2+} from the SR (70;199). Wave-like $[Ca^{2+}]_i$ oscillations in VSM are efficient in activating myofilaments because the SR network penetrates deep into the myoplasm (133), and the frequency-encoded Ca^{2+}-signals provide more precise contractile modulation than global changes in average $[Ca^{2+}]_i$. In resistance arteries, asynchronous waves have a dilatory effect due to the opening of Ca^{2+}-activated K^+-channels (K_{Ca}) (113); however, oscillatory vasomotion is induced when they become synchronized during exposure to agonists (172). While the exact mechanisms underlying vascular heterogeneity of smooth muscle Ca^{2+} signaling are unresolved, differences in the ion transporters found in junctional complexes could be important. Furthermore, $[Ca^{2+}]_i$ oscillations could serve to modulate frequency-encoded Ca^{2+}-sensitive mitochondrial dehydrogenases and gene expression.

A detailed description of the ionic mechanism of smooth muscle Ca^{2+} oscillation has been reported for adrenergicaly-stimulated rabbit IVC and is illustrated in Figure 1.3. First, α_1-adrenergic receptor stimulation leads to saltatory SR Ca^{2+}-release from IP_3R, spreading across

the cell from Ca^{2+}-wave initiation sites, which may be similar to so called "hot spots." Secondary activation of ryanodine receptors (RyR) also occurs in some tissues. Subsequently, a PM channel permeable to both Na^+ and Ca^{2+} is activated, either by store depletion or receptor activation (11). The resultant inward current depolarizes the PM activating VGCCs. In the IVC and trachea, where VGCC play a modulatory but not permissive role in contractile regulation, Na^+ is postulated to enter the PM-SR junctional space to increase the local Na^+ concentration ($[Na^+]_{PM-SR}$) sufficiently to cause NCX reversal (133). There is convincing evidence that $[Na^+]_{PM-SR}$ is separately regulated by the α2- and α3-isoforms of the Na^+/K^+-ATPase (NKAα2/3) (12). The reverse-mode NCX bring Ca^{2+} into the cell, which is taken up into the SR by SERCA in preparation for the next wave of Ca^{2+}-release. Ca^{2+}-influx associated with SR refilling also balances the loss of cell Ca^{2+} through augmented Ca^{2+} extrusion during elevated $[Ca^{2+}]_i$. In support of the above model, separation of PM-SR junctions with calyculin A has been shown to abolish Ca^{2+} oscillations (131;132). Blockade of IP_3R with 2-aminoethoxy-diphenylborate (2-APB) immediately terminates the $[Ca^{2+}]_i$ oscillations, while blockade of SOCs and VGCCs allows continuation of a few oscillations before silencing the Ca^{2+} waves (132). Site directed mutagenesis of the IP_3 receptor to reduce its Ca^{2+} sensitivity also abolished VSM Ca^{2+}-waves, convincingly demonstrating the primary importance of the IP_3-mediated Ca^{2+} release in this process (109).

1.2.2.3 Ca^{2+} spark/wave-STOC coupling in relaxing smooth muscle. Spatially restricted membrane currents through K_{Ca}, or spontaneous-transient outward currents (stocs), are activated by local increases in sub-plasmalemmal $[Ca^{2+}]$ resulting from spontaneous RYR-mediated Ca^{2+}-release events (sparks) (254). Although spark-mediated $[Ca^{2+}]$ elevations can spread over a much larger distance than the 20 nm PM-SR junctional width (113), kinetic considerations for the relationship between sparks and stocs indicate that the RyRs producing sparks are within 20 nm of the K_{Ca} in the PM (for current reviews on sparks see (32;102). This suggests for instance that cerebral resistance vessels possess PM-SR junctions that are different from those in the IVC, being specifically designed to hyperpolarize the PM and mediate relaxation. The presence of $K_{Ca,}$, as opposed to say NCX, in PM-SR junctions of cerebral resistance arteries further explains why Ca^{2+}-waves in this tissue are linked to relaxation (112).

1.2.2.4 CICR in activating smooth muscle. Calcium entering smooth muscle through VGCC can activate RyR, and the SR Ca^{2+}-release amplifies the contraction-inducing Ca^{2+} signal.

Although there is a very close relationship between VGCC and RyR in cardiac muscle, a large body of evidence indicates that Ca^{2+}-induced Ca^{2+}-release (CICR) is not a common mechanism in most smooth muscle types. For example in the uterus, which is mainly dependent on L-type Ca^{2+} channels, spontaneous contractile activity is not accompanied by fluctuations of SR Ca^{2+} content (207). However, CICR has been demonstrated in myocytes of some blood vessels, *vas deferens* and urinary bladder (124). It has been argued that, since CICR in the bladder depends more on the net Ca^{2+} influx than on the open probability of individual VGCC, and because there is a delay between the current and the subsequent spark, the VGCC are loosely coupled to the RyR with a distance between them in excess of 100 nm (124). This is consistent with the aforementioned idea that the VGCC are not located within the 20 nm cleft of the junction, but rather in the tips of the caveolae.

1.2.3 Structural considerations of mitochondrial junctions

Recent years have seen an resurgence of interest in mitochondrial (MT) Ca^{2+} transport with novel evidence for its influence on both plasmalemmal and SR/ER Ca^{2+} transport that compliments rather than detracts from more traditional roles for mitochondrial in ATP production and apoptosis (190). A popular view of mitochondrial Ca^{2+}-uptake is that mitochondria form diffusionally restricted domains with the PM or SR/ER, as in Figure 1.4, that develop Ca^{2+} levels sufficiently high to overcome the low affinity of mitochondrial Ca^{2+}-uniporter, as measured in isolated mitochondria. However, the Ca^{2+}-affinity of the uniporter *in situ* is hotly debated. In HELA and luteal cells, mitochondrial Ca^{2+}-uptake occurs upon modest $[Ca^{2+}]_i$ elevation (<300 nM) (47;219), but these reports do not preclude the involvement of MT-ER junctions. Indeed, sustained MT-ER interactions were recently reported in HELA cells (74), and mitochondria are known to take up the Ca^{2+} sparks released by nearby RyR (168), which occur more frequently as $[Ca^{2+}]_i$ increases (254). In smooth muscle, direct measurement of $[Ca^{2+}]_{MT}$ revealed substantial mitochondrial Ca^{2+}-uptake in response to agonist-mediated SR-Ca^{2+} release, but only modest mitochondrial Ca^{2+} uptake in response to sustained influx as discussed below (220). The aforementioned report is one of very few direct investigations of VSM mitochondrial Ca^{2+}-signaling. Consequently, much of the following discussion is based on evidence from non-muscle cells, and awaits verification in VSM.

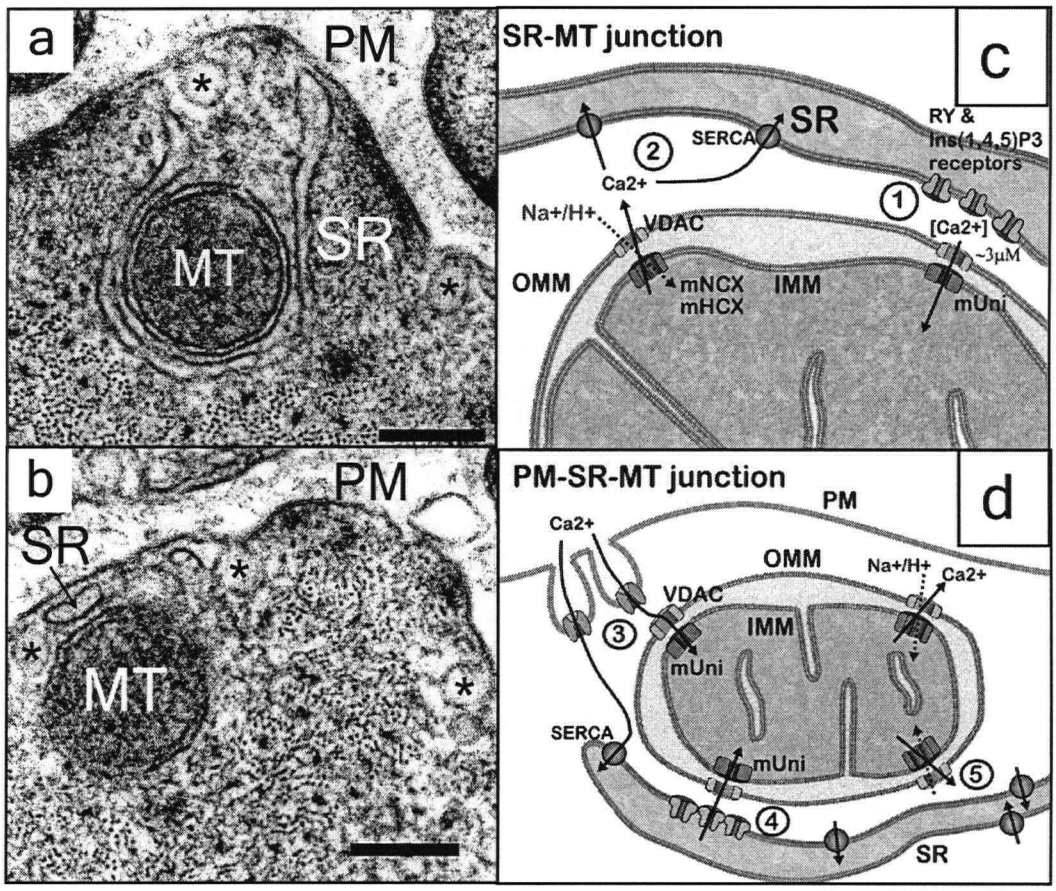

Figure 1.4. Mitochondrial junctions with the sarcoplasmic reticulum and plasmalema. (a) This smooth muscle electron micrograph shows the close contact between the SR and mitochondria (MT) that can often enshroud the MT. (c) Close apposition between MT and PM or MT, SR and PM can also be observed. In restricted regions, caveolae (asterisk) and MT are separated by less than 200 nm. (c & d) *Probable junctional complexes at MT-SR junctions (c) and PM-SR-MT junctions (d) drawn to relative scale based on current literature.* (1 & 4) SR release channels (RY & IP_3 receptors) cluster in regions facing MT, likely near contact sites of the inner (IMM) and outer (OMM) mitochondrial membranes. Ca^{2+} released into the MT-SR junctional space crosses the OMM via the voltage-dependent anion channel (VDAC) and reaches sufficiently higher $[Ca^{2+}]$ to activate the MT uniporter (U). (2 & 5) The mitochondrial Na^+/Ca^{2+}-exchanger (mNCX) or H^+/Ca^{2+}-exchange (mHCX) extrude Ca^{2+} and help to refill the SR. (3) VGCC and TRPC channels likely localize in caveole, and mitochondria can buffer Ca^{2+} entry through these channels implying a close association. *Other abbreviations:* IP_3 – inositol(1,4,5)-trisphosphate, mUni – mitochondrial Ca^{2+} uniporter, RY – ryanodine. Scale bar = 400 nm

The junctions between mitochondria and SR/ER are more diverse than those between PM and SR discussed above. The width of the MT-SR junctional space in VSM varies between 15 to 50 nm, both within one junction and amongst different junctions within a given cell. The extent of apposition ranges from minor to apparently complete mitochondrial envelopment by SR, and the degree of MT-SR association can vary significantly depending on the state of cellular activation (personal communication – Dr. Kuo-Hsing Kuo, 2005) (250). This implies that MT-SR junctions have a dynamic nature. Indeed, lateral movement of mitochondria relative to the SR has been described (142). This dynamic behaviour is reduced upon physiological elevations of $[Ca^{2+}]_i$, which has been attributed to inhibition of mechano-chemical enzymes that are proposed

to be involved in providing a framework for local MT-ER connections (241;250;262). Potentially important enzymes include dynamin GTPases, dynamin related proteins, microtubules, microfilaments and kynesins (241). Moreover, the long-lasting MT-ER interactions in HELA were reported in the context of mitochondria exhibiting typical motion and fusion/fission behaviour (74). Consistent with these concepts, the autocrine motility factor receptor appears to be a marker of ER regions in close contact with mitochondria (250). Ion channels of the outer mitochondrial membranes cluster at contact sites between the two membranes (52), and IP_3 and RyR have also been shown to localize at SR/ER regions facing the mitochondria hinting at the existence of an anchoring mechanism (98). Supporting the concept of intimate ER-MT signaling, mast cell ER release channels have been estimated to be no more than 100nm from mitochondrial Ca^{2+}-uptake sites (55).

1.2.4 Function of mitochondrial junctions

Mitochondrial serve numerous functions in all cells, and not surprisingly the function of the close associations of mitochondria with the SR/ER and PM is a complex and multi-faceted story that can be examined from many perspectives. From the biosynthesis point of view, the close contacts of MT and ER has long been thought to permit the exchange of mitochondrial derived lipids to the ER (128). In terms of Ca^{2+} signaling, it is now widely accepted that these close junctions are required to locally generate micromolar elevations of $[Ca^{2+}]_i$ to activate the low-affinity Ca^{2+}-uniporter (K_d ~10μM) (54;94;179). As a consequence of the ensuing and rapid Ca^{2+} uptake into the mitochondrial matrix, mitochondria modulate the release and refilling of SR Ca^{2+} stores in addition to buffering the sub-plasmalemmal Ca^{2+} gradients that modulate the gating of Ca^{2+}-sensitive PM ion channels. However, the role of mitochondria in VSM Ca^{2+} signaling extends far beyond the Ca^{2+} microdomain. Consequently, the function of PM-MT and SR-MT junctions is discussed below in the context of the integral role of mitochondria in VSM Ca^{2+} signaling.

1.3 MITOCHONDRIA AT THE CROSSROADS OF Ca^{2+} SIGNALING[2]

In vascular smooth muscle, Ca^{2+} signaling regulates vascular tone by an integrated response to endogenous agonists, membrane potential, oxygen supply, and the cellular oxidation-reduction potential. Meanwhile, mitochondrial Ca^{2+} signaling in VSM is often viewed simply as a means to match ATP production to cellular energy demands by virtue of the Ca^{2+}-dependence of mitochondrial dehydrogenases and the F_1F_0-ATPase (38;61). This has led to the proposition that VSM mitochondria may act as integrators of three aspects of Ca^{2+} signaling seldom discussed together (Figure 1.5). First, mitochondria modulate the activation and inactivation of plasmalemmal ion channels and intracellular Ca^{2+}-release channels by buffering localized Ca^{2+} gradients in the cytoplasmic microdomains formed by close mitochondrial associations with the plasmalemma and sarco/endoplasmic reticulum (SR/ER) (13;37;67;93;251). These microdomains, subsequently referred to as PM-MT and SR/ER-MT junctions, in combination with tissue-specific channel expression are proposed to contribute to the heterogeneity of Ca^{2+} signaling observed in different types of VSM (164). Second, mitochondria are thought to contain the VSM oxygen sensor acting through the production of radical oxygen species (ROS) that modulate ion channels and second messenger production, which are central to the regulation of vascular tone. Finally, mitochondria contribute to regulation of cellular redox-potential in response to changes in the availability of metabolic substrates (18). For example, changes in the NADH:NAD ratio can alter the metabolism of cyclic-ADP ribose (cADPr) via NADH-mediated cADPr hydrolase inhibition (257). As cADPr alters ryanodine receptor (RyR) Ca^{2+} sensitivity, the subsequent effect will depend on the tissue-specific role of RyR-mediated Ca^{2+}-release. This model provides a working hypothesis to describe many of the effects of mitochondrial inhibition reported in VSM, but requires further evidence to validate whether or not mitochondria are indeed a central axis in VMS Ca^{2+} signaling.

Before the importance of mitochondria in Ca^{2+} signaling was clearly established (13;193), the clinical relevance of mitochondrial function in VSM was illustrated by mitochondrial encephalomyopathies that are caused by specific insufficiencies within the electron transport chain and exhibit altered mitochondrial morphology and possibly Ca^{2+} signaling (51). In spite of the extensive MT-SR associations first reported in VSM more than 10

[2] A version of section 1.3 has been published as: Poburko D, Lee CH, van Breemen C. (2004) Vascular smooth muscle mitochondria at the cross roads of Ca(2+) regulation. **Cell Calcium.** 35 (6): 509-521.

years ago (164), few details are known of the mitochondrial role in VSM Ca^{2+} signaling. Aspects like the mitochondrial contribution to cytosolic Ca^{2+} clearance or the time courses of mitochondrial Ca^{2+} transients are still unclear. At the same time, several studies clearly illustrate the importance of mitochondria in VSM Ca^{2+} signaling (139;217;231) and ROS production (154). Our current understanding of mitochondrial Ca^{2+} signaling in VSM is not only limited by the scarcity of studies employing organelle-specific Ca^{2+} probes, but also by the potential for vascular heterogeneity to confound extrapolation of findings between different blood vessels. Furthermore, hypotheses based on data from experiments in VSM prior to recognition of the central role of cytosolic microdomains in mitochondrial Ca^{2+} signaling have largely gone unchallenged. The few available studies using organelle-specific calcium probes report mitochondrial Ca^{2+}-signals consistent with those reported in other cell types and underscore the need to define the detailed mitochondrial interactions with SR and PM transporters in VSM (160;220).

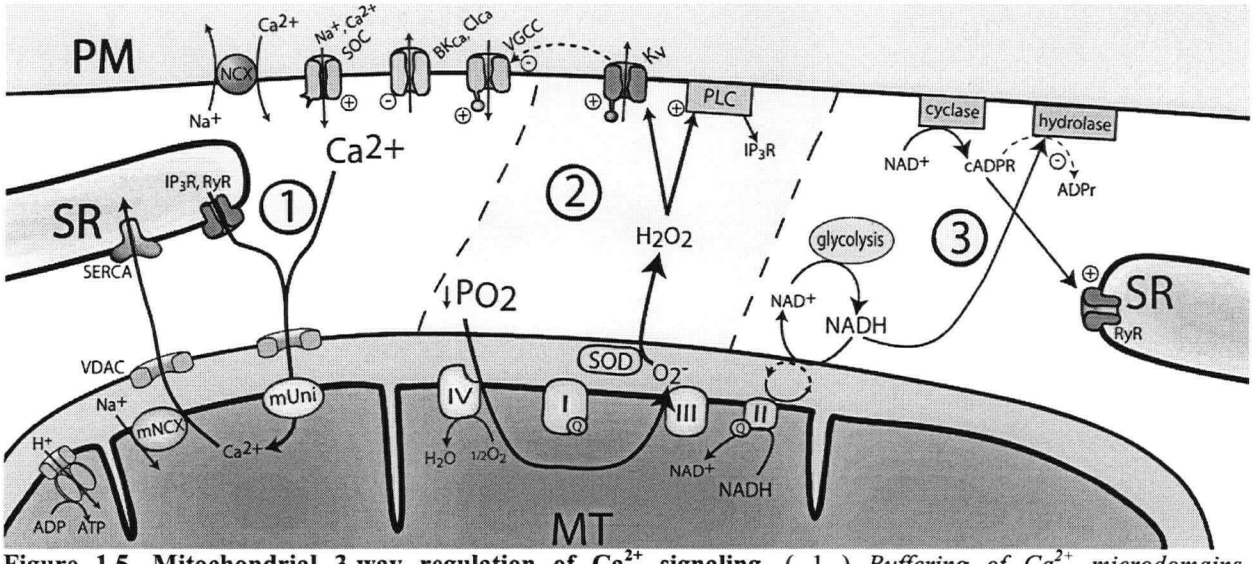

Figure 1.5. Mitochondrial 3-way regulation of Ca^{2+} signaling. (1) *Buffering of Ca^{2+} microdomains.* Mitochondria buffer Ca^{2+} entry and release to modulate the local [Ca^{2+}] near Ca^{2+}-sensitive PM and SR ion channels and to help refill the SR. (2) *Relaying P_{O2} to Ca^{2+} signaling.* Hypoxia or proximal electron transport chain inhibition influence mitochondria-derived H_2O_2 production. O_2^- and H_2O_2 act on K_v, phospholipase C and SERCA in different blood vessels. (3) *Relaying metabolic perturbations to Ca^{2+} signaling.* Perturbations in oxidative respiration and metabolite recycling affects the cytosolic NADH:NAD ratio, which can inhibit cADPr hydrolysis and modulate RyR and BK_{Ca} gating properties. Plus signs denote increased activity. Minus sign denotes reduced activity.Abbreviations: ; I - IV, electron transport chains complexes I – IV; ADPr, ADP ribose; BK_{Ca}, large-conductance Ca^{2+}-activated K^+-channel; cADPr, cyclic ADP ribose; Cl_{Ca}, Ca^{2+}-activated Cl^--channel; K_v, voltage-gated K^+-channel; P_{O2}, oxygen tension; SOD, superoxide dismutase.

A word of caution is in order before delving into the available data. I have discussed the available data on smooth muscle mitochondria in the context of advances made in other cell types and with an emphasis on how "mitochondrial inhibition" can affect Ca^{2+} signaling

pathways in at least three different ways. Much of the evidence from VSM describes effects of "mitochondrial inhibition" on cytosolic [Ca^{2+}] ($[Ca^{2+}]_i$) responses, and substantial confusion stems from the term "mitochondrial inhibitor," which describes a diverse group of drugs acting by very different mechanisms (see table 1). We begin with a brief review of Ca^{2+}-related mitochondrial ion transporters before considering the immediate effects of "mitochondrial inhibition" that include, but are not limited to, altered Ca^{2+} buffering, ATP production and ROS generation.

Table 1.2. Abridged list of mitochondrial inhibitors

Class	*Drug (EC_{50})*	*Comments*	*Ref*
Protonophores	FCCP (1 μM) CCCP (1 μM) DNP (3 mM)	depolarize PM at ~10μM	(73) (127) (205)
Complex I inhibitors	Rotenone (1 nM) capsaicin DPI (23 nmol/mg)	depolarize $\Delta\psi_m$, alter radical production inhibits PM-bound oxidases	(125) (59) (182)
Complex II Inhibitors	Carboxin TTFA (0.6 μM) antimycin A	 depolarizes $\Delta\psi_m$, alters radical production	(184) (265) (45)
Complex III inhibitors	HQNO (37 μM)) Myxothiazol Stigmatellin antimycin A (3 pM) benzoyl peroxide	complex IIIb/c(1) - Qi site complex IIIb/c(1) - Qo site complex IIIb/c(1) - Qo site complex IIIb(562)	(189) (189) (189) (104) (122)
Cytochrome c	DCCD (10μM)		(239)
Complex IV	Cyanide		(46)
	azide (10 nM)		(242)
F_o subunit of ATPase	Oligomycin A & B (3μM) Apoptolidin (5 μM)		(239)
F_1 subunit of ATPase	Aurovertin (25μM)		(200)
Uniporter blockers	ruthenium red (~0.2 nM)	inhibits RyR at higher concentration	(260)
	RU360 (0.2 nM)		(150)
RaM blockers	ruthenium red		(212)
mNCX inhibitor	CGP-37157 (0.4 μM)	selective over PM NCX	(50;111)
$_{mito}K_{ATP}$ activator	Diazoxide (0.4 μM) Cromakalim (1 μM)	selective over PM K_{ATP}	(81) (81)
$_{mito}K_{ATP}$ inhibitor	Glibenclamide (60 nM) 5-hydroxydecanoate	non-selective for $_{mito}K_{ATP}$	(17) (111)

Abbreviations: CCCP, carbonyl cyanide m-chlorophenylhydrazone; CN, cyanide; DCCD, dicyclohexyl carboniimide; DNP, dinitrophenol; DPI, diphenyleneiodonium; FCCP, carbonyl cyanide 4-trifluoromethoxyphenylhydrazone; HQNO, 2-heptyl-4-hydroxyquinoline-N-oxide; N_3, azide; TTFA, theonyltrifluoroacetate;

1.3.1 Pertinent mitochondrial ion transporters

1.3.1.1 Ca^{2+} uptake mechanisms. The mitochondrial Ca^{2+} uniporter (mUni) is activated by Ca^{2+} concentrations > 3μM (K_m ~ 10μM) in the inter membrane space (IMS) (55;94;179). Such concentrations are thought to result from Ca^{2+} release or influx into cytosolic

microdomains at SR-MT and PM-MT junctions, which exhibit restricted diffusion (193). Uniporter activation mediates Ca^{2+}-uptake by virtue of the negative membrane potential across the inner mitochondrial membrane ($\Delta\psi_m$), and the mUni appears to possess a Ca^{2+}-calmodulin-dependant mechanism that sustains some degree of Ca^{2+}-uptake after $[Ca^{2+}]_{IMS}$ has fallen below the threshold for activation indicated above (56;65). This is referred to as mitochondrial memory, plasticity or facilitation. Mitochondria experimentally loaded with high $[Ca^{2+}]$ are partially depolarized, in which case activation of the uniporter with a pulse of appropriate extra-mitochondrial $[Ca^{2+}]_i$ will permit Ca^{2+} diffusion out of the mitochondria through the uniporter (155). Ruthenium red is the prototypical mUni blocker (K_i ~0.2 μM) (260), but it is poorly membrane permeable, can inhibit the ryanodine receptor (K_i ~0.5μM, block at ~10μM) and binds to numerous Ca^{2+}-binding proteins such as calsequestrin (K_d 0.7μM) (44;158;202). The ruthenium red derivative, RU360, appears to be specific for the mUni (K_i ~10nM), but it is also poorly membrane permeable and rapidly oxidized (264;267).

The Rapid Mode of Calcium Uptake (RaM) is a Ca^{2+}-uptake mechanism demonstrating a high initial uptake velocity, and its steady-state uptake is reduced at $[Ca^{2+}]_i$ above 150nM and completely inhibited at $[Ca^{2+}]_i$ > 180nM (93). This likely limits the RaM to a role in resting VSM. RaM is also inhibited by a [ruthenium red], but at ~10-fold greater concentration than required to inhibit the uniporter, which thus also blocks RyR. Currently, no direct investigations of RaM activity have been reported in SMC.

1.3.1.2 Ca^{2+} extrusion & release mechanisms. Differences in the kinetics of Ca^{2+} extrusion from mitochondria in intact cells *versus* isolated mitochondria are difficult to reconcile given the potential for artifacts associated with each technique and the fact that these transporters have not been isolated or reconstitute in lipid bilayers. Calcium extrusion from polarized mitochondria is thought to occur via two pathways, a Na^+/Ca^{2+}-exchanger (mNCX) and a H^+/Ca^{2+}-exchange (mHCX) (22;174). The contribution of each transporter to mitochondrial Ca^{2+} extrusion varies in different cells. Early studies of isolated SMC mitochondria suggested a lack mNCX activity (53), but recent evidence clearly shows Na^+-dependant Ca^{2+} release in SMC mitochondria (228). Using CGP-37157, a selective mNCX inhibitor, we have found a modest contribution of mNCX to mitochondrial Ca^{2+} extrusion in cultured VSM cells (Figure 2.2). Both extrusion mechanisms have eluded molecular characterization, and mHCX has also eluded

pharmacological characterization perhaps because of the large number of H^+-translocating proteins on the inner mitochondrial membrane.

The permeability transition pore (PTP) is generally thought to be activated under pathophysiological conditions, and here I view it as a Ca^{2+}-releasing mechanism acting as an emergency release valve at high $[Ca^{2+}]_{MT}$ (174). It is important to note that Ca^{2+}-release upon pore opening requires mitochondrial depolarization, which has been observed in stimulated VSMC (141). In cells other than smooth muscle, PTP-mediated Ca^{2+}-release can stimulate ER Ca^{2+}-uptake (36). The molecular nature, regulation and pharmacology of the PTP are a complicated matter more comprehensively reviewed in (174).

1.3.1.3 Outer mitochondrial membrane. The outer mitochondrial membrane (OMM) is sometimes viewed as being freely permeable to Ca^{2+}, but this permeability is mediated via porins, also known as voltage-dependant anion channels (VDAC). Mitochondrial Ca^{2+}-uptake is thought to occur at junctions with the SR/ER and PM, and VDAC preferentially localizes to regions of the OMM closely apposing (<100nm) the ER such that the VDAC expression level limits mitochondrial Ca^{2+}-uptake (174). Numerous pro- and anti-apoptotic proteins, such as members of the Bcl-2 family, also appear to regulate mitochondrial and ER Ca^{2+} transport; however, these proteins will not be discussed due to a lack of information specific to VSM. For general information we suggest the following reference (60).

1.3.2 Interpreting mitochondrial inhibition

The term "mitochondrial inhibitor" is often used to describe any drug that partially or completely collapses the $\Delta\psi_m$, thereby preventing mitochondrial Ca^{2+}-uptake. This term is applied to protonophores and inhibitors of the electron transport chain (ETC). The resulting $\Delta\psi_m$ depolarization can cause F_1F_0-ATPase reversal whereby the hydrolysis of ATP mediates proton pumping to sustain a moderate $\Delta\psi_m$. Accordingly, an F_0-proton channel blocker, oligomycin, is often used to prevent ATPase reversal. ETC complexes influence the oxidation state of metabolite redox pairs and contribute to cellular ROS production; consequently, interpretation of the effects of their inhibition on mitochondrial Ca^{2+}-buffering and $[Ca^{2+}]_i$ signaling warrants caution and suitable controls to account for altered radical production, ATP supply, SR refilling and SR release. Moreover, since mitochondria are thought to contain the oxygen-sensor mediating hypoxic pulmonary vasoconstriction, the majority of studies on mitochondrial radical

production in SMC are based in pulmonary vessels in which regulation of ROS differs from systemic vessels (8;154;251;252).

1.3.2.1 Protonophores & Oligomycin. Protonophores like CCCP and FCCP are the most common agents used to depolarize mitochondria in attempts to prevent mitochondrial Ca^{2+}-uptake. At appropriate concentrations these agents are selective for mitochondrial *versus* plasmalemmal depolarization (127). Again, protonophore-mediated $\Delta\psi_m$ collapse commonly reverses F_1F_0-ATPase, which can alter local [ATP], ATP:ADP ratio, local pH, and sustain some degree of Ca^{2+}-uptake by maintaining a moderate $\Delta\psi_m$ via ATP hydrolysis. Oligomycin prevents these effects, and alone is an effective tool to assess the influence of mitochondrial ATP production on Ca^{2+} signaling mechanisms. Protonophores are sometimes used to "release" mitochondrial Ca^{2+}, but release *per se* is unlikely without some kind of stimulation to open the uniporter or PTP.

In smooth muscle it is unclear whether protonophores selectively inhibit mitochondrial Ca^{2+}-buffering or if the loss of oxidative ATP production also affects SERCA activity. On the one hand, ionic homeostasis in VSM is generally accepted to be sustained by glycolytic ATP production (100;213), and glycolysis has been shown to support sustained vascular contraction (130). Thus glycolysis should also be able to sustain SERCA activity given that SERCA has a higher affinity for ATP than does myosin ATPase (K_d ~2 μM vs. ~50 μM) (65). On the other hand localized [ATP] has not yet been directly recorded, so indirect evidence is used to argue that $\Delta\psi_m$ collapse does not deprive SERCA of ATP. In electrophysiological experiments the typical pipette [ATP] of ~2-5mM is assumed to support SERCA activity (91), which is a reasonable assumption given that maximal SR-filling rate requires only 200μM ATP in permeabilized BHK-21 cells (129). Dialysis with millimolar [ATP] might abolish localized regulation of SERCA by [ATP] microdomains (129), in which case the effects of oligomycin reported in smooth muscle would be consistent with preventing modest mitochondrial Ca^{2+}-buffering through inhibition of F_1F_0-ATPase reversal rather than oligomycin A depriving SERCA of ATP (121). Oligomycin additively inhibited Ca^{2+} clearance on top of FCCP in pulmonary artery SMC (121) and increased Ca^{2+} clearance in femoral artery in a manner consistent with F_0 inhibition causing mitochondrial hyperpolarization (120). While these observations cannot exclude the involvement of mitochondria locally supplying ATP to SERCA, they do indicate that bulk SERCA activity does not explicitly rely on oxidative phosphorylation.

The appropriate application of RU360 could greatly simplify this type of experiment and clarify to what extent $\Delta\psi_m$ collapse affects processes other than mitochondrial Ca^{2+}-uptake.

1.3.2.2 ETC inhibition alters ROS production, redox state and $\Delta\psi_m$. The electron transport chain is central to mitochondrial function. It creates the pH gradient that supports the $\Delta\psi_m$ as a result of complexes I, III and IV pumping protons across the inner mitochondrial membrane (IMM), and it produces oxygen radicals and recycles metabolites essential to aerobic respiration. Inhibition of any one of these complexes can depolarize mitochondria to some extent, while protonophores depolarize $\Delta\psi_m$ without preventing electron transport (48;141;154). The ETC is sometimes divided into the proximal and distal ETC such that complexes I and II are proximal and supply complex III with reduced ubiquinol. Complex I recycles matrix NADH and may be an important regulator of the PTP (75), while complex II recycles glycolytic NADH via the malate-aspartate and glycerol-3-phosphate shuttles. Thus complex II inhibition, perhaps more so than complex I inhibition, could indirectly induce anaerobic respiration by increasing the cytosolic NADH:NAD ratio (8;19). NADH additionally inhibits cADPr-hydrolase thus increasing [cADPr] and promoting SR Ca^{2+}-release (257). None the less, complex I inhibition with rotenone prevented refilling of IP_3-releasable Ca^{2+} stores in cultured VSMC (231). While the underlying mechanism in this case is unclear, it illustrates the need to assess the tissue-specific and inhibitor-specific effects of mitochondrial inhibition in a given preparation. For instance, rotenone and antimycin A increased hydrogen peroxide (H_2O_2) levels in renal artery SMC resulting in voltage-gated K^+-channel (K_V) activation while producing exactly the opposite effect in pulmonary artery SMC (154). In this case the differences are associated with differential expression levels of the ETC complexes. At the same time, complex $III_{b/c}$ and IV inhibition with myxothiazol and cyanide did not alter radical production in pulmonary and renal artery SMC (154). Thus the release of internal Ca^{2+} stores by cyanide in mesenteric artery could illustrate differential control of Ca^{2+} and ROS signaling by specific ETC complexes (251) (but see (65)).

Clearly, "mitochondrial inhibition" refers to complex interventions with multiple effects that should be considered when investigating the role of mitochondria in smooth muscle Ca^{2+} signaling.

1.3.3 Mitochondria buffer Ca^{2+} influx & release

Mitochondria can both accelerate and retard clearance of $[Ca^{2+}]_i$ elevations depending on the cell type being studied (95;170;217). In smooth muscle, mitochondrial depolarization

consistently reduces the rate of cytosolic Ca^{2+} clearance following Ca^{2+} influx across the PM or release from internal stores (65;66;91;118;120;151). These altered kinetics are interpreted as the loss of mitochondrial Ca^{2+}-buffering, which might occur at $[Ca^{2+}]_i$ as low as 300nM (120). In one case, ruthenium red (50-200 μM) mimicked the effect of FCCP on clearance of voltage-gated Ca^{2+}-influx, strongly indicating that $\Delta\psi_m$ collapse inhibited mitochondrial buffering (65). Increased $[Ca^{2+}]_{MT}$ has also been directly observed in response to SR Ca^{2+} release in vascular and nonvascular SMC with indications that the pattern of mitochondrial stimulation could be agonist-specific (65;95;151;160;220). Subtle differences amongst these observations have lead to discordant views on the details of uptake into and efflux from VSM mitochondria and whether or not mitochondria modulate the resting $[Ca^{2+}]_i$ set-point, but there is little doubt that mitochondria do buffer Ca^{2+} in VSM.

1.3.3.1 Uniporter vs. RaM activation. Most of the evidence that uniporter activation depends on high $[Ca^{2+}]$ in PM-MT and ER/SR-MT junctions comes from non-smooth muscle cells (10;55;156;193). Electron micrography has revealed extensive, close association of mitochondria with SR in smooth muscle (164), and mitochondrial Ca^{2+}-uptake in VSM appears to be dependant on localized $[Ca^{2+}]$ elevations in junctional microdomains. Mitochondrial-targeted aequorin in permeabilized A10 SMC was largely insensitive to low concentration (< 1.8μM) Ca^{2+}-buffers if SR release was prevented (160). This illustrates that calcium-induced Ca^{2+}-release, not the global elevation of $[Ca^{2+}]_i$ expected during stimulation, activated mitochondrial Ca^{2+}-uptake (160). In cultured aortic SMC, vasopressin and ATP stimulated similar increases in bulk $[Ca^{2+}]_i$, while ATP produced a much greater response in $[Ca^{2+}]_{MT}$, and in both cases the stimulated $[Ca^{2+}]_i$ plateau was not reflected in $[Ca^{2+}]_{MT}$ (160;220). These finding are consistent with activation of the mUni by focal elevations of $[Ca^{2+}]$ above average $[Ca^{2+}]_i$. They also suggest that the uniporter inactivates in, and is insensitive to, moderate global elevations of $[Ca^{2+}]_i$. As such, changes in average $[Ca^{2+}]_i$ do not necessarily predict changes in $[Ca^{2+}]_{MT}$, and measurement of bulk $[Ca^{2+}]_i$ does not detect the occurrence of elevated cytosolic $[Ca^{2+}]$ microdomains. Mitochondria mediate rapid clearance of high $[Ca^{2+}]_i$ as would be expected for activation of uniporters in close proximity to Ca^{2+} sources in the PM and SR (65;120), but it is less clear how mitochondria-mediated Ca^{2+} clearance can also occur at $[Ca^{2+}]_i \leq 300$ nM (120). This could be explained in several ways: 1) the Ca^{2+} affinity of mUni is significantly lower *in situ*, 2) the initial evoked $[Ca^{2+}]_i$ elevation activates a Ca^{2+}-CaM dependent mechanism that sustains uniporter Ca^{2+}-permeability at low $[Ca^{2+}]$ (56;120), 3) the RaM is

mediating mitochondrial uptake at low $[Ca^{2+}]_i$, or 4) the uniporter is activated by localized Ca^{2+} elevations (such as Ca^{2+} sparks) that are not reflected in bulk $[Ca^{2+}]_i$. The insensitivity of mitochondrial uptake to low microM Ca^{2+} buffers argues against a reduced K_d for the mUni *in situ* (160), while the return of $[Ca^{2+}]_{MT}$ to baseline levels during sustained $[Ca^{2+}]_i$ elevation argues against RaM activation as considered below (120;220). This favors the last explanation (4). Mitochondria have been shown to take up Ca^{2+} in response to near-bye Ca^{2+} sparks (168), but these events were visualized by sub-cellular confocal analysis of $[Ca^{2+}]_i$ and $[Ca^{2+}]_{MT}$ at sub-second temporal resolution, which has not been performed in VSM.

1.3.3.2 Mitochondrial Ca^{2+}-cycling at rest & $[Ca^{2+}]_i$ set-point. In most vascular smooth muscle protonophores (FCCP/CCCP), cyanide and oligomycin or rotenone increase resting $[Ca^{2+}]$ (95;220;231;251), as has also been reported in bladder SMC (127). However, in *Bufo marinus* stomach smooth muscle cyanide does not affect basal $[Ca^{2+}]_i$ (65). Thus it appears that VSMC mitochondria help sustain low $[Ca^{2+}]_i$ by buffering or regulating Ca^{2+}-influx and release (see sections 5 and 6). CGP-37157 and PTP inhibition with cyclosporin A elevated resting $[Ca^{2+}]_{MT}$ in VSMC mitochondria indicating basal Ca^{2+}-uptake and therefore Ca^{2+}-cycling in resting VSMC (Figure 1.6). Similar observations have also been observed in HeLa cells (10). Direct observation of mitochondrial Ca^{2+}-influx at very low $[Ca^{2+}]_i$ implies that either: 1) leak of PM/SR Ca^{2+} creates few, but significant, Ca^{2+} microdomains that permit basal Ca^{2+}-uptake, or 2) that RaM is important for buffering of these basal fluxes. RaM is not inhibited by a $[Ca^{2+}]$ of 100 nM, so a physiological role for RaM in cells with resting $[Ca^{2+}]_i$ near 100 nM is possible. On the other hand, focal Ca^{2+} elevations at resting $[Ca^{2+}]_i$, termed "marks," occur in response to RyR-mediated Ca^{2+} sparks in cardiac myotubes (168). However, the increased resting $[Ca^{2+}]_{MT}$ upon inhibition of the mNCX and PTP does not prove or disprove either mechanism. In addition, removal of extracellular Ca^{2+} decreases resting $[Ca^{2+}]_{MT}$, but this too could result from either reduced SR filling and Ca^{2+} spark frequency or reduced basal $[Ca^{2+}]_i$ (176). Resolution of this issue requires the use of RU360 to specifically inhibit the uniporter.

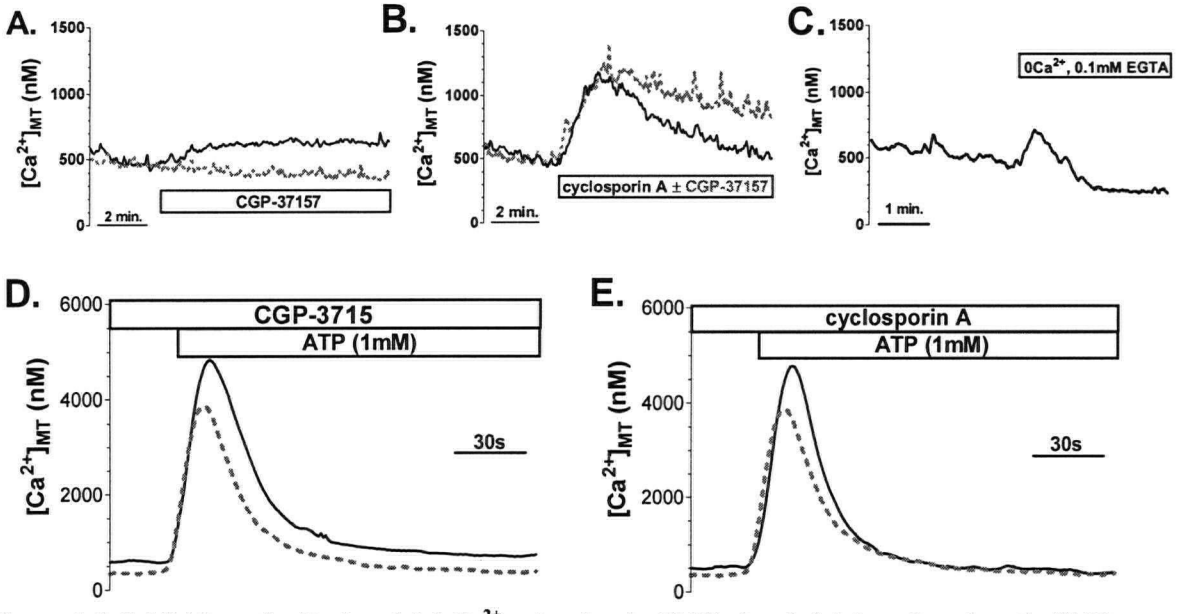

Figure 1.6. Inhibition of mitochondrial Ca^{2+}-extrusion in SMC. (top left) In cultured aortic SMC expressing mito-aequorin, inhibition of the mitochondrial NCX with CGP-37157 (10μM) reveals mitochondrial Ca^{2+} cycling at rest. (top middle) The transient increase in resting $[Ca^{2+}]_{MT}$ upon inhibition of the permeability transition pore with cyclosporin A (CsA, 10μM) is returned to resting levels by the mitoNCX (dotted trace). (top right) Removal of extracellular Ca^{2+} also reduced resting $[Ca^{2+}]_{MT}$. (bottom left) CGP-37157 impaired extrusion of Ca^{2+} from mitochondria in cells stimulated with ATP (1mM) as revealed by the increased peak $[Ca^{2+}]_{MT}$ and a reduced rate of $[Ca^{2+}]_{MT}$ recovery. (bottom right) CsA increased peak stimulated $[Ca^{2+}]_{MT}$ without prolonging recovery, indicating that the PTP mediates mitochondrial Ca^{2+}-release but not extrusion.

1.3.3.3 Kinetics of mitochondrial versus cytosolic Ca^{2+} elevations. Two types of mitochondrial Ca^{2+} responses have been observed with respect to their recovery kinetics in smooth muscle. In pulmonary artery smooth muscle cells Rhod-2, a cationic dye with good mitochondrial selectivity, reported $[Ca^{2+}]_{MT}$ transients that decayed slowly over minutes, long outlasting the cytosolic Ca^{2+} transients (66), whereas in colonic SMC Rhod-2 reported $[Ca^{2+}]_{MT}$ transients decaying with a half-time of 47 seconds (151). Only in the latter study cytosolic Rhod-2 dialyzed from the cell to reduce the likelihood of cytosolic artifacts. In aortic SMC loaded with Mag-fura-2, RyR- and IP_3R-mediated Ca^{2+} release produced $[Ca^{2+}]_{MT}$ elevations that outlasted the cytosolic response by minutes. This time course of decay was suggested to match SR refilling (95). But in cultured aortic SMC, aequorin targeted to the mitochondrial matrix reported transient $[Ca^{2+}]_{MT}$ elevations in response to SR Ca^{2+} release that decayed with half-times of less than one-minute (160;220).

To determine which trend more accurately describes the physiological response we must consider the characteristics of both the Ca^{2+} sensors as well as the experimental methodologies. Without sub-cellular analysis, non-specific localization of fluorescent dyes can confound interpretation. Dispersion of Rhod-2 from depolarized mitochondria is not uncommon, nor is its

nucleolar accumulation. Mag-fura-2 loads into both the mitochondria and SR, and reciprocal $[Ca^{2+}]$ changes within these organelles make it difficult to interpret the kinetics of cell-averaged mag-fura-2 responses. In addition the ultraviolet and or intense laser light used to excite these dyes can produce free radicals that can inhibit proteins of the ETC and alter the activity of SR Ca^{2+} transporters (1). These considerations are discussed at length in a recent review (68). The above reports using fluorescent dyes were performed at room temperature, which can slow Ca^{2+} handling mechanisms (149). In contrast, the aequorin experiments were performed at 37°C and do not require illumination of the cells. Consumption of aequorin in subpopulations of mitochondria could undermine accurate reporting of $[Ca^{2+}]_{MT}$ kinetics. However, we have observed that the kinetics of the agonist-mediated mitochondrial-aequorin response very closely match those of the cytosolic $[Ca^{2+}]$ transient measured with fura-2 up to the onset of the cytosolic plateau at which point the mitochondrial signal continues to fall (see chapter III). The close temporal relationship of the mitochondrial and cytosolic signal indicates that aequorin consumption did not significantly affect the observed mitochondrial kinetics. The similarity of the aequorin and dialyzed Rhod-2 decay half-times points to fast $[Ca^{2+}]_{MT}$ recovery as the more physiological response. In cultured cardiomyocytes, $[Ca^{2+}]_{MT}$ oscillations followed $[Ca^{2+}]_i$ oscillations with a period of ~1 s (196). If VSM mitochondria are also capable of such rapid Ca^{2+} oscillations this would support rapid cycling of Ca^{2+} between the mitochondria and SR, allowing the mitochondria to enhance the apparent SR buffer capacity by facilitating SR refilling.

1.3.4 Mitochondria modulate SR Ca^{2+} release channel gating

Mitochondria mediate multifaceted regulation of SR release channels by buffering local $[Ca^{2+}]$ and controlling local [ATP] and possibly via ROS signaling and cADPr metabolism. RyR and IP_3R are sensitive to cADPr and IP_3/ATP, respectively (25;208), and both channels have separate Ca^{2+}-sensitive activating and inactivating sites. By influencing channel modulators and buffering localized $[Ca^{2+}]_i$, mitochondria can modulate both the Ca^{2+}-sensitivity and the duration of opening of RyR and IP_3R. In various cell types, including VSM, mitochondria affect the frequency and amplitude of sparks (91;168), and regions of ER in close proximity to MT paradoxically exhibit increased rates of ER Ca^{2+} release and reduced ER $[Ca^{2+}]$ depletion upon IP_3R stimulation (10;99). While this later point at first appears paradoxical, the fact that mitochondria facilitate ER refilling may help to explain how mitochondria can both enhance the rate and reduce the extent of ER Ca^{2+} depletion. While these phenomena are at least in part a consequence of diffusional restriction and linked Ca^{2+}-transport at MT-SR junctions (99;176),

few details are known about the specific interactions between mitochondria and SR release channels in SMC. Moreover, reports in SMC rely primarily on altering $[Ca^{2+}]_i$ signaling with pharmacological tools without monitoring subcellular events with confocal microscopy. Thus, these findings are subject to the uncertainties associated with the mitochondrial inhibitors. Below we summarize the available SMC data with reference to recent advances made in other cell types.

VSMC mitochondria appear to regulate Ca^{2+} release events from both IP_3R and RyR that are important in the propagation of oscillating Ca^{2+} waves and the generation of Ca^{2+} sparks (254). In pulmonary and mesenteric artery SMC, moderate inhibition of complex IV increased both spark frequency and amplitude, which translated to increased Ca^{2+}-induced Cl^--current ($I_{Cl(Ca)}$) (133;251). Increased spark frequency could indicate increased $[Ca^{2+}]_{SR}$, increased $[Ca^{2+}]$ near the channel activating site, or Ca^{2+}-sensitization of the RyR (254). Since mitochondrial inhibition is unlikely to increase SR filling (see section VI), it is most likely that moderate complex IV inhibition impedes local mitochondrial Ca^{2+} buffering or increases cytosolic [cADPr] by preventing oxidation of NADH. While the latter explanation is somewhat unorthodox, it is consistent with the fact that further inhibition of complex IV, but not $\Delta\psi_m$ collapse, increased bulk $[Ca^{2+}]_i$ primarily by releasing SR Ca^{2+} (251). An ROS mechanism could also be involved, but in pulmonary and renal arteries cyanide (a complex IV inhibitor) did not alter radical production (154). Thus mitochondria might tonically suppress Ca^{2+} sparks, as seen in H9c2 cardiac myotubes (168), which is consistent with a report that mitochondrial depolarization by activation of mito-K_{ATP} increased $[Ca^{2+}]_i$ in a manner consistent with RyR activation (261). Similarly, depolarization of mitochondria with FCCP slowed the time to peak of caffeine responses in pulmonary artery SMC, consistent with notion that mitochondrial Ca^{2+}-buffering delays Ca^{2+}-mediated RyR-inactivation (66). We propose that these seemingly paradoxical observations illustrate separate mitochondrial mechanisms to modulate cell-wide RyR Ca^{2+}-sensitivity and site-specific Ca^{2+}-mediated RyR inhibition. In addition, mitochondrial regulation of SR filling creates an indirect mechanism by which mitochondria can influence RyR activity.

Regulation of IP_3R by mitochondria has been reported in colonic, but not yet vascular, smooth muscle (151). CCCP caused progressive loss of IP_3-mediated $[Ca^{2+}]_i$ transients, and oligomycin did not alter the effect of CCCP. This indicates that loss of oxidative-ATP production did not account for the effect of CCCP despite suggestions of IP_3R sensitivity to [ATP] (129). Gross depletion of SR Ca^{2+} stores was not observed, thus CCCP was assumed to

prevent mitochondrial Ca^{2+} buffering near IP_3R resulting in greater Ca^{2+}-mediated inactivation of the release channels. As discussed below, several mitochondrial inhibitors also impaired adrenergicaly-driven oscillating $[Ca^{2+}]_i$ waves, which presumably require Ca^{2+} release from IP_3R (217). However, it was not directly demonstrated that the effects of the $[Ca^{2+}]_i$ signals were directly due to mitochondrial modulation of IP_3R gating.

The above studies clearly illustrate that mitochondrial Ca^{2+}-buffering is important for physiological RyR and IP_3R mediated Ca^{2+} signaling, but many details remain to be described.

1.3.5 Mitochondrial modulation of PM channels

Mitochondria modulate the activity of plasmalemmal ion channels such as CRAC channels, store-operated channels (SOCs), voltage-gated calcium channels (VGCC), Ca^{2+}-activated K^+-channels (K_{Ca}) and Ca^{2+}-activated Cl^--channels (Cl_{Ca}) by buffering local Ca^{2+} gradients (106;146;147;156;226). Varying degrees of evidence support mitochondrial regulation of PM ion channels in VSM, which can indirectly affect SR refilling (and consequently SR release) and global Ca^{2+} signaling.

Calcium-activated K^+-channels and Cl_{Ca} are essential to the regulation of vascular tone in many small blood vessels, and are primarily activated by Ca^{2+} sparks from SR elements in close proximity to the PM (254). In endothelial cells, Mali *et al.* elegantly showed that mitochondria situated in close proximity to large-conductance K^+-channels (BK_{Ca}) reduced channel activation by buffering Ca^{2+} sparks (146), and similar findings are observed in SMC. In pulmonary and coronary artery, mitochondrial depolarization increases BK_{Ca} open probability up to nine-fold by enhancing the diffusion of Ca^{2+} released by the SR toward BK_{Ca} (126;261). Moreover, stimulation of SR Ca^{2+} release in aortic SMC with caffeine can activate both K_{Ca} and Cl_{Ca}, and the observation that FCCP alters the ratio of Cl^- *versus* K^+-channels open at any demonstrates the complexity of mitochondrial regulation of the spatio-temporal profile of sub-plasmalemmal $[Ca^{2+}]$ gradients (95). While mitochondria acutely buffer the SR Ca^{2+} release or influx through VGGC that activates K_{Ca} and Cl_{Ca} (91), they also facilitate the refilling of the SR that is required to sustain the generation of sparks (section 7). In cultured aortic SMC, in which voltage-gated Ca^{2+} influx plays a minor role in contractile regulation, we observed only modest $[Ca^{2+}]_{MT}$ increases upon depolarization with 80mM K^+ and no effect of nifedipine on basal $[Ca^{2+}]_{MT}$ (unpublished observations– Poburko & van Breemen). Paradoxically, in pulmonary artery, mitochondrial inhibition with cyanide increased spark and stic frequency (251). These findings highlight the heterogeneity of mitochondrial regulation of $[Ca^{2+}]_i$ throughout the vascular tree,

and caution against extrapolation of findings between functionally different vessels. However, we must also acknowledge mechanistic differences between protonophores and cyanide. Though speculative, current results are consistent with the proposition that cyanide alters [cADPr], while CCCP inhibits mitochondrial Ca^{2+}-buffering.

In several cell types, mitochondria promote store-operated Ca^{2+} entry (SOCE) by preventing Ca^{2+}-mediated channel inactivation (106;147;169;226), but current evidence in VSM provides few conclusions. One study in VSMC, mitochondria buffered SOCE but did not directly affect the gating of SOC according to Mn^{2+}-quench in Ca^{2+}-free solution (121). Here it is important to consider that SOCs may not be permeable to Mn^{2+}. In VSM, store-depletion can also cause Ca^{2+}-influx via reversal of the plasmalemmal NCX secondary to Na^{+}-entry through ROC/SOC (134), and studies in cultured SMC indicate a functional linkage between the mitochondria and NCX via regulation of SR-Ca^{2+} extrusion (220). As discussed in chapter III, NCX reversal can directly stimulate mitochondrial Ca^{2+}-uptake, which but the physiological relevance of this is not yet clear.

1.3.6 Mitochondria facilitate SR refilling

In addition to promoting opening of SOCE pathways, mitochondria facilitate refilling of SR Ca^{2+}-stores (10;79;106;147;169;226). Direct measurement of $[Ca^{2+}]_{MT}$ and $[Ca^{2+}]_{ER}$ in HeLa has shown mitochondrial Ca^{2+} extrusion via mNCX to be crucial for refilling of the ER (10;147). At the same time, localized regulation of [ATP] or ATP:ADP ratio may also be important for SERCA activity (129). As mentioned previously, in permeabilized cells the maximal rate of ER–refilling is achieved at only 200μM ATP, and FCCP does not affect this process. In intact cells, however, FCCP or oligomycin can dramatically inhibit SR refilling (129). Half-maximal SERCA ATPase activity is reported to occur at 335 nm Ca^{2+}, and SERCA exposed to resting $[Ca^{2+}]_i$ near 100nM may operate at only 30% of maximal capacity (16). Thus, it is tempting to postulate that mNCX and SERCA co-localize at MT-SR junctions where elevated $[Ca^{2+}]$ would increase SERCA activity and the rate of SR-refilling. Furthermore, the plasmalemmal Na^{+}/K^{+}-ATPase is believed to utilize a compartmentalized ATP supply (100), thus it is conceivable that SERCA could be driven by ATP from closely juxtaposed mitochondria.

In cerebral and femoral artery SMC, recovery from $[Ca^{2+}]_i$ elevations occurs in three stages. FCCP abolishes the fast first stage and latent third stage, such that clearance becomes monotonic. Presumably, this monotinic clearance is mediated by the PMCA and NCX, as SERCA blockade does not affect the first or second phase. SERCA blockade does however

abolish the third stage, typically occurring at $[Ca^{2+}]_i$ <300nM (119;120). Susceptibility of the third stage to both FCCP and SERCA reflects an interrelationship between SERCA and mitochondrial Ca^{2+}-uptake, whether by directed Ca^{2+} transfer toward SERCA or by Ca^{2+}-stimulated mitochondrial ATP production. The former mechanism is supported by reports of CCCP abolishing stics in rabbit portal vein in a manner consistent with depletion of SR-Ca^{2+} and abolition of Ca^{2+} sparks (92). An earlier study in cultured VSMC, which employed calcium green and mag-fura-2 to simultaneously measure $[Ca^{2+}]_i$, $[Ca^{2+}]_{SR}$ and $[Ca^{2+}]_{MT}$, also indicated that mitochondria facilitate SR-refilling. In this case, FCCP reduced the peak $[Ca^{2+}]_i$ response to caffeine, retarded $[Ca^{2+}]_i$ clearance and appeared to prevent recovery of $[Ca^{2+}]_{SR}$ subsequent to stimulation (95). Together, these reports strongly support a mitochondrial role in SR refilling in vascular smooth muscle, and mechanisms described in other cell types set the stage for future studies employing confocal microscopy and agents like CGP-37157 to further elucidate the underlying mechanisms.

1.3.7 Mitochondria influence Ca^{2+} oscillations

Oscillations of $[Ca^{2+}]_i$ are an important signaling modality in VSM (133). Repetitive intracellular wave-like Ca^{2+}-oscillation are usually driven by ER/SR Ca^{2+}-release, whereas PM Ca^{2+} influx is more important in repetitive spatially uniform transient rises in $[Ca^{2+}]_i$. Cytosolic $[Ca^{2+}]$ oscillations result in mitochondrial $[Ca^{2+}]$ oscillations in VSMC (66), non-vascular SMC (78) and other cells (29;195;196;245), where the oscillations rely upon close ER-MT coupling. The $[Ca^{2+}]_{MT}$ oscillations are also associated with temporally-coupled oscillations in [NADH] via stimulation of intra-mitochondrial dehydrogenases that are regulated by the frequency of Ca^{2+} oscillations (195). Thus, mitochondrial metabolism appears to depend on repetitive SR/ER Ca^{2+} release.

Just as $[Ca^{2+}]_i$ oscillations modulate mitochondria, mitochondria also modulate $[Ca^{2+}]_i$ oscillations. In preparations like rat tail artery VSMC that exhibit asynchronous SR-mediated wave-like $[Ca^{2+}]_i$ oscillations, mitochondrial inhibitors (rotenone, FCCP, ruthenium red, cyanide, antimycin-A, dinitrophenol) increased the frequency and decreased the amplitude of $[Ca^{2+}]_i$ oscillations (217;269). This modulatory role for mitochondria Ca^{2+} oscillations in vascular smooth muscle contrasts with observations in chromaffin cells, where mitochondria provide a Ca^{2+} buffer barrier that limits the spread of oscillatory Ca^{2+}-waves (170). Recent evidence further suggests that differences in mitochondrial Ca^{2+} buffering underlie the differences in propagation of Ca^{2+} cytosolic Ca^{2+} waves in ventricular versus atrial cardiomyocytes (204).

Results obtained in hepatocytes and HeLa cells shed some light on why mitochondrial inhibition reduces the amplitude while increasing the frequency of Ca^{2+}-oscillations in VSMC. In hepatocytes, mitochondria decrease the apparent IP_3-sensitivity of nearby IP_3R, and regions of ER not in close contact with mitochondria exhibit reduced rates of ER-release and more extensive $[Ca^{2+}]_{ER}$ depletion (10;40;99). At a constant $[IP_3]_i$ the activation of the IP_3R depends on the local $[Ca^{2+}]_i$ generated by spontaneous SR Ca^{2+}-release and loss of mitochondrial Ca^{2+}-buffering increases $[Ca^{2+}]_i$ during the troughs between oscillations. This reduces the time required to achieve the threshold $[Ca^{2+}]$ for IP_3R activation and thus shortens the interval between the transients. At the same time Ca^{2+}-release from IP_3R more rapidly reaches inhibitory concentrations (IC_{50} ~250 nm for type 1 IP_3R) thus shortening the time to peak of the transients. The combined effect will be an increase in the frequency of Ca^{2+} oscillations. In addition, impaired mitochondrial refilling of the SR coupled with the reduced inter-wave period would result in relative depletion of the SR, which may contribute to the reduced Ca^{2+}-wave amplitude following mitochondrial inhibition.

1.3.8 Mitochondrial ROS production , O_2 detection

Reactive oxygen species are important signaling molecules in VSM acting via a multitude of mechanisms (143;186;253;258;259), and mitochondrial ROS are important physiological regulators of $[Ca^{2+}]_i$ signaling (43;143;186;253). This is especially true in pulmonary artery SMC where mitochondria are believed to contain the oxygen sensor underlying hypoxic pulmonary vasoconstriction (reviewed in (8)). The effects of ROS on smooth muscle K^+-channels and SR Ca^{2+} stores are discussed in recent reviews (143;186;253). The prominent radical produced by mitochondria is super oxide (O_2^-), generated primarily at complex III and I (82;130;186;253)Superoxide dismutase converts O_2^- to H_2O_2, which can activate phospholipase A, phospholipase-C γ, increase cADPr levels, release intracellular Ca^{2+} stores and activate voltage-gated and Ca^{2+}-activated K^+-channels (86;154;211;257). Enhanced O_2^- formation can also increase conversion of mitochondrial NO into reactive peroxynitrites that affect Ca^{2+} handling and energy homeostasis (180).

Rotenone and myxothiazol, but not CN, attenuated flow-induced radical production and dilation of coronary resistance vessels (139). Since coronary VSMC originate from different precursor cells than most VSMC, these vessels might exhibit Ca^{2+} signaling mechanisms unique from other vessels (144). For example, (246) in renal artery SMC, rotenone and antimycin A increased $[H_2O_2]$ and stimulated dilatory K_V currents, while the opposite occurred in pulmonary artery. Myxothiazol and CN had no effect in either tissue (154), yet others report that CN

increases [Ca^{2+}] in both pulmonary and mesenteric arteries (251). Clearly, radical-mediated signaling qualitatively differs between systemic and pulmonary vessels. Inhibition of complex I, II and III tends to alter radical production, while complex IV inhibition causes effects more consistent with NADH:NAD regulation. These data offer a glimpse at the integration of ROS and Ca^{2+} signaling mechanisms, and illustrates the need to characterize the specific details of these mechanisms in any given preparation.

1.3.9 Summary of mitochondria & Ca^{2+} signaling

Mitochondria are integral to Ca^{2+}-transport, ROS production and metabolite recycling in VSM, and these three systems are amalgamated in the orchestration of Ca^{2+} signaling that is central to physiologically regulation of blood flow. By buffering Ca^{2+}-elevations in cytoplasmic microdomains mitochondria can modulate Ca^{2+}-mediated activation and inactivation of ion channels underlying control of membrane potential in resistance vessels and oscillatory SR Ca^{2+}-release in larger conduit vessels, while rapid Ca^{2+}-cycling between mitochondria and the SR effectively permits the mitochondria to extend the SR-buffering capacity. At a more cell wide level, modulation of membrane potential and second messenger pathways by mitochondrial ROS permits the vascular response to regional oxygen supply to be superimposed on responses to paracrine and endocrine factors and physical factors such as pressure and flow. Moreover, oxygen and metabolic substrates co-regulate recycling of metabolic intermediates and the cellular redox potential through both mitochondrial and cytosolic mechanisms from which the consequent modulation of NADH:NAD and ATP:ADP can alter second messenger metabolism and ion channel gating. These mechanisms place mitochondria at the cross-roads of VMS Ca^{2+} signaling and reconcile otherwise discordant observations in the VSM literature. However, this remains a working model and many of the details remain to be investigated.

1.4 PURPOSE AND SPECIFIC AIMS

To better understand Ca^{2+} homeostasis in vascular smooth muscle, I studied Ca^{2+} movements and protein localization in cultured rat aorta cells using a variety of techniques. I had 3 specific aims.

- To determine the basic mechanism of the Ca^{2+} leak and to estimate the molar flux of this basal Ca^{2+} entry, I:
  - optimized conditions for the specific measurement of $^{45}Ca^{2+}$ uptake into resting cells.
  - screened a series of pharmacological agents for their effect on the basal rate of Ca^{2+} influx.
  - estimated the average volume of the cultured cells. This was accomplished by capturing images of cells expressing SNAP-25 targeted GFP (targeting the plasma membrane), deconvolving the image stacks, and reconstructing the cell volumes.
  - determined whether these particular cells expressed L-type voltage-gated channels, and canonical transient receptor potential (TRPC1-7) proteins.
- To characterize the interaction of the plasmalemmal Na^+/Ca^{2+}-exchanger and mitochondria and to determine whether peripherally localized mitochondria contribute to the superficial buffer barrier in vascular smooth muscle cells, I:
  - transfected cells with aequorin targeted to the mitochondrial matrix (or inner leaflet of the PM) to directly measure mitochondrial (or sub-plasmalemmal) Ca^{2+} levels upon reversal of the Na^+/Ca^{2+}-exchanger.
  - performed parallel fura-2 experiments to measure changes in bulk $[Ca^{2+}]_i$ in the same smooth muscle cell line.
- To dissect the relative contributions of inositol-1,4,5-trisphosphate receptors (IP_3R) and ryanodine receptors (RyR) to agonist-mediated mitochondrial $[Ca^{2+}]$ elevations, and to determine whether IP_3R and RyR stimulated separate populations of mitochondria, I:
  - measured the effect of pharmacological inhibition IP_3R and RyR on the ATP-mediated and $[ARG^8]$-vasopressin-mediated $[Ca^{2+}]_{MT}$ elevations reported by aequorin targeted to the mitochondria.
  - determined whether two separate agonists consumed aequorin from individual or overlapping populations of mitochondria.
  - measured the effect of pharmacological inhibition IP_3R and RyR on the ATP-mediated cytosolic $[Ca^{2+}]_{MT}$ elevations reported by untargeted inverse-pericams.

- semi-quantitatively analyzed the spatial relationships of immuno-fluorescently labelled IP_3R and RyR and GFP-labeled mitochondria using digital reconstruction of deconvolved images acquired by confocal microscopy.

CHAPTER II
Basal Ca^{2+} entry in vascular smooth muscle cells[3]

2.1 INTRODUCTION

Described in smooth muscle 30 years ago, the phenomenon of basal calcium entry has received little attention especially in smooth muscle cells, where it plays a substantial role in resting calcium homeostasis and the maintenance of vascular tone (71;166;236). For example exposure of "resting" cells to Ca^{2+} free ambient solution causes a loss of sarcoplasmic reticulum Ca^{2+} content. This is due to leakage of Ca^{2+} from the sarcoplasmic reticulum (40), and sarcoplasmic reticulum Ca^{2+} can be restored upon replenishment of Ca^{2+} without the development of force (42;62). Conversely blockade of Ca^{2+} extrusion in the presence of extracellular Ca^{2+} leads to a net gain in cellular Ca^{2+}. Thus it has long been clear that the inactive smooth muscle is not static with respect to Ca^{2+} metabolism, but supports continuous physiological cycling of Ca^{2+} between the intra and extracellular compartments. While it is generally accepted that efflux is mediated by the plasma membrane Ca^{2+}-ATPase and the Na^{+}/Ca^{2+}-exchanger we have little knowledge to date regarding the components of the resting Ca^{2+} influx (166;240). The objective of this investigation is therefore to characterize the nature of Ca^{2+} transport across the plasma membrane of non-stimulated smooth muscle cells.

Three different techniques are commonly employed for the measurement of cellular Ca^{2+} fluxes: 1) imaging of fluorescent Ca^{2+} indicators, 2) patch clamp electrophysiology and 3) radioactive tracer analysis, each of which has several advantages and disadvantages. While fluorescent Ca^{2+} indicators have allowed us to investigate Ca^{2+} signalling at the subcellular level with high temporal and spatial resolution (198), this technique is not suited to measurement of resting Ca^{2+} influx because fluorescent measurements do not differentiate between intra and extracellular sources of Ca^{2+}. This is a complicating issue since release of intracellular Ca^{2+} stores often activates capacitative calcium entry through store-operated channels. Electrophysiology is an invaluable tool that has provided great insight into the nature of ion channel behaviour. While the technique is capable of detecting tiny single channel currents of spontaneous channel activity, it is unable to detect electro-neutral transport as seen in some ion-exchange mechanisms. Additionally, the leak current associated with the patch seal is difficult to adequately distinguish from resting Ca^{2+} influx. The third method for measuring Ca^{2+} influx is to

[3] A version of this chapter has been published as: Poburko D, Lhote P, Szado T, Behra T, Rahimian R, McManus B, van Breemen C, Ruegg UT. (2004) Basal calcium entry in vascular smooth muscle. **European Journal of Pharmacology.** 505 (1-3): 19-29.

label the calcium of the bathing solution with $^{45}Ca^{2+}$ and measure the cellular uptake of radioactive label. This method is theoretically the most direct, but is subject to two drawbacks. First, its temporal resolution is relatively poor and therefore sub-optimal for measurement of stimulated Ca^{2+} fluxes. Second, a background signal is generated by non-specific adsorption of $^{45}Ca^{2+}$ to sites within the extracellular space as previously described (71). Nevertheless we chose this third method as the most likely to provide direct information on the nature of basal Ca^{2+} entry in monolayers of cultured smooth muscle cells, a preparation that lends itself well to removal of extracellular radioactive label. In addition the fact that net non-stimulated Ca^{2+} fluxes have a relatively slow time course reduces the requirement for high temporal resolution in these experiments.

Given that pure lipid bilayers are not inherently leaky to inorganic ions, several mechanisms have been proposed to account for the resting Ca^{2+} permeability of physiological membranes (39;232). The first possibility is that imperfect junctions between phospholipid domains and membrane proteins are permeable to small ions. Second, pinocytosis may bring significant amounts of calcium into the cell, considering the ~10,000-fold difference between extracellular and intracellular Ca^{2+} concentration (89). Third, excitable Ca^{2+}-permeable membrane channels may exhibit a degree of basal activity, or flickering, and thereby contribute to basal calcium influx (165). Our results provide experimental support for the latter hypothesis, and reveal the complexity and importance of the phenomenon of basal calcium entry.

2.2 METHODS

2.2.1 Cultures of smooth muscle cells. Rat aortic smooth muscle cells were previously prepared from aortae of male Wistar Kyoto rats (200-300g) as described elsewhere (140). Cells were cultured in Dulbecco's Modified Eagles Medium supplemented with essential and non-essential amino acids, vitamins, 0.001% ciproxin and 10% fetal calf serum, and kept at 37°C in a humidified atmosphere of 5% CO_2 in air. Cells were seeded at 20,000 cells (between passages 6 and 11) per 16 mm diameter culture well and grown to confluence (ca. 400,000 cells per well) for 7 to 9 days. .

2.2.2 $^{45}Ca^{2+}$ influx measurement. $^{45}Ca^{2+}$ uptake was recorded as previously described with minor modifications (140). After two washes in physiological salt solution (physiological saline solution, in mM: NaCl 145, KCl 5, $MgCl_2$ 1, Hepes [4-(2-hydroxyethyl)piperazine-1-ethanesulfonic acid] 5, glucose 10 and $CaCl_2$ 1.2, pH 7.6), the cellular monolayers were pre-

incubated at 37°C for 15 min (20 min when 2-APB (2-aminoethoxy-diphenylborate) was used) in 200 µl physiological saline solution containing the inhibitors. Twenty micro-liters of $^{45}Ca^{2+}$ at 0.02 mCi/ml were added to this solution and cells were incubated for 10 min at 37°C, or as specifically indicated. Influx was stopped by washing the cells 4 times at 0.5 min intervals with 0.5 ml of ice-cold 3 mM $LaCl_3$ or 0.2 mM EGTA (ethylene glycol-bis(2-aminoethylether)-N,N,N¢,N¢-tetraacetic acid) in physiological saline solution without calcium, and cells were detached with 50 µl of physiological saline solution containing trypsin (0.25%), EDTA (ethylenediaminetetraacetic acid, 0.1%) and lysed with 250 µl of SDS (sodium dodecyl sulfate, 1%). Radioactivity in the lysates was assessed by scintillation counting (Ultima Gold™, Packard, Groningen, NL, and LKB Wallac 1217 Rackbeta™, Turku, Finland). See Appendix I for conversion of cpm to moles of $^{45}Ca^{2+}$.

2.2.3 Curve fitting: 1. Wash out kinetics: Extracellular tracer was removed by sequential washes of the cells at times denoted in Fig. 2.1. We subtracted the sum of cpm collected in washes previous to each point from the sum of cpm in all washes collected and in the final cell lysate. This treatment depicts the $^{45}Ca^{2+}$ activity present in the wells immediately prior to each wash. These values were fitted to a single exponential decay using GraphPad Prism 3.0 to determine the rate of tracer removal. *2. Uptake kinetics:* An initial fast component was observed in the raw uptake data. The magnitude of this component was estimated by back extrapolation of the curve to time zero based on the assumption that the rate of uptake would be relatively constant during the first three minutes of influx. Linear regression of these data points (0.5 - 3.0 min) indicated a y-intercept of 96 ± 12 cpm/well. This rapid uptake occurred within the first 30 seconds of exposure and was subtracted from each data point. The corrected data set was fitted to a single exponential association using GraphPad Prism 3.0. *3. Curve Peeling:* Visual inspection of the gadolinium (Gd^{3+}) concentration-response relationship suggested that Gd^{3+} had a biphasic effect but overlapping concentration-response relationships. GraphPad Prism does not contain an equation to fit such a curve or to estimate the parameters of these two effects (pIC_{50}, Hill slope, and magnitude) and to peel the two curves apart. We wrote an equation describing the sum of two sigmoid curves such that the top of the combined curve would be the sum of the two separate curves each with a bottom equal to zero and each with independent IC_{50}s and Hill slopes. The equation is shown below:

$$Y = 2*\text{Bottom} + \frac{(\text{T1-bottom})}{(1+10^{\wedge((\text{LogIC}_{50\text{-}1}-X)*\text{Hill Slope1})})} + \frac{(\text{Top-T1-bottom})}{(1+10^{\wedge((\text{LogIC}_{50\text{-}2}-X)*\text{Hill Slope2})})}$$

Top-T1 is the top of the second curve. Using GraphPad Prism, the experimental data were fitted to this equation to estimate the individual curve parameters with the initial values set based on visual inspection of the raw data: Bottom = 0, T1 = 70%, Top = 100%, Log($IC_{50\text{-}1}$) = -6.0, Log($IC_{50\text{-}2}$) = -3.0, and Hill slope(1and2) = -1.0. The individual curves were then simulated from the best-fit parameters (dotted curves, Fig. 2.4).

2.2.4 Confocal microscopy and 3-D reconstruction: Cells were transfected with a plasmid encoding a green fluorescent protein (GFP) construct that is targeted to the inner leaf of the plasmalemma with a SNAP-25 pre-sequence (148). Using an Olympus BX50WI microscope fitted with an Ultraview Nipkow confocal disk (Perkin-Elmer, location), z-series of images were captured with a 60x water-dipping lens (numerical aperture 0.90) at 200 nm intervals (Prior H128 motor drive). Image stacks were deconvolved using a Nipkow-optimized classic maximum likelihood estimation algorithm (Huygens, Scientific Volume Imaging, Netherlands). We then reconstructed the image stacks into 3-dimensional volumes with Imaris 3.3 (Bitplane, Zurich, Switzerland) and estimated cell volume with the Surpass function using a voxel size of 0.24 x 0.24 x 0.20 μm (Fig. 2.3b).

2.2.5 RNA extraction: Total cellular RNA from low- and high- confluent rat aortic smooth muscle cell lysates were extracted using a RNeasy mini kit™ (Quiagen) according to manufacturer's instructions. RNA was quantified by measuring absorbance spectrophotometrically at 260 nm, and its integrity was assessed after electrophoresis in non-denaturating 1% agarose gels stained with ethidium bromide.

2.2.6 Semi-quantitative RT-PCR: Reverse transcription of 5 μg total RNA was performed in 60 μl reaction volumes containing 200 units of Superscript II™ reverse transcriptase, 60 units RNase inhibitor, 3 mM $MgCl_2$, 1× Buffer II (Sigma) and 0.3 μg of random primers and 1 mM dNTP for 50 min at 42°C. Contaminating genomic DNA present in the RNA preparations was removed by digesting the reaction with 5 units of DNase I for 45 min at 37°C prior to the addition of reverse transcriptase. RT product (5 μl) was used in each 100 μl PCR

reaction. The PCR mixture contained 250 μM dNTP, 2 mM $MgCl_2$, 1× volume of Buffer and 2.5 units Hotstar™ Taq polymerase, and 1 μl of forward and 1 μl of reverse primers. Amplification consisted of 40 cycles of 1 min at 94°C, 1 min at 55°C and 1 min at 72°C. The final extension was completed at 72°C for 7 min. Ten μl of 6× loading buffer (containing 0.25% bromothymol blue, 0.25% xylene cyanol FF, and 15% Ficoll type 400 (Pharmacia) in distilled water treated with DEPC (diethyl pyrocarbonate)) was added to the PCR products. Twenty μl of PCR products were then analyzed by electrophoresis on 2% agarose gels stained with ethidium bromide and gels were photographed under ultraviolet light. 18S ribosomal RNA expression was used as an internal control. The exemplary gels shown in this report (fig. 2.6) represent findings from a minimum of six different low confluency and four high confluency lysates. Rat brain mRNA was used as a positive control for the expression of TrpC1, 2, 3, 4, 5, 6, 7. Primers used for different amplifications were designed from published reports (152;247) or sequences available in Genebank (Table 2.1). RT-PCR (reverse transcriptase polymerase chain reaction) reactions run in the absence of reverse transcriptase or cDNA were used as negative controls (data not shown). Amplified PCR products from cell lysates were isolated from agarose gel, sequenced and found to be 100% identical to the authentic sequences of rat TrpC1-7.

2.2.7 Data analysis: Results are presented as the means of at least three independent experiments with vertical bars indicating standard error (S.E.). IC_{50} values were calculated by non-linear regression using GraphPad Prism 3.0 (GraphPad Software, San Diego, USA). Statistical evaluation was performed using one-way analysis of variance (ANOVA) followed by Bonferroni or Dunnett post-tests. Differences with a value of $P < 0.05$ were considered significant.

2.2.8 Materials: Unless specified otherwise drugs and chemicals were purchased from Sigma Aldrich, Switzerland. 2-APB was purchased from Fluka, Switzerland. Ultima Gold™ scintillation cocktail was purchased from Packard, Groningen, NL, and isotopic $^{45}Ca^{2+}$ was purchased from NEN Life Sciences Products, Geneva. SuperscriptII™ reverse transcriptase, RNase inhibitor and random primers were obtained from Gibco/BRL, Canada. Buffer II (10×) was obtained from Sigma/Aldrich, Canada. $MgCl_2$, dNTP, 10x volume PCR Buffer, Hotstar™ Taq polymerase and RNeasy mini kit™ were purchased from Qiagen, Canada. Primers for ribosomal RNA (18S) and RNAseZap were purchased from Ambion Inc., TX, USA.

2.3. RESULTS

2.3.1 Washout of extracellularly bound tracer Ca^{2+}: Figure 2.1 illustrates the process of washing out the surface bound $^{45}Ca^{2+}$ from the culture wells as described in the methods. The $^{45}Ca^{2+}$ content of the cellular monolayer falls initially very rapidly when exposed to ice cold solutions containing either La^{3+} (3 mM) or EGTA (0.2 mM) and then stabilizes with a very slow decay. It appeared that the displacement of $^{45}Ca^{2+}$ by La^{3+} ($k = 3.113 \pm 0.077$) was not appreciably faster than chelation by EGTA ($k = 3.323 \pm 0.112$). However, it is known that high concentrations of La^{3+} block Ca^{2+} extrusion (238), and this is most probably the reason for the significantly higher plateau following La^{3+} washes ($5.28 \times 10^3 \pm 0.12 \times 10^3$ cpm·well^{-1}) than when cells were washed with EGTA ($4.46 \times 10^3 \pm 0.22 \times 10^3$ cpm·well^{-1}). On the basis of these results we subsequently use two minutes of washing with ice-cold La^{3+} solution to remove $^{45}Ca^{2+}$ from the wells and outer cell surfaces, thereby permitting the determination of $^{45}Ca^{2+}$ uptake into the cells.

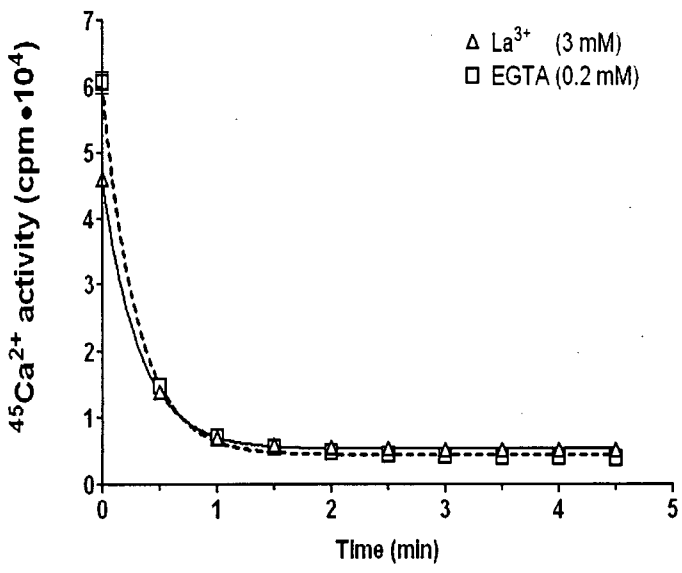

Figure 2.1. Optimizing washout of excess tracer. At each time point cells were washed with 0.5 ml ice-cold physiological saline solution containing $LaCl_3$ (3 mM) or EGTA (0.2 mM). $^{45}Ca^{2+}$ activity in the well at each time point was determined by subtracting the sum of $^{45}Ca^{2+}$ activity collected in previous 1 ml washes from the total $^{45}Ca^{2+}$ collected in all washes plus the cell lysate. The t_0 point indicates the total $^{45}Ca^{2+}$ activity loaded onto the cells Wash out is best fitted by single exponential decay. Wash out with $LaCl_3$ was described by $k = 3.11 \pm 0.08$ min^{-1} and plateau = $5.28 \pm 0.12 \times 10^3$ cpm·well^{-1}. Wash out with EGTA was described by $k = 3.32 \pm 0.11$ min^{-1} and plateau = $4.46 \pm 0.22 \times 10^3$ cpm·well^{-1}. Given the equivalent rates of tracer removal using EGTA or $LaCl_3$, $LaCl_3$ was chosen as the superior washing agent in that it resulted in a higher plateau than EGTA.

2.3.2 Rate of basal Ca^{2+} influx: The SMC were exposed to $^{45}Ca^{2+}$-labelled physiological saline solution (3.9×10^4 cpm·well^{-1} in 0.22 ml) for various times before washout of the surface bound label followed by scintillation counting of cell lysates. Close inspection of the curve revealed an initial very fast component of 96 ± 12 cpm·well^{-1} that was determined by back extrapolation of the linear portion of the curve. This was followed by a mono-exponential component reaching a steady state of $1.92 \times 10^3 \pm 0.04 \times 10^3$ cpm·well^{-1} after about 60 min (see methods). The size of the initial fast component increased considerably when the time period of the cold lanthanum (La^{3+}) incubation was decreased to 30 sec (data not shown). This strongly indicated that the fast phase was due to extracellular binding of tracer, so it was subtracted from the curve. The corrected uptake of $^{45}Ca^{2+}$ into the cells (Figure. 2.2) is best fitted to a single exponential process with a rate constant of 0.084 ± 0.005 cpm·min^{-1}. This suggests that, at rest, permeation through the plasma membrane is rate limiting. For the purpose of obtaining highly reproducible measurements of resting Ca^{2+} influx in the presence of a variety of Ca^{2+} transport inhibitors we exposed cells to $^{45}Ca^{2+}$ for 10 min after pre-incubation in absence or presence of inhibitors before washing with cold La^{3+} solution. Cells were exposed to a $[^{45}Ca^{2+}]_{tracer}$ of ~ 0.12 nM in a 1.2 mM solution of $^{40}Ca^{2+}$ resulting in a $^{45}Ca^{2+}$:$^{40}Ca^{2+}$ ratio of 9.7×10^6. The initial rate of tracer influx is approximated by the slope or first derivative of the exponential uptake curve at time 0 (Figure. 2.2). This is equal to Y_{max} (plateau) multiplied by the rate constant (k) giving an instantaneous influx rate of 161 cpm·min^{-1}, which was then converted to moles of $^{45}Ca^{2+}$-labeled Ca^{2+} (see Appendix I). This conversion gives the instantaneous influx rate of $^{45}Ca^{2+}$, and the rate of $^{40}Ca^{2+}$ influx was assumed to be proportional to the ratio of $^{40}Ca^{2+}$: $^{45}Ca^{2+}$ in the tracer solution. We estimate the instantaneous influx of Ca^{2+} into the SMC to be 5.9×10^{14} Ca^{2+}·min^{-1}·well^{-1}. Each well contained an average of 4.0×10^5 cells, so cellular Ca^{2+} influx was approximately 1.5×10^9 Ca^{2+}·cell^{-1}·min^{-1}. The average volume of 14 cells from 3 individual experiments was calculated to be 9.6 ± 1.2 picolitres (volumes ranged from 3.6 to 15.8 picolitres) (Figure 2.3). Therefore, we estimate the molar minute influx of Ca^{2+} in our cultured smooth muscle cells to be on the order of 2.5×10^{-4} M·min^{-1}, which corresponds to a whole cell current of approximately 7.5 pA.

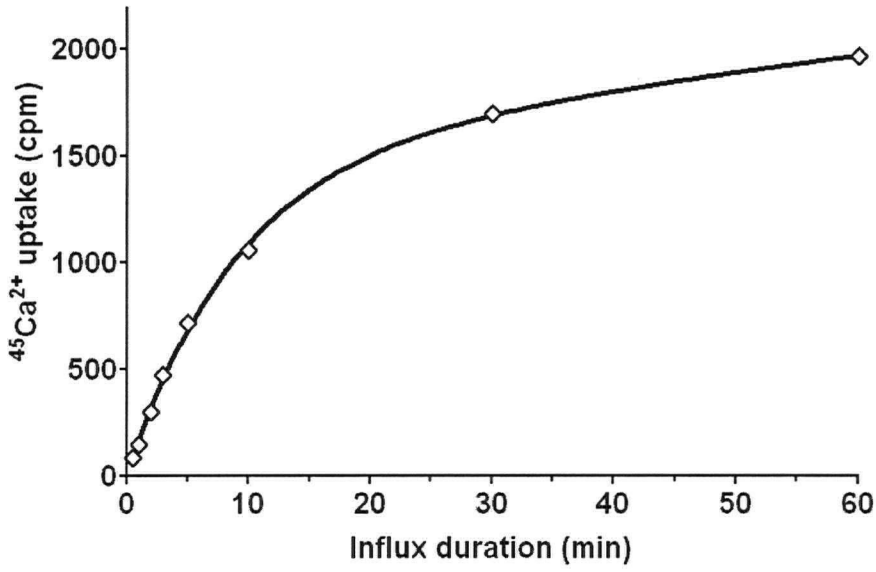

Figure 2.2. Exponential $^{45}Ca^{2+}$ uptake. Cells were exposed to $^{45}Ca^{2+}$ (0.6 μCi, 0.9 μM) in the presence of 1.2 mM $^{40}Ca^{2+}$ for the indicated times, and excess tracer was removed with four 30-second washes in ice-cold $LaCl_3$ (3 mM). Linear back extrapolation of the first four points to t = 0 revealed a y-intercept of 96 ± 12 cpm·well^{-1} indicating an initial fast component of tracer uptake that was interpreted as extracellular binding (see discussion). Following subtraction of this fast component, data were well described by a single exponential process with a plateau of 1.92 x 10^3 ± 0.04 x 10^3 cpm·well^{-1} and a rate constant of 0.084 ± .005 (fitted parameters ± S.E. of estimates). Data points represent the mean ± S.E. (n = 6).

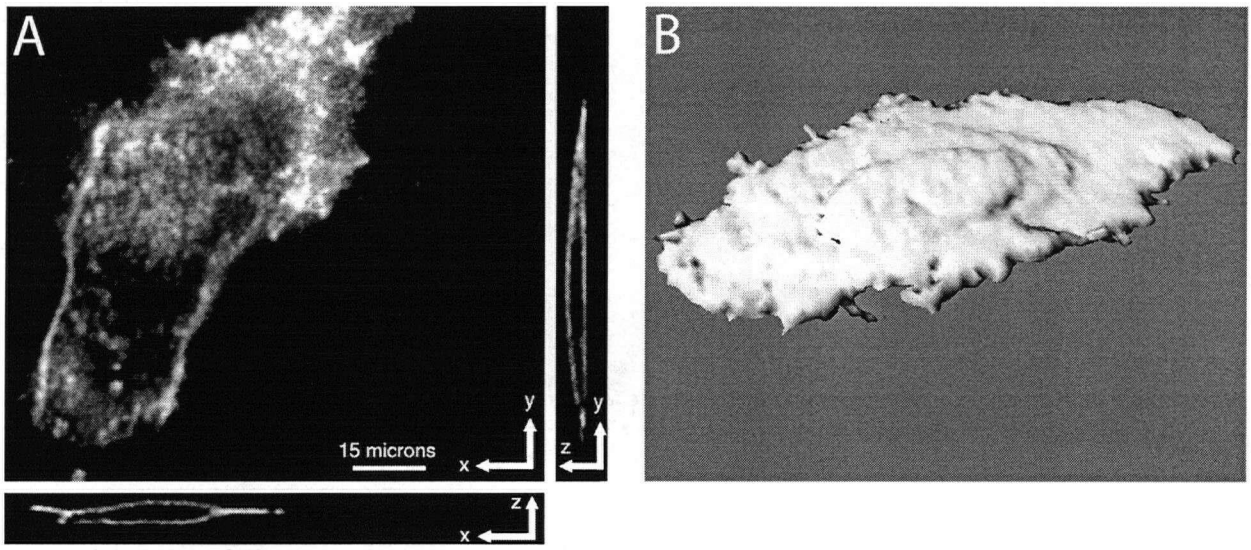

Figure 2.3. SNAP-GFP expression pattern and 3-D reconstruction of a representative cell. A.The peripheral localization of SNAP-GFP is evident in a single image in the x-y plane (bird's eye) of a single rat aortic smooth muscle cell amongst a confluent lawn. This localization of also revealed in slices through the z-x and z-y planes that were produced from deconvolved z-stacks using Imaris 3.3 software (Bitplane, Zurich, Switzerland). Scale bar equals 15 μM. *B.* These image stacks were then reconstructed into fractal-based volumes using the Surpas feature of Imaris to approximate cell volume (voxel size of 0.24(x) x 0.24(y) x 0.2(z) μm), in this case 9 pl.

2.3.3 Inhibition by gadolinium ion: Lanthanides have long been known to inhibit membrane Ca^{2+} transport (248), and it has been suggested that Gd^{3+} can selectively inhibit SOC (229). We investigated the concentration response relationship of Gd^{3+} on inhibition of resting

Ca^{2+} influx (Figure. 2.4). The semi-log plot of this relation yields two well-separated inhibitory processes with Hill slopes for both of about -1. The first process accounts for 65-70 % of total inhibition and has an IC_{50} of 1 μM. The second process accounts for 30 % of total inhibition with an IC_{50} of 2 mM. As illustrated below the larger more sensitive component is the result of inhibition of various Ca^{2+} channels, which are also sensitive to more selective organic channel blockers. The smaller less sensitive component may be related to competition between Gd^{3+} and Ca^{2+} for negative binding sites on the plasma membrane (see discussion).

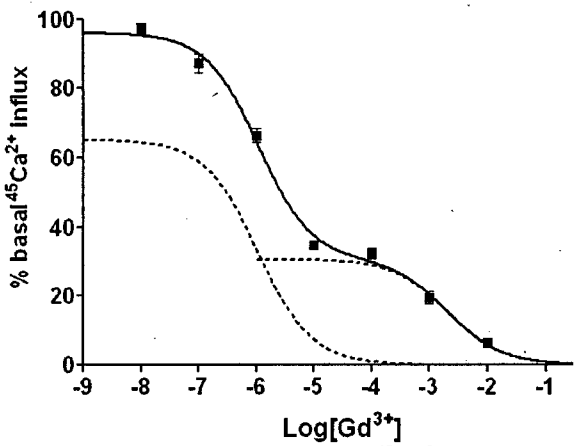

Figure 2.4. Complex concentration-dependent inhibition of $^{45}Ca^{2+}$ uptake by gadolinium ion. Cells were incubated for 15 minutes in $GdCl_3$ then exposed to $^{45}Ca^{2+}$ tracer (0.4 μCi) for 10 minutes followed by removal of excess tracer as described above. The concentration-effect relationship was closely fit using a custom programmed bi-sigmoidal equation in GraphPad Prism (see methods) where the initial values for iteration of the fit were set at: Hill $slopes_{1and2} = -1$, $pIC_{50\text{-}1} = 6$ (visually estimated), $pIC_{50\text{-}2} = 3$ (visually estimated), $Top_1 = 70$, $Top_2 = 30$, both bottoms = 0). Two overlapping sigmoids were simulated from the resulting parameters (left dotted curve: pIC_{50} = 6.0, Hill slope = -0.95, right dotted curve: pIC_{50} = -2.7, Hill slope = -0.92).

2.3.4 Non-stimulated Ca^{2+} entry through excitable Ca^{2+} channels: We tested the hypothesis that part of the "resting" Ca^{2+} influx was due to entry through the same types of Ca^{2+} channels that support stimulated Ca^{2+} entry. In other words we hypothesized that voltage-gated Ca^{2+} channels, receptor-opeated channels and store-operated channels display a background activity when the cells are not stimulated either electrically or chemically. Figure 2.5 shows the inhibition of $^{45}Ca^{2+}$ uptake by maximally effective concentrations of nifedipine (10 μM; for L-type calcium channels), SKF 96365 (1-[b-[3-(4-Methoxyphenyl)propoxy]-4-methoxyphenethyl]-1H-imidazole) (50 μM; for L-type and receptor-operated channels) and 2-APB (75 μM; selective, but not specific for inisitol-1,4,5-trisphosphate (IP_3) receptor and some store-operated channels in addition to partial inhibitory effect on L-type channels).

From these results (Figure 2.5) we deduced that distinct pathways contribute to resting Ca^{2+} influx. Thus 45% of the resting Ca^{2+} influx is mediated by voltage-gated Ca^{2+} channels,

which are completely blocked by nifedipine and SKF 96365 and are inhibited 50% by 75 μM 2-APB. 7% of the resting Ca^{2+} influx is mediated by Ca^{2+} channels exclusively blocked by SKF 96365 and, 23% of the resting Ca^{2+} influx is mediated by channels blocked exclusively by 2-APB. This conclusion is dependent on the use of optimally blocking concentrations of the various agents as demonstrated for SKF 96365 and 2-APB in the presence of nifedipine (10 μM) (Fig. 2.5B & C). Note that effective concentrations of 2-APB for inhibition of resting Ca^{2+} influx are more consistent with those reported for inhibition of the IP_3R (IC_{50} = 42 μM) in the SR than SOC in the PM (reported to be 0.5 μM) (215). We have previously shown 10 μM to be a maximally effective concentration of nifedipine (173).

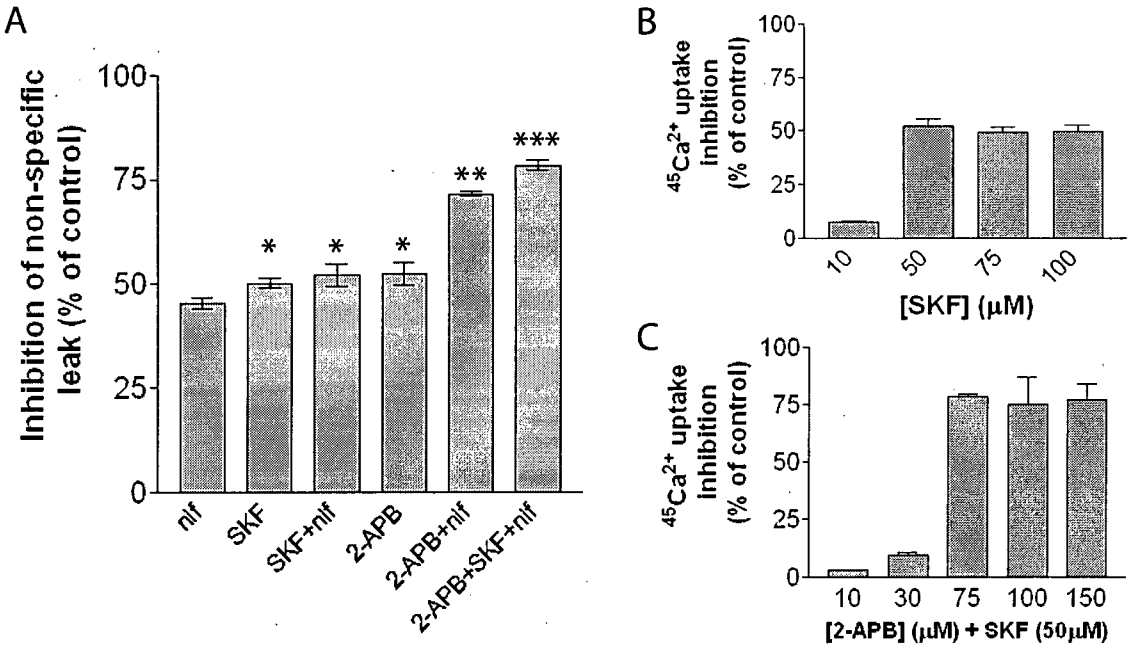

Figure 2.5. Excitable calcium channels mediate calcium leak. A) Investigation of known organic calcium channel blockers. Cells were pre-incubated with nifedipine (nif, 10 μM) or SKF 96365 (50 μM) for 15 minutes or 2-APB (75 μM) for 20 minutes before $^{45}Ca^{2+}$ tracer (0.4 μCi) was added to cells for a 10-minute incubation period. Analysis of additivity: SKF 96365 inhibits $Ca_v1.2$ at this concentration, so $Ca_v1.2$ carries ~45% of the leak influx and channels exclusively sensitive to SKF 96365 carry ~7% of the influx. Channels uniquely sensitive to 2-APB carry ~23% of the resting Ca^{2+} influx. (n = 6-15). (* = different from nif, ** = different from SKF 96365, *** = different from 2-APB ± SKF 96365. Determined by ANOVA ($p < 0.05$) and pair-wise post-hoc analysis) B) Concentration-response relationship for SKF 96365: This compound shows a very steep concentration-response relationship with a Hill slope ~3.0, and a maximal effective concentration of 50 μM. (n = 3) C) Concentration-response relationship for 2-APB: The concentration-response relationship of 2-APB was determined in the presence of SKF 96365 (50 μM) to negate any cross-reactivity with SKF 96365-sensitive channels (n = 3). Error bars represent SE.

2.3.5 Comparison of organic Ca^{2+} entry blockers with inorganic gadolinium: Due to the clear separation of the two inhibitory components of Gd^{3+}, we used a concentration of 100 μM Gd^{3+} to completely block the more sensitive phase of $^{45}Ca^{2+}$ up-take, while leaving the less sensitive component essentially untouched (Figure 2.4). This permitted us to address the question

of whether there is a Ca^{2+} channel that is uniquely and potently inhibited by Gd^{3+}. Three independent experiments showed that a combination of 75 μM 2-APB and 50 μM SKF 96365 exerts the same degree of inhibition (79.6 ± 3.5%) as 100 μM Gd^{3+} (83.7 ± 1.2%). Furthermore, the Ca^{2+} leak is not additively inhibited by organic and inorganic blockade (83.8 ± 4.0%) (Figure 2.6). This indicates that at concentrations below 100 μM, Gd^{3+} blocks all three types of Ca^{2+} channels: L-type Ca^{2+} channels, "receptor-operated channels" and "store-operated channels". Moreover, the first phase of influx blockade by Gd^{3+} occurs with a Hill Slope of ~1, which is commonly interpreted to indicate a single binding site. In this case we take this to indicate a lack of selectivity by Gd^{3+} for any one of these channels.

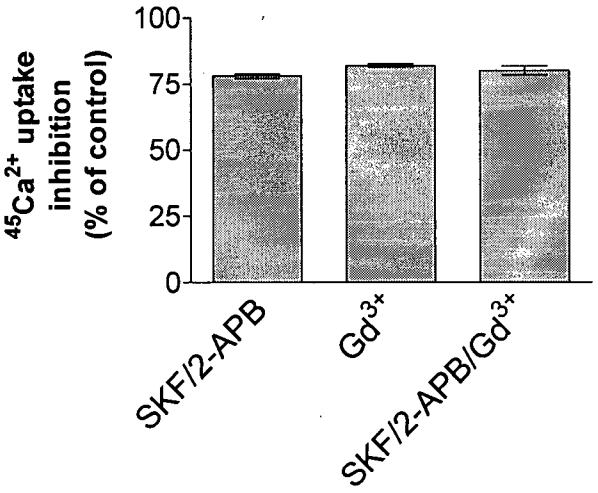

Figure 2.6. A combination of SKF 96365 and 2-APB fully blocks resting influx through membrane channels. 100 μM Gd^{3+} is an approximation of the maximal effective concentration for the first phase of Gd^{3+}-mediated inhibition of resting $^{45}Ca^{2+}$-influx, with little effect on the second phase of inhibition. SKF 96365 and 2-APB were used at their maximally effective concentrations. There is no significant difference between inhibition of resting Ca^{2+} entry by organic inhibitors alone or in combination with Gd^{3+} (100 μM), or by Gd^{3+} (100 μM) alone (ANOVA with Bon Ferroni pair-wise comparison, p = 0.07). Cells were pre-treated with inhibitors for 20 minutes before addition of $^{45}Ca^{2+}$ (0.4 μCi) for 10 minutes. Experiments represent the mean ± standard error of 8 replicates.

2.3.6 Expression of candidate genes for channels responsible for non-stimulated Ca^{2+} entry:

The above experiments have helped to functionally characterize the channels contributing to the spontaneous background Ca^{2+} leak, but do not identify the molecular identities involved with the exception of the L-type channel ($Ca_v1.2$), by virtue of the high degree of selectivity of nifedipine. Accordingly, RT-PCR detected expression of the L-type channel-specific α-subunit (data not shown). To date the most likely candidate molecules for receptor-operated and store-operated channels in mammalian cells are the cannonical transient receptor potential channels (TRPC channels) (137;163). Confluent cultured rat aortic smooth muscle cells expressed TrpC1, 4 and 6

mRNA, while homogenized rat brain, used as a positive control, revealed expression of TrpC1-7 mRNA (Figure 2.7).

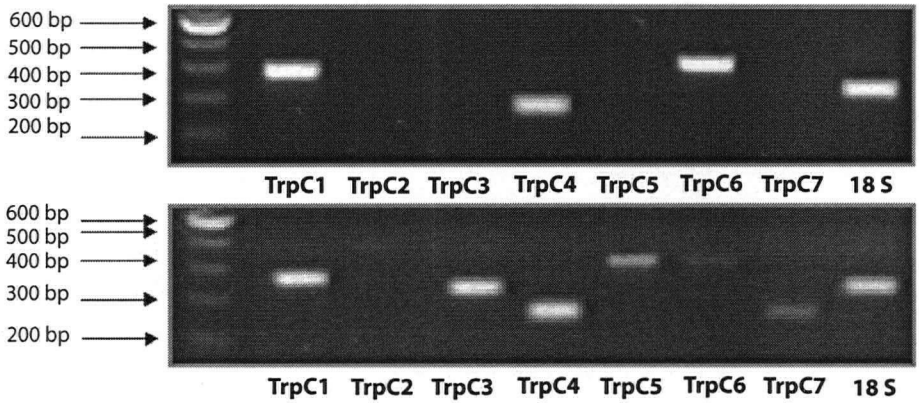

Figure 2.7. TrpC mRNA expression profile in cultured rat aortic smc. Upper panel shows cDNA amplified by RT-PCR of total RNA isolated from confluent rat aortic smooth muscle cells at 7-9 days in culture. Lower panel shows a positive control for the probes using total RNA isolated from rat brain homogenate. All primers used amplified rat brain transcripts. (primer sequences in Table 2.1)

Table 2.1. Oligonucleotide sequences of RT-PCR primers

Channel	*GenBank Accession No.*	*Predicted Size, bp*	*Sense/ Antisense*	*Location, nucleotides*
mTrpc1	U40980	372	5'-CAAGATTTTGGGAAATTTCTGG-3' 5'-TTTATCCTCATGATTTGCTAT -3'	1-22 352-372
rTrpc2	AF136401	487	5'-CAGTTTCACCCGATTGGCGTAT-3' 5'-CTTTGGGGATGGCAGGATGTTA -3'	1606-1627 2071-2092
hTrpc3	U47050	331	5'-ATTATGGTGTGGGTTCTTGG-3' 5'-GAGAAGCTGAGCACAACAGC -3'	1483-1502 1795-1814
mTrpc4	U50922	265	5'-CAAGGACAAGAGAAAGAAT-3' 5'-CCTGTTGACGAGTAATTTCT -3'	2535-2553 2781-2800
mTrpc5	AF029983	419	5'-CCTCGCTCATTGCCTTATCA-3' 5'-TGGACAGCATAGGAAACAGG -3'	675-694 1075-1094
mTrpc6	U49069	410	5'-CTGCTACTCAAGAAGGAAAAC-3' 5'-TTGCAGAAGTAATCATGAGGC -3'	738-758 1128-1148
mTrpc7	AF139923	260	5'-TGACAGCCAATAGCACCTTCA-3' 5'-GCAGGTGGTCTTTGTTCAGAT -3'	2397-2417 2637-2657

Trpc, transient receptor potential; m, mouse; r, rat; h, human.

2.4 DISCUSSION

We have analyzed basal Ca^{2+} entry in non-stimulated, "resting" cells and have identified four pharmacologically distinct components: 1. voltage gated channels, 2. receptor operated channels, 3. store operated channels and 4. a smaller undefined components sensitive only to millimolar Gd^{3+}. This complements recent electrophysiological and molecular studies (159;166;240), and we illustrate here that basal Ca^{2+} entry in smooth muscle cells is mainly

mediated by a background open probability of electrically- and chemically-sensitive Ca^{2+} permeable channels, which may be of similar molecular composition to "Ca^{2+} leak channels" described in skeletal myotubes (105;240). A large component, 70-80% of the total Ca^{2+} influx, is carried by L-type Ca^{2+} channels, receptor-operated channels and store-operated channels in proportions that will most probably vary markedly with cell type, culture conditions and TRPC expression profile. It is important to note that the cells used in this study do not necessarily reflect the properties of vascular smooth muscle under physiological conditions. For example, the large basal entry through the L-type Ca^{2+} channels may indicate that these cells are partly depolarized after reaching confluency (123). Indeed preliminary experiments indicated that nifedipine inhibited considerably less influx (about 25% of total influx) in younger, non-confluent cells (data not shown). However, the most surprising finding was the large inhibition by 2-APB, which indicates the presence of open store-operated channels under resting conditions even though the sarcoplasmic reticulum contains ample stored Ca^{2+} (209;220). This finding is compatible with constant cycling of Ca^{2+} between the sarcoplasmic reticulum and the extracellular space independent of changes in bulk cytoplasmic $[Ca^{2+}]_i$ (234). This illustrates that the plasmalemmal Ca^{2+} leak is to some extent linked to the well-known sarcoplasmic reticulum Ca^{2+} leak (40). The TRP family of proteins are likely candidates for the molecular constituents forming receptor-operated and store-operated channels, and these proteins can form non-selective cation channels (163). Therefore, this may explain the resting activity of voltage-gated Ca^{2+} channels, since opening of non-selective cation channels will tend to partially depolarize the cells (263).

In addition to the Ca^{2+} leak carried by excitable Ca^{2+} channels, a smaller component of 20-30% of basal $^{45}Ca^{2+}$ uptake is only inhibited by high concentrations of inorganic polyvalent cations such as La^{3+} and Gd^{3+}. At present we do not know the mechanism for this uptake nor its physiological significance, but the concentrations of La^{3+} or Gd^{3+} required to inhibit this uptake are far greater than the IC_{50}'s reported for inhibition of activated Ca^{2+} channels (227;248). Close inspection of the uptake kinetics reveals a small component of uptake with a $t_{1/2}$ of approximately 7 seconds, which is faster than would be energetically favourable for channel permeation. In addition, the magnitude of this rapid component was dramatically reduced after enhancing the stringency of the $^{45}Ca^{2+}$ washout protocol (Fig. 2.1). This suggests the presence of a protected extracellular Ca^{2+} pool that is not readily displaced from its binding sites such as described Darby et al. (58). If extracellular binding sites are involved, the 15-minute Gd^{3+} pre-

incubation used to create the Gd^{3+} concentration-effect curve may effectively act as a blocking step, or alternatively may block internalization of the tracer. However, this conclusion remains speculative.

It is particularly interesting that the Ca^{2+} channels contributing to basal Ca^{2+} entry that are sensitive to low micromolar concentrations of lanthanides appear to be the same channels already functionally identified in smooth muscle: voltage-gated, receptor-operated and store-operated channels. Other candidates for channels contributing to basal Ca^{2+} entry are stretch-activated channels and the "leak channels" recorded in skeletal muscle (105). Setoguchi *et al.* showed that stretch-activated channels are inhibited by Gd^{3+} with an IC_{50} of 14 μM and are completely blocked by 100 μM Gd^{3+}(206). We cannot confirm or dispute a role for stretch-active channels in these cultured cells, but the lack of additivity of Gd^{3+} on top of SKF 96365 and 2-APB would imply that if stretch-activated channels are expressed and are contributing to the Ca^{2+} leak then they are also sensitive to these organic compounds. The skeletal muscle "leak channels," which may also be stretch-sensitive, are activated by nifedipine and inhibited by two unique dihydropyridines, AN-1043 (dimethyl 2,6-dimethyl-4-(4-bromophenyl)-1,4-dihydropyridine-3,5- dicarboxylate) and AN-406 (dimethyl 2,6-dimethyl-4-(4-trifluoromethylphenyl)-1,4-dihydropyridine-3,5-dicarboxylate) (5;105). However there is no evidence to date as to their sensitivity to SKF 96365, 2-APB or Gd^{3+}. On the other hand Obejero-Paz et al. have electrophysiologically characterized two distinct "leak channels" in A7r5 cultured smooth muscle cells(166). One channel was divalent cation-selective (6pS), and the other was a relatively non-selective channel (17 pS), and these channels are inhibited by 50 μM Gd^{3+}. Moreover, the 17 pS channel shares some electrophysiological characteristics with the skeletal muscle leak channels and the drosphila TRPC-L channel.

Of the known excitable Ca^{2+} channels, current literature overwhelmingly points towards the TRPC channels as mediating the phenomena of receptor-activated and store-activated calcium influx. Generally, TRPC6 and 7 are thought to be activated by diacylglycerol (79;117;243), while different reports show TRPC1, 3, 4 and 5 to be activated by both receptor-activation or store-depletion depending on the experimental conditions (137;163;167;175). This variable activation most likely reflects extensive species- and tissue-specific signaling, which makes it difficult to definitively label these channels as receptor-operated or store-operated channels (163). More importantly however, Gailly's group showed TRPC1 and 4 to be

constitutively active in A7r5 smooth muscle cells (240), and TRPC7 has been implicated as contributing to basal plasmalemmal permeability to divalent cations by virtue of it's activation by intracellular Mg·ATP and Mg·GTP (159). On the other hand Vanderbrouke et al. found that TRPC6 was not constitutively active, which is consistent with its specific roll as a receptor-operated channel. TRPC1 is linked to the type-2 IP_3 receptor in some cells, which might confer sensitivity to the release of intracellular Ca^{2+} stores (145). Furthermore, it is important to note that heteromeric TRPC channels often exhibit radically different characteristics from those reported for the respective homomeric channels. (83). Thus since the cultured rat aortic smooth muscle cells in our study expressed TRPC1, 4 and 6, we propose that these cells express at least two forms of store-sensitive cation channel (TRPC1 and TRPC4) and at least one of type of channel that is selectively regulated by receptor activation (TRPC6).

Although the pharmacology of TRPC channel modulation is still in its infancy, initial reports indicate that TRPC1 and 6 are inhibited by La^{3+} (2-50μM) and are also sensitive to SKF 96365, which incidentally has been shown to inhibit TRPC3 (35;268). Several reports have shown 2-APB to inhibit store-operated Ca^{2+} entry, presumably carried by TRPC channels (34). To be specific 2-APB can inhibit TRPC3 (229;230). In rabbit inferior *vena cava*, which expresses only TrpC1 mRNA, SKF 96365, but not 2-APB, inhibited store refilling (135). Thus we hypothesize that the portion of the Ca^{2+} leak that is selectively blocked by 2-APB is carried by TRPC4. However, the potency that we observed for 2-APB's action on Ca^{2+} leak inhibition is more consistent with inhibition of IP_3 receptors than direct inhibition of a plasmalemmal channel (215). This implies: 1) that the IP_3 receptor channels have a basal open probability, which could represent one pathway for the sarco/endoplasmic reticulum Ca^{2+} leak, and 2) that the resting Ca^{2+} leak from the sarcoplasmic reticulum is required and sufficient for the activation of TRPC4. This activity of 2-APB is in addition to partial inhibition of L-type Ca^{2+} channels at the concentrations used, which as mentioned above may be an indirect effect. The fact that TRPC6 was shown to not be active in resting A7r5 smooth muscle cells (240), further indicates that 2-APB was selectively inhibiting TRPC4 in our cultured smooth muscle cells. By corollary, this would infer that the portion of the Ca^{2+} leak that was specifically blocked by SKF 96365 may have been purely mediated by TRPC1. This would be consistent with the report from Scarpa's group that only two single channel currents were active in the A7r5 cell Ca^{2+} leak (166).

Having characterized the nature of the calcium leak in the RASMC, we must question the physiological significance of 2.4 femtomoles of Ca^{2+} permeating the cell membrane per minute. Is this influx sufficient to maintain intracellular calcium stores? In relation to cell volume, this corresponds to a turnover of 250 μM per minute, which at first seems excessive given a resting $[Ca^{2+}]_i$ of ~100 nM. Yet for comparison, Ganitkevich calculated a single episode of Ca^{2+} release from the endoplasmic reticulum to be 680 attomoles of Ca^{2+} (80). Thus, resting Ca^{2+} influx could provide sufficient Ca^{2+} to compensate for spontaneous Ca^{2+} sparks and puffs in resting cells, and in fact may be stimulated by these quantal release events from sarcoplasmic reticulum Ca^{2+} On the other hand, this rate of resting calcium leak is equivalent to an inward current of ~7.5 pA, compared to a single open L-type channel carring 0.3 pA (84), and this magnitude of unstimulated influx is amenable to the concept of "leaky" or "flickering" excitable channels, being equivalent to 250 channels with a basal opening probability 0.1. However, it is important to consider how these findings in cultured cells relate to intact vascular smooth muscle. Given that removal of extracellular Ca^{2+} depletes intracellular Ca^{2+} stores (162), which implies that basal Ca^{2+} influx is required to maintain the resting Ca^{2+} concentration in the sarcoplasmic reticulum of intact vascular smooth muscle. The compounds used herein to inhibit the Ca^{2+} leak are also known to inhibit vascular contraction, thus it is of immediate interest to assess whether this is in part due to a loss of reticular Ca^{2+} stores in a manner analogous to removing extracellular Ca^{2+}.

2.5 APPENDIX I: Converting tracer uptake to $^{40}Ca^{2+}$ influx.

$[^{45}Ca^{2+}]_{stock}$: Stock tracer solution was diluted 1000-fold, and the activity in six 20 μl alliquots was counted giving an average diluted activity of 3.90 x 10^4 cpm. Accordingly, the stock contained 1.95 x 10^9 cpm/ml. Given a half life of 163 days and 90% counting efficiency, the concentration of $^{45}Ca^{2+}$ ion required to give this activity is 7.31 x 10^{14} ions/ml based on simple exponential decay. This is equivalent to 1.22 x 10^{-6} moles/liter, and gives a conversion factor of 3.76 x 10^5 $^{45}Ca^{2+}$/cpm. This values was then corrected to account for decay of the stock from the time when the uptake measurements were performed (30 days prior) to give a $[^{45}Ca^{2+}]_{stock}$ of 1.37 x 10^{-6} M.

$[^{45}Ca^{2+}]_{on\ cells}$ and $^{40}Ca^{2+}$-to-$^{45}Ca^{2+}$ ratio : Upon addition of tracer to the experimental wells, the $[^{45}Ca^{2+}]_{stock}$ had been diluted 11 000-fold giving a $[^{45}Ca^{2+}]_{on\ cells}$ of 1.24 x 10^{-10} M. The physiological saline solution used contained nominally 1.2mM Ca^{2+} giving a $^{40}Ca^{2+}$-to-$^{45}Ca^{2+}$ ratio of 9.68 x 10^6.

Basal Ca^{2+} permeability: the instantaneous $^{45}Ca^{2}$ uptake rate of 161 cpm·min^{-1} was calculated as the first derivative of the influx kinetics curve at t = 0, which is equivalent to a rate constant multiplied by the curve plateau (k = 0.084, y_{max} = 1920). Converting cpm to $^{40}Ca^{2+}$ ions gives 5.86 x 10^{14} $^{40}Ca^{2+}$·min^{-1}·$well^{-1}$. Given that each well contained 4.04 x 10^{5}cells on average, the basal cellular influx of Ca^{2+} was 1.45 x 10^{9} Ca^{2+}·min^{-1}.

CHAPTER III
Direct communication between peripheral mitochondria and the Na^+/Ca^{2+}-exchanger[4]

3.1 INTRODUCTION

It has long been known that high salt intake may lead to hypertension. Demographic studies have shown that populations with limited dietary sodium chloride (NaCl) have lower blood pressures, while lowering one's salt intake to 75 mmoles/day can reduce systolic blood pressure by 5 mm Hg in ~50% of hypertensive patients (101). Blaustein and co-workers originally suggested that the vascular smooth muscle (VSM) Na^+/Ca^{2+}-exchanger (NCX) provides the mechanistic basis for the above clinical correlation between blood pressure and $[NaCl]_{plasma}$ (27). This hypothesis is based on the fact that the plasmalemmal Na^+ gradient governs the rate and direction of the Ca^{2+} flux mediated by the NCX (27). While early mechanistic investigations failed to provide a consistent correlation between extracellular Na^+ concentration and cytoplasmic $[Ca^{2+}]_i$ in VSM, it was later recognized that the NCX communicated more efficiently with the sarcoplasmic reticulum (SR) than with the myoplasm (3;28). The concept of preferential Ca^{2+} transport between the extra-cellular space and SR (or ER in non-muscle cells) was first proposed by van Breemen and co-workers (3;233;235) and is highly dependant on junctional complexes between the plasmalemma (PM) and the peripheral membranes of the superficial SR observed to cover about 10% of the inner PM surface (176;210). These junctional complexes consist of patches of PM and SR membranes separated by a narrow cytoplasmic space ~20 nm in width and are often neighboured by mitochondria. Both the NCX and the ouabain-sensitive Na^+/K^+-ATPase-$\alpha 2$ have been reported to co-localize with the superficial SR, which is enriched in the low affinity Ca^{2+} binding protein calsequestrin (116;157). This coupling of proteins is thought to provide local regulation of the sub-plasmalemmal $[Na^+]$ that regulates the activity of the NCX and its interaction with the junctional SR (28), but the consequence or function of the mitochondria neighbouring these junctions has yet to be investigated.

Traditionally the NCX has been studied in resting cells and during recovery from elevations of $[Ca^{2+}]_i$, at which time the NCX operates in the forward mode to unload the SR and to extrude Ca^{2+} from the cytoplasm (28;161). Recently, several studies have revealed that the NCX can also operate in reverse mode during receptor mediated activation (11) to refill the SR

[4] A version of this chapter has been submitted for publication in Cell Calcium as: Damon Poburko, Kathryn Potter, Edo van Breemen, Nicola Fameli, Olivier Basset, Urs Ruëgg, Cornelis van Breemen. (2005) Mitochondria buffer NCX-mediated Ca^{2+}-entry and limit its diffusion into vascular smooth muscle cells.

between recurrent waves of SR Ca^{2+} release ((134) – also see (64). These oscillating Ca^{2+} waves are also dramatically affected by mitochondrial Ca^{2+} transport (217), but the underlying mechanism has not been completely defined.

The development of aequorin targeted to the MT matrix by Pozzan and co-workers has led to the discovery of linked Ca^{2+} transport between SR/ER and mitochondria (194). We recently reported that such linked transport between MT and the peripheral SR led to indirect NCX control over mitochondrial Ca^{2+} signaling (220). In this communication we employ aequorin targeted to either the MT or the PM to demonstrate a direct interaction between the NCX and the mitochondrial uniporter, which may be relevant to agonist-mediated Ca^{2+} signaling in vascular smooth muscle.

3.2 METHODS

3.2.1 Smooth muscle cell culture: Cells were cultured as described previously (220). A proprietary line of cultured rat aortic smooth muscle cells (RASMC), stored in 90% DMEM/10% DMSO in liquid nitrogen, were thawed and used between passages 8–12. Cells were incubated at 37°C in a humidified atmosphere of 5% CO_2.

3.2.2 Expression of aequorins and green fluorescent proteins (GFP): RASMCs were transiently transfected with one of two pcDNAI expression vectors encoding apo-aequorin containing the amino terminal targeting sequences for human cytochrome oxidase subunit VIII (mito-aequorin) or SNAP-25, which localizes to the inner leaflet of the plasmalemma (PM-aequorin) (148;194). We also transfected cells with SNAP-targeted GFP (PM-GFP) to confirm the fidelity of the SNAP-25 localization sequence. RASMC were seeded onto 13 mm Thermanox™ cover slips coated with Matrigel™ for 30 minutes at 37°C (Nunc, Life Technologies). After 1 day in culture, culture dishes were washed with Ca^{2+}/Mg^{2+}-free PBS and refilled with 500 μL of DMEM (10% FCS) before transfecting cells with Effectene® (Qiagen) as per manufacturer's instructions (1 μg DNA per 2.77 μL Effectene). Cells were used for experiments on the following day.

3.2.3 Immuno-labeling & imaging PM-targeted proteins: The localization PM-GFP was directly imaged in live cells, and the localization of PM-aequorin assessed in fixed cells by immunocytochemistry. Cells were fixed in 4% paraformaldehyde for 10 minutes in Tris-buffered solution (TBS). Excess fixative was quenched for 5 minutes in glycine (0.2 M) prior to

permeabilizing cells Triton X-100 (0.1%, 10 min.). Following a block-step (1% goat serum, 1% bovine serum albumin, 1 hr), cells were exposed to monoclonal anti-haemaglutinin (HA) antibody (1:400, Boehringer Ingelheim, 12CA5 clone) over-night at 4°C. Cells were washed in TBS 3 times and incubated with a goat anti-mouse $F(ab_2)$' Alexa-488 antibody (1:100, Molecular Probes, Oregon) for 1 hour (23°C). Control cells were treated identically but were not exposed to primary antibody.

Images were acquired on an upright Olympus BX50WI microscope with a 60x water-dipping objective (NA 0.9) and equipped with an Ultraview confocal imaging system (Perkin Elmer). Images were collected at 400 nm z-steps (Prior H-128 motor drive) and were reconstructed into 3D volumes using Imaris software (Bitplane, Switzerland). Immuno-fluorescence images were thresholded based on the intensity of non-specific binding in control images.

3.2.4 Measurement of mitochondrial & sub-plasmalemmal [Ca^{2+}]: Mito-aequorin was reconstituted (coelenterazine 5 μM) in serum free DMEM for 2–4 hrs before experiments. SNAP-aequorin was reconstituted in serum free DMEM with 0.1 mM Ca^{2+} with coelenterazine (5 μM) for 2-4 hrs. Cells were superfused at 1 mL/min with physiological salt solution (PSS, in mM: NaCl 145, KCl 5, $MgCl_2$ 1, HEPES 5, glucose 10, and $CaCl_2$ 1.2, pH 7.4). Luminescence was detected by photomultiplier tubes (PMTs) (EMI 9789 and P25232, Electron Tubes Inc, USA) and photon emission was recorded 1 Hz with EM6 photo-counting software (Electron Tubes Inc, USA). The EMI 9789 was coupled to an AD6 analog-digital converter and a CT-2 counting module (Electron Tubes Inc.). The P25232 is a self-contained counting-photon counting system. PMTs were cooled to 4-10°C to reduce dark counts. The off-line calibration of photon emission to [Ca^{2+}] has been described in detail previously (148;220).

3.2.5 Measurement of cytosolic [Ca^{2+}]: Cells (30,000 per cover slip) were seeded onto ethanolized and flame-sterilized 12 mm culture-coated glass cover slips (VRW Scientific) treated with Matrigel™. After 3 days in culture, cover slips were washed 6x with warm PSS and incubated with fura-2AM (5 μM, 0.05% DMSO, 0.05% pluronic acid F-127) for 45 min at room temperature (18-20°C). Cells were washed 6x with PSS (37°C) and allowed to equilibrate for 10 min at 33-35°C on the microscope stage. Ratiometric image capture and analysis are described elsewhere (221). Background fluorescence was measured in cell-free regions of interest and subtracted in a frame-wise manner. At the end of each experiment fura-2 fluorescence was

quenched with Mn^{2+} (15 mM) in the presence of 20 μM ionomycin to determine auto-fluorescence values. In experiments with KB-R7943, fura-2 responses were expressed as the change in ratio from the pre-stimulatory baseline in order to compensate for a fluorescent artefact caused by absorption of UV light by KB-R7943 between 300-390 nm that produced a parallel shift in the absolute F340 and F380 values.

3.2.6 Statistical Analysis: Values are expressed as mean ± standard error (SE) with the number of replicates indicated for each experiment. Means were compared using the most robust test appropriate to each experimental design. Groups of three or more means were compared by ANOVA with pair-wise comparisons made by Bonferroni post-hoc tests. Data were compiled and analyzed using GraphPad Prism 4.0 in coordination with Microsoft Excel, and NCSS was used to perform statistical tests.

3.3 RESULTS

3.3.1 Reversal of NCX stimulates mitochondrial Ca^{2+}-uptake: Acute removal of extracellular Na^+ reverses the plasmalemmal Na^+-gradient causing transient reversal of the NCX and Ca^{2+} entry (3). Although removal of extracellular Na^+ creates an un-physiological condition, it provides an effective means to study local interactions between the plasmalemmal NCX, mitochondria and the SR. Iso-osmotic replacement of extracellular Na^+ with N-methyl-D-glucamine (NMDG), referred to as "$0Na^+$", caused a rapid and transient increase of $[Ca^{2+}]_{MT}$ to a maximal value of 2-4 μM (Figure 3.1A), which declined to a plateau 1.5- to 2-fold above resting levels (~700 nM). The mitochondrial response to $0Na^+$ was entirely dependent on extracellular Ca^{2+} (data not shown) indicating that the elevation of $[Ca^{2+}]_{MT}$ is due to Ca^{2+} influx rather than Ca^{2+} release from intracellular stores (220). The selective blocker of reverse-mode NCX, KB-R7943 (5-10 μM), completely inhibited the transient phase of the mitochondrial response to $0Na^+$ without affecting the plateau phase of the response (plateau: control - 662 ± 46 μM, n = 14; KB-R7943 - 761± 49 μM, n = 8, p=0.18, 2-sample t-test) (Figure 3.1A). This indicated that the $[Ca^{2+}]_{MT}$ plateau, in the absence or the presence of KB-R7943, was due to inhibition of forward mode Na^+/Ca^{2+}-exchange and a reduction in the extrusion of basal Ca^{2+} entry.

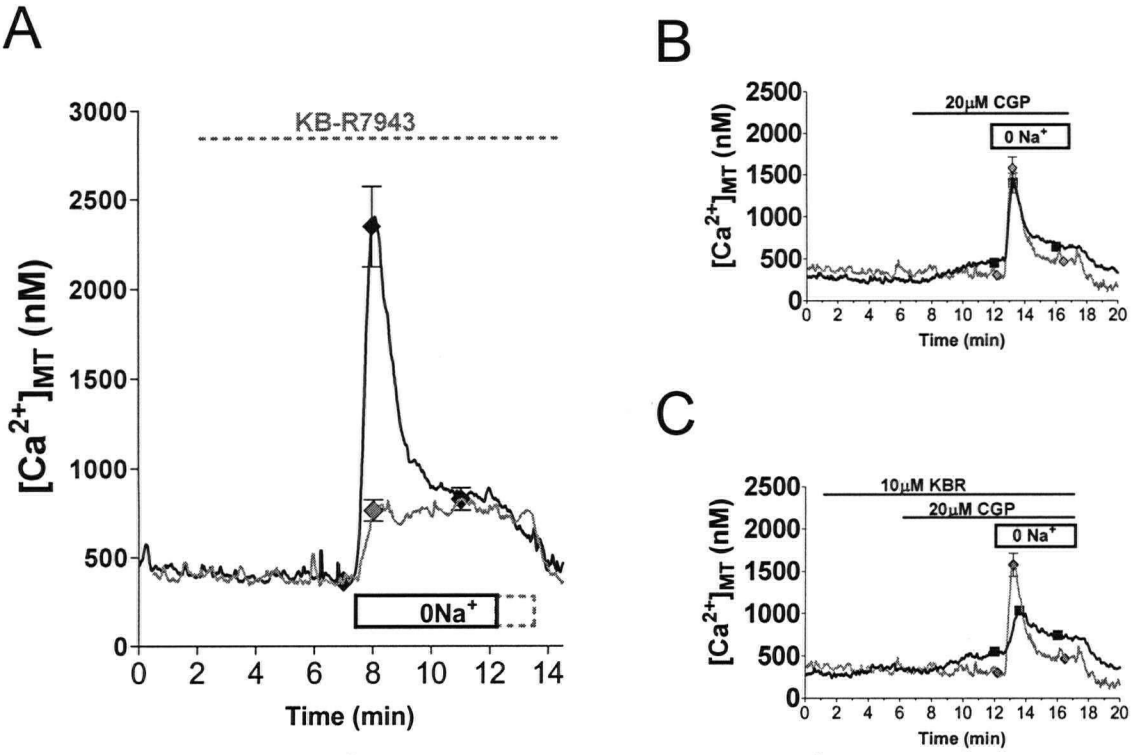

Figure 3.1. Reversal of Na^+/Ca^{2+}-exchange stimulates mitochondrial Ca^{2+}-uptake in cultured smooth muscle cells. A. Elevation of mitochondrial $[Ca^{2+}]$ upon external Na^+ replacement with NMGD (black trace, n = 14). KB-R7943 (10 μM) inhibits the transient phase of this response (gray trace, n = 8). **B**. Selective inhibition of the mitochondrial Na^+/Ca^{2+}-exchanger with CGP-37157 (10-20 μM, black trace, n = 8) demonstrates that $0Na^+$ treatment alone (gray trace, n = 8) does not block the mitochondrial Na^+/Ca^{2+}-exchanger. **C**. Inhibition of NCX reversal by KB-R7943 (black and grey traces) does not alter the effect of CGP-37157 (black trace, n = 10) Traces are averaged responses with standard error shown for selected points.

It is also possible that the $0Na^+$-mediated $[Ca^{2+}]_{MT}$ plateau was due to loss of intracellular Na^+ and subsequent inhibition of the mitochondrial Na^+/Ca^{2+}-exchanger (mitoNCX) (147). Incubation of the cells with a selective inhibitor of the mitoNCX, CGP-37157 (10-20 μM), caused a state-state increase in $[Ca^{2+}]_{MT}$ that was additive with the plateau caused by $0Na^+$ (Figure 3.1B). This additivity was also observed in cells that were pre-treated with KB-R7943 to reduce the depletion of intracellular Na^+ (Figure 3.1C). Thus it is unlikely that the steady-state elevation of $[Ca^{2+}]_{MT}$ in $0Na^+$ is due to inhibition of the mitoNCX.

3.3.2 Ca^{2+} influx through revNCX increases $[Ca^{2+}]$ in the sub-plasmalemmal space:

It is often assumed that rapid increases in $[Ca^{2+}]_{MT}$ require mitochondria to be closely apposed to their Ca^{2+} source. We therefore investigated whether $0Na^+$ caused an increase in $[Ca^{2+}]_{subPM}$ in parallel with the $[Ca^{2+}]_{MT}$ elevation using PM-aequorin, which localizes to the inner leaflet of the plasmalemma and has previously been used A7r5 cells (148). We observed pronounced plasmalemmal accumulation and a variable degree of cytosolic localization of SNAP-25-tagged proteins in live cells expressing PM-GFP (Figure 3.2A) and in fixed cell that were immuno-

fluorescently labeled at the HA-epitope on the recombinant PM-aequorin construct (Figure 3.2B). Localization was examined in deconvolved image stacks both in individual images and in xz and yz cross-sections reconstructed cells. The high density of SNAP-targeted proteins at the cell periphery supports the assumption that PM-aequorin preferentially reported changes in $[Ca^{2+}]_{subPM}$.

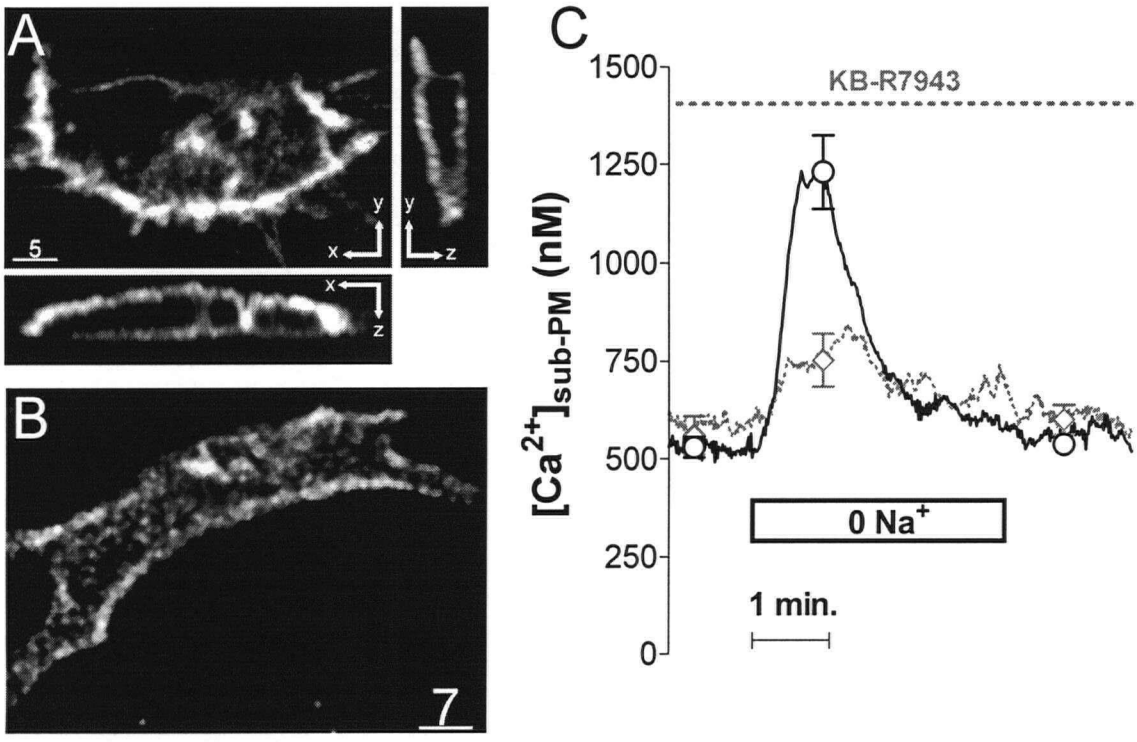

Figure 3.2. Reverse-NCX increases sub-plasmalemmal $[Ca^{2+}]$. A. Localization of transiently expressed PM-GFP shown in an x-y mid-cell slice and cross-sections in the x-z and y-z planes. **B.** Localization of transiently expressed PM-aequorin by immuno-fluorescent labelling of aequorin at the recombinant HA-epitope. Cells are amongst a confluent lawn of cells. Scale bars are in microns. **C.** The PM-aequorin response to Na^+-removal (black trace, n = 12) was similar in shape to that reported by mito-aequorin. KB-R7943 (10 μM) attenuated the transient phase of the response (grey trace, n = 12). Traces are averaged responses with data points showing standard error.

The PM-aequorin response to $0Na^+$ was similar in nature to the mitochondrial response exhibiting a transient increase in $[Ca^{2+}]_{subPM}$ (to 1.2 – 2.5 μM) that fell to a plateau of ~100-300 nM above resting levels (Figure 2C). The transient phase of the PM-aequorin response was also inhibited by KB-R7943 (10 μM) indicating that revNCX caused the transient elevation of $[Ca^{2+}]_{subPM}$ upon removal of extracellular Na^+. Thus it was likely that mitochondria in the periphery of the cell could have responded to this elecation of $[Ca^{2+}]_{subPM}$. To determine further whether this elevation of cytosolic $[Ca^{2+}]$, and subsequent mitochondrial stimulation was restricted to the subplasmalemmal microdomain, we investigated the global change in cytosolic $[Ca^{2+}]$ in response to revNCX.

3.3.3 $0Na^+$ causes a delayed increase in global cytosolic $[Ca^{2+}]$: Since the fura-2 ratio is linearly related to $[Ca^{2+}]_i$ it is ideally suited for measurement of average $[Ca^{2+}]_i$ in the bulk of the myoplasm (see discussion) (187). $0Na^+$ caused a delayed and tonic increase in the fura-2 ratio (Figure 3.3A). Assuming that changes in the fura-2 ratio represent changes in the average cytosolic $[Ca^{2+}]$, we hypothesized that the delay in the $[Ca^{2+}]_i$ elevation might be due the superficial SR buffering revNCX-mediated Ca^{2+} influx (187;237). As predicted, blocking SERCA with cyclopiazonic acid (CPA, 30 μM) abolished the delay in the response to $0Na^+$ and increased the amplitude of the fura-2 response upon NCX reversal with $0Na^+$ (Figure 3.3B). To a lesser extent mitochondrial inhibition has a similar effect, allow the transient phase of the response to be translated to the bulk cytosol (data not shown).

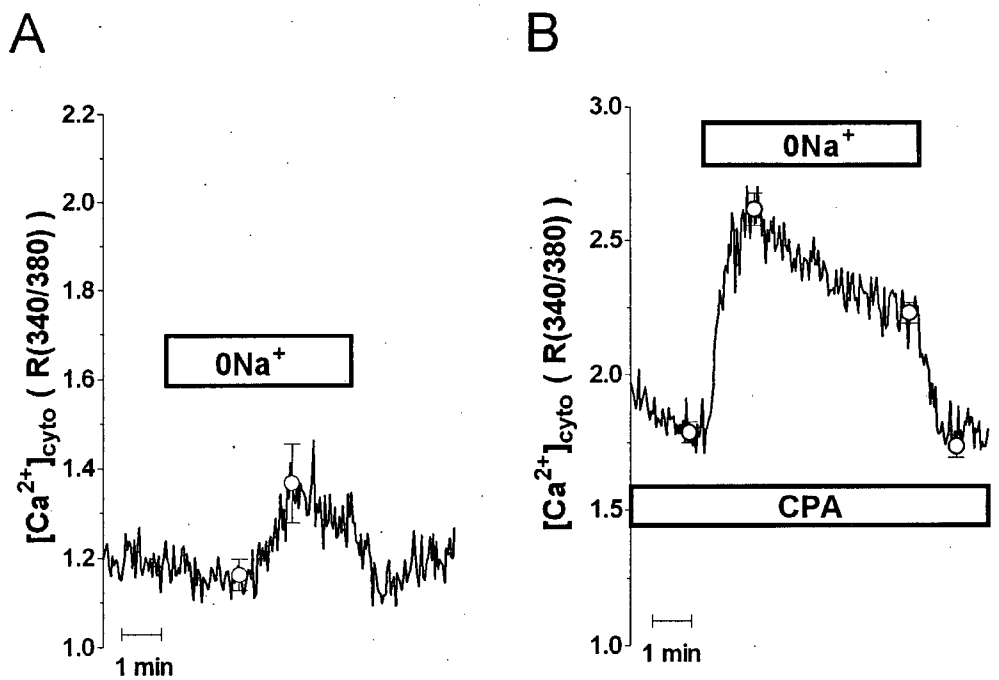

Figure 3.3. Effects of Na^+ substitution and SERCA blockade on $[Ca^{2+}]_i$. A. Fura-2 reported changes in cytosolic $[Ca^{2+}]$ ($[Ca^{2+}]_i$) in response to $0Na^+$ (Average trace of 4 independent experiments). **B.** Effect of SERCA inhibition with cyclopiazonic acid (CPA, 30 μM) average cytosolic response to $0Na^+$ (Average trace of 13 independent experiments). Data points show mean ± standard error.

3.3.4 SR and mitochondria compete for uptake of reverse-NCX mediated Ca^{2+} entry: Ca^{2+} released from the peripheral SR under resting conditions is extruded from the cell by forward-mode NCX in a vectorial manner (161). In the absence of extracellular Ca^{2+} this extrusion process reduces the amount of SR Ca^{2+} available to stimulate mitochondria (220). Previous reports combined with our current findings with fura-2 and CPA suggest that the superficial SR may play an important role in buffering revNCX-mediated Ca^{2+}-influx (28). Inhibition of SERCA with CPA, which depletes releasable SR Ca^{2+} (220), increased the peak

mitochondrial response to $0Na^+$ by ~20% (from 3.10 ± 0.20 to 3.76 ± 0.16 μM, $p < 0.01$, 2-sample t-test) (Figure 3.4A) and slowed the decay of $[Ca^{2+}]_{MT}$ following stimulation. This indicated that SR Ca^{2+} buffering influences the amplitude and kinetics of $[Ca^{2+}]_{MT}$ elevations, presumably by competing for Ca^{2+} influx upon NCX reversal. Fitting the decays of $[Ca^{2+}]_{MT}$ in the absence or presence of CPA to double exponential equations ($R^2 > 0.99$) and plotting the instantaneous rate of decay ($-d[Ca^{2+}]/dt$) as a function of $[Ca^{2+}]_{MT}$ (Figure 3.4B) showed that CPA slowed the decay of $[Ca^{2+}]_{MT}$. Such an effect would indicate that inhibition of SERCA-mediated Ca^{2+} buffering slowed the decay of the ambient $[Ca^{2+}]_{subPM}$ near the mitochondria upon NCX reversal or that SERCA blocked somehow impaired mitochondrial Ca^{2+} extrusion.

In parallel experiments using PM-aequorin, SERCA inhibition increased the peak $[Ca^{2+}]_{subPM}$ response to $0Na^+$ from 1.27 ± 0.15 μM to 2.13 ± 0.17 μM ($n = 6$ & 7, $p = 0.01$, 2-sample t-test), and caused a notable increase in the steady-state $[Ca^{2+}]_{subPM}$ (Figure 3.4C). This observation does not exclude the possibility that CPA impaired mitochondrial Ca^{2+} extrusion (see ref), but parallel changes in $[Ca^{2+}]_{MT}$ and $[Ca^{2+}]_{subPM}$ are indicative of a causal relationship. Moreover, $0Na^+$ and CPA produced synergistic increases in steady-state $[Ca^{2+}]_{subPM}$ ($0Na^+$ 112 ± 77 nM; CPA 146 ± 46 nM; combined 390 ± 86 nM above resting levels), which led us to propose that the peripheral mitochondria are sensitive to steady-state changes in $[Ca^{2+}]_{subPM}$ that reflect inhibition of mechanisms that buffer basal Ca^{2+} influx into the sub-plasmalemmal cytosol.

3.3.5 Mitochondrial Ca^{2+} buffering moderates reverse-NCX mediated elevation of $[Ca^{2+}]_{subPM}$: Mitochondria clearly take up Ca^{2+} upon revNCX-mediated Ca^{2+} influx, but it was unclear if the amount of Ca^{2+} uptake was sufficient to moderate changes in $[Ca^{2+}]_{subPM}$ (see (146)), which are also buffered by the superficial SR. Collapse of the mitochondrial membrane potential with FCCP (2 μM) impairs mitochondrial Ca^{2+} uptake (220), and FCCP increased the elevation of $[Ca^{2+}]_{subPM}$ mediated by $0Na^+$ from 1.42 ± 0.13 μM to 2.15 ± 0.11 μM ($n = 6$ pairs, $p < 0.01$ by paired t-test) (Figure 3.4D). The selective blocker of the Ca^{2+} uniporter, ruthenium red (2 μM, 30 min), reduced stimulated mito-aequorin responses by 35 ± 5% ($n = 6$, $p < 0.01$, data not shown) and increased the PM-aequorin response to $0Na^+$ from 1.87 ± 0.13 μM to 2.26 ± 0.25 μM ($n = 8$ pairs, $p < 0.05$ by paired t-test) (Figure 3.4E). Thus, we conclude that peripheral mitochondria buffer revNCX-mediated Ca^{2+} influx, and by doing so regulate $[Ca^{2+}]_{subPM}$ in co-ordination with the superficial SR.

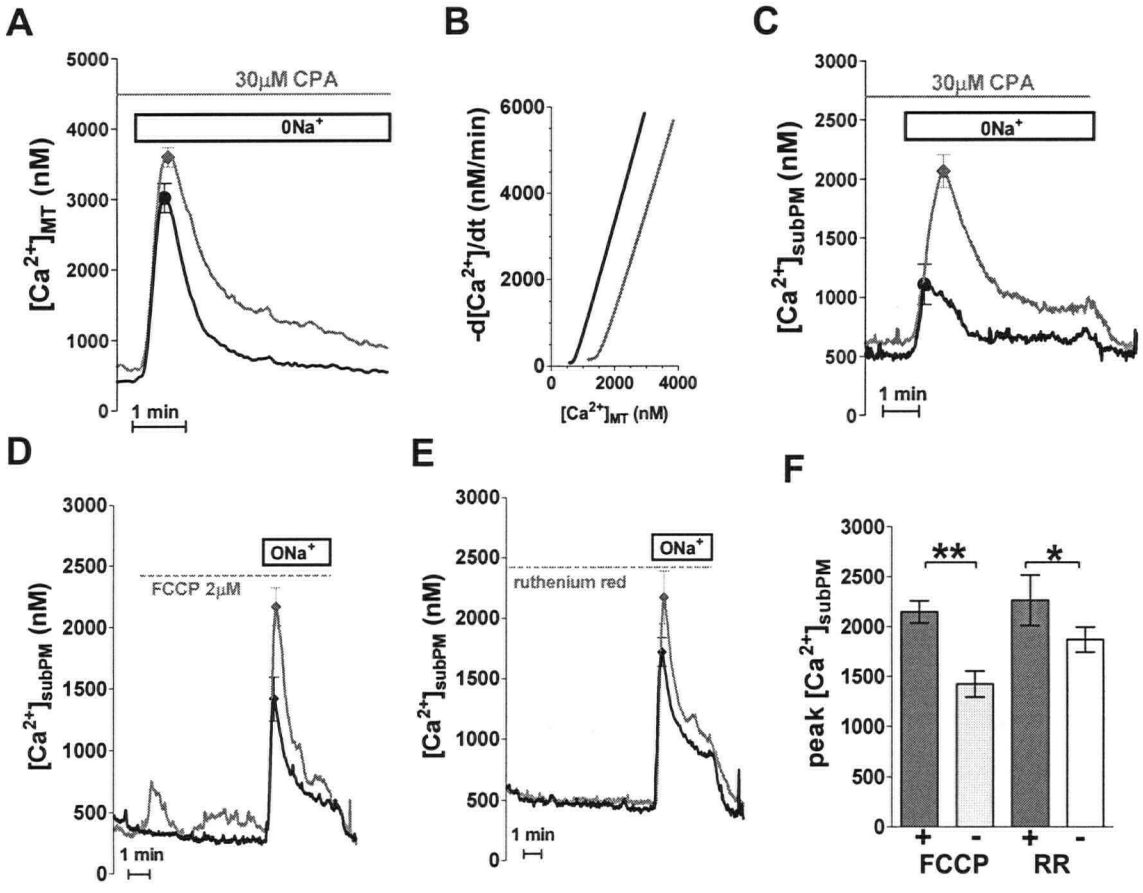

Figure 3.4. The sarcoplasmic reticulum and mitochondria buffer and compete for revNCX-mediated Ca^{2+} influx. A. Cyclopiazonic acid (CPA, 30 μM) increased the peak $[Ca^{2+}]_{MT}$ response to $0Na^+$. **B.** The instantaneous slope of the down stroke of the traces in A plotted as a function of $[Ca^{2+}]_{MT}$ (black trace – control; gray trace – CPA). **C.** CPA increased the peak $[Ca^{2+}]_{subPM}$ response to $0Na^+$ (black trace - control, n = 6; CPA - grey trace, n = 7). **D & E.** Mitochondria depolarization with FCCP (2 μM, n = 4) or inhibition of the Ca^{2+} uniporter with ruthenium red (2 μM, n = 9) increased the $[Ca^{2+}]_{subPM}$ response to $0Na^+$. **F.** Comparison of treatments in D & E with paired controls. Error bars show standard error. * - p-value < 0.05; ** - p-value < 0.01.

3.3.6 NCX reversal influences the tail of the mitochondrial response to ATP: In light of reports that revNCX contributes to agonist-induced Ca^{2+}-entry (64;134), we investigated whether revNCX occurred during agonist-induced stimulation and whether this caused mitochondrial Ca^{2+} uptake. In fura-2 loaded cells, activation of purinergic receptors with adenosine 5'-trisphosphate (ATP, 1 mM) produced a transient $[Ca^{2+}]_i$ peak and a subsequent plateau typical of agonist-mediated responses (Figure 3.5A). Incubation in Ca^{2+} free PSS did not significantly reduce the peak stimulated $[Ca^{2+}]_i$ elevation (without Ca^{2+} 2.56 ± 0.30 R340/380, n = 6; with Ca^{2+} 2.58 ± 0.14 R340/380, n = 15; $p > 0.90$), but the $[Ca^{2+}]_i$ plateau was abolished (data not shown). When the mitochondrial and cytosolic responses were scaled and superimposed to compare the time course of the responses, the transient $[Ca^{2+}]_{MT}$ elevation closely matched the transient phase of the fura-2 response, but $[Ca^{2+}]_{MT}$ continued to decline to

resting levels as the fura-2 signal reached a plateau. This initially indiciated that mitochondria were insensitive to agonist-induced Ca^{2+} influx. However, when Ca^{2+} was removed from the super-perfusate ~10 seconds before stimulation with ATP, the tail of the $[Ca^{2+}]_{MT}$ response declined faster than in the presence of extracellular Ca^{2+} and established a steady-state level below resting $[Ca^{2+}]_{MT}$ (Figure 3.5B). This brief $0Ca^{2+}$ treatment did not affect the $[Ca^{2+}]_{MT}$ peak height (Figure 3.5Ci), but reduced the area under the curve to 84 ± 5% (n = 11, p = 0.01, paired t-test) of paired control responses (Figure 3.5Cii) and caused a significant suppression in the tail of the $[Ca^{2+}]_{MT}$ response (682 ± 121 nM vs 350 ± 84 nM, $p < 0.01$, n = 11) at the point of maximum separation between the tails of the responses in the presence and absence of extracellular Ca^{2+} (Figure 3.5Ciii). Apparently, ATP-stimulated Ca^{2+} entry had a small, but measurable, effect on mitochondrial Ca^{2+} uptake.

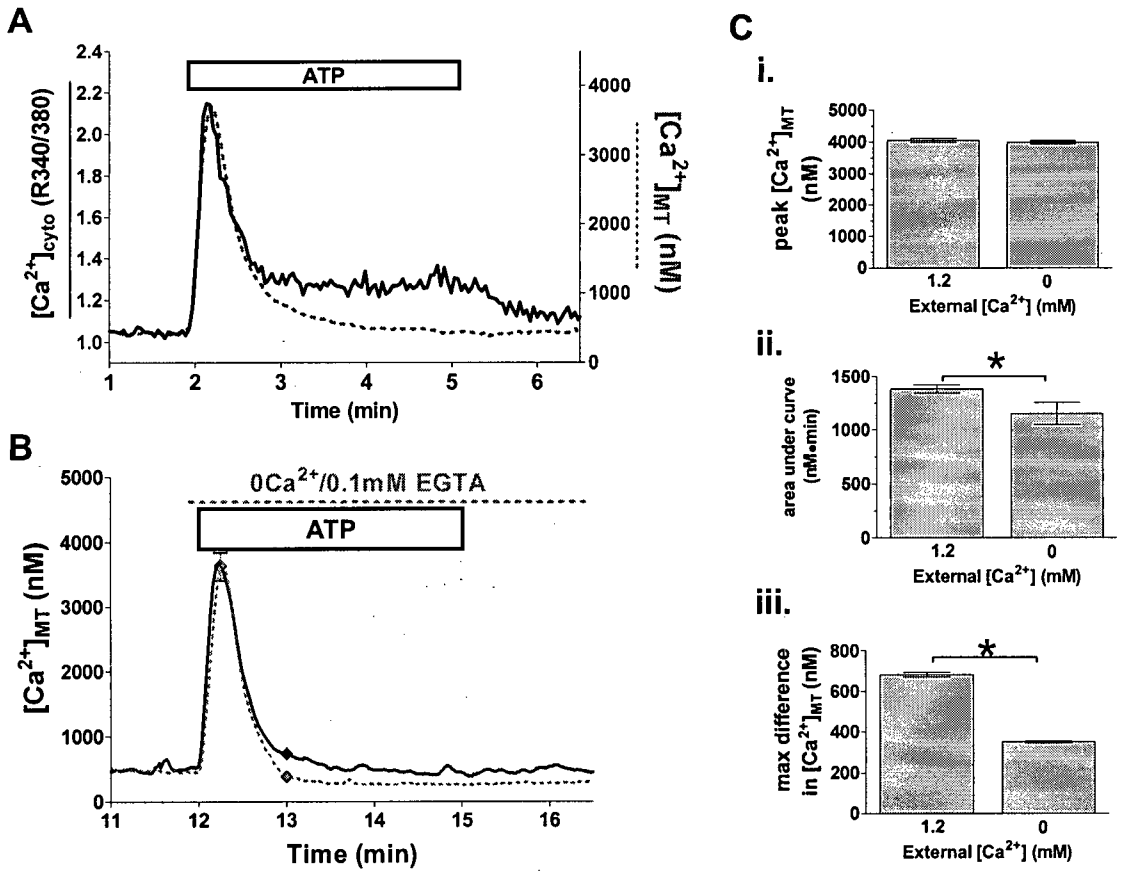

Figure 3.5. Ca^{2+} influx contributes to the tail of the mitochondrial responses to ATP. **A.** Mitochondrial (grey dotted trace) and cytosolic (solid black trace) responses to ATP. **B.** Superposition of averaged mito-aequorin responses to ATP with extracellular Ca^{2+} present (black trace) or removed from the bathing solution (dotted gray trace) 10-30 seconds before stimulation. **C.** Paired analysis of the effect of brief Ca^{2+} removal: (i) peak stimulated $[Ca^{2+}]_{MT}$, (ii) area under the curved, (iii) $[Ca^{2+}]_{MT}$ at point of maximum separation between the traces. * $p < 0.05$.

Blockade of revNCX with KB-R7943 revealed a similar, subtle reduction in the tail of the $[Ca^{2+}]_{MT}$ response to ATP in addition to a small decrease in the peak $[Ca^{2+}]_{MT}$ elevation (Figure 3.6A). Paired analysis revealed that KB-R7943 reduced the area under the curve by 22 ± 5% (1.72 ± 0.13 μM·min control *vs* 1.35 ± 0.10 μM·min KB-R7943, $p < 0.001$, paired t-test) and the peak $[Ca^{2+}]_{MT}$ elevation by 11 ± 5% (4.51 ± 0.28 μM control *vs*. 4.00 ± 0.28 μM KB-R7943, $p = 0.001$, paired t-test) (Figures 3.6Bi & Bii). Inhibition of revNCX also caused a significant separation in the tails of the $[Ca^{2+}]_{MT}$ traces (612 ± 59 nM control *vs*. 421 ± 24 nM KB-R7943, $p < 0.01$, $n = 15$ pairs) (Figure 3.6Biii). In contrast, the transient phase the ATP-mediated increase in average cytosolic $[Ca^{2+}]$ was unaffected by inhibition of revNCX (KB-R7943: 2.56 ± 0.33 R340/380, $n = 12$; control: 2.44 ± 0.14, $n = 14$ R340/380; $p > 0.05$, 2-sampled t-test), but the plateau phase was abolished (KB-R7943: 0.92 ± 0.04 R340/380, $n = 12$; control: 1.11 ± 0.06, $n = 14$ R340/380; $p < 0.05$, 2-sampled t-test) (Figures 3.6C & D). Similar to treatment with Ca^{2+} free solution, KB-R7943 caused both mitochondrial and cytosolic traces to diverge from their respective controls 40 - 45 seconds after stimulation. Collectively, these observations provided compelling evidence that revNCX contributed to Ca^{2+} entry during the sustained cytosolic $[Ca^{2+}]$ plateau stimulated by ATP. This revNCX-mediated Ca^{2+} entry also caused a detectable mitochondrial Ca^{2+} uptake.

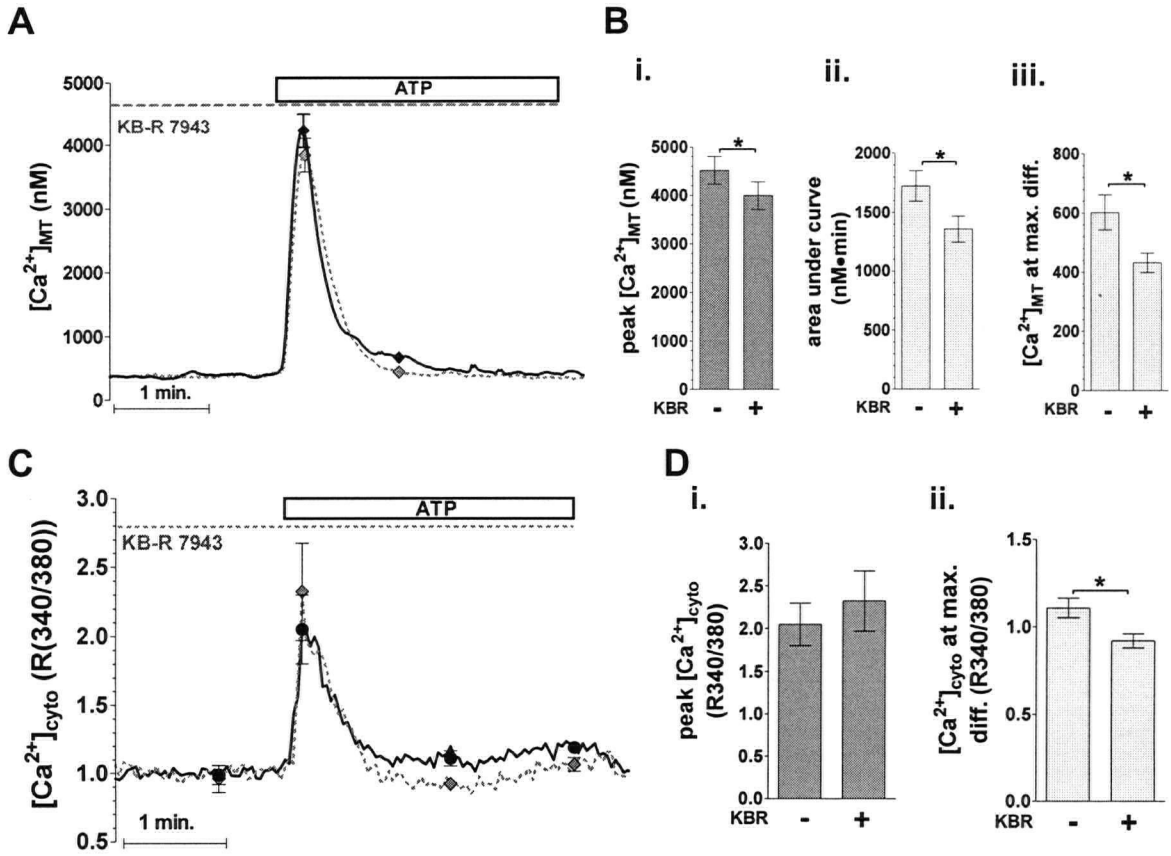

Figure 3.6. NCX-reversal causes mitochondrial Ca^{2+}-uptake during agonist stimulation. A. KB-R7943 (10μM) significantly reduced the mitochondrial response to ATP (1 mM) (gray dotted trace) compared to control experiments (black trace). Traces are average of 17 replicates for each treatment. Error bars show mean ± standard error. **B.** Quantitatifive analysis of KB-R7943 effect on (i) peak $[Ca^{2+}]_{MT}$, the (ii) area under the curve and (iii) the point of maximal separation in the tail of the responses to ATP. **C.** Average cytosolic $[Ca^{2+}]$ responses to ATP in the presence of KB-R7943 (grey dotted trace) or absence of KB-R7943 (black trace) **D.** Analysis of KB-R7943 effects on (i) peak $[Ca^{2+}]_i$ response to ATP rand the subsequent (ii) $[Ca^{2+}]_i$ plateau.

3.3.7 Agonist-mediated up-regulation of mitochondrial Ca^{2+} extrusion: While the arguably modest effect of KB-R7943 on the mitochondrial response to ATP could be attributed to the fact that only peripheral mitochondria are expected to respond to NCX reversal, the return of $[Ca^{2+}]_{MT}$ to resting levels in the sustained presence of the agonist suggested that stimulation of mitochondria by revNCX was only transient. However, it has been reported that both mitochondrial Ca^{2+} uptake and extrusion are stimulated during receptor activation (147). We tested whether receptor stimulation enhanced mitochondrial Ca^{2+} turnover by inhibiting the mitochondrial NCX with CGP-37157 (20 μM) prior to and during purinergic stimulation. CGP-37157 caused a steady-state $[Ca^{2+}]_{MT}$ elevation that was significantly larger in the presence of ATP compared to resting cells (ATP = 184 ± 23 nM; control = 72 ± 31 nM; n = 14 pairs; $p < 0.01$, paired t-test) (Figure 3.7). Similar findings have been reported in endothelial cells by Malli and co-workers (146;147). Pre-incubating cells with KB-R7943 (10 μM) reduced the height of

the CGP-mediated $[Ca^{2+}]_{MT}$ plateau following ATP-stimulation from 235 ± 22 nM to 139 ± 18 nM ($p < 0.005$, Wilcoxon signed rank t-test, n = 11 pairs). This effect of KB-R7943 was similar to the inhibition of the ATP-mediated cytosolic $[Ca^{2+}]$ plateau illustrated in Figure 3.6. Together these findings strongly suggest that during ATP-mediated stimulation of vascular smooth muscle cells reverse-mode NCX contributes to agonist-induced Ca^{2+} influx across the PM and stimulates mitochondrial Ca^{2+} turnover.

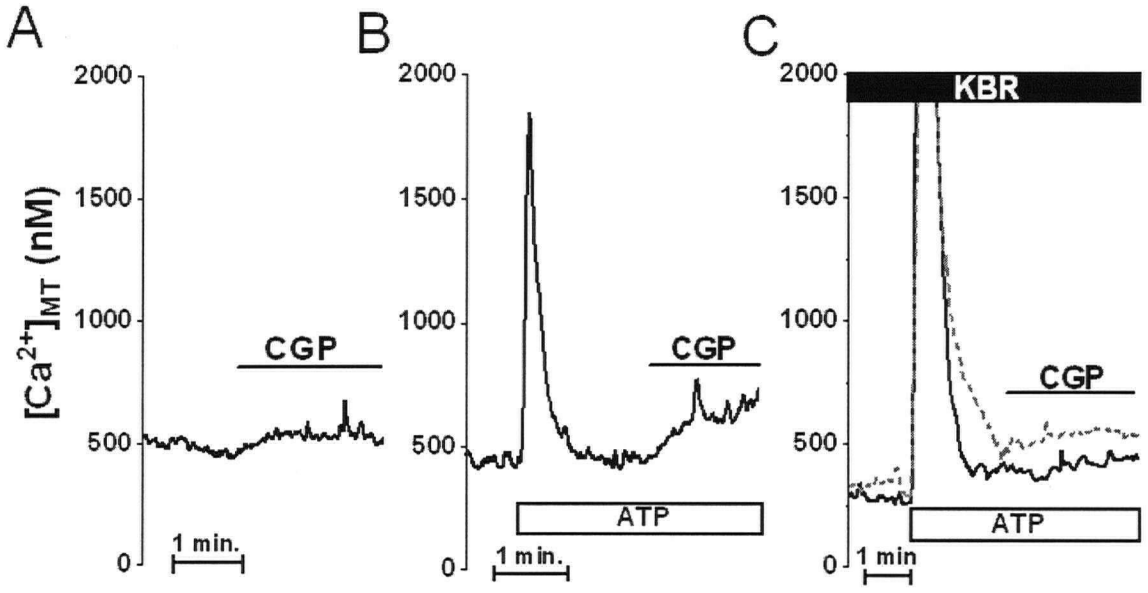

Figure 3.7. Reverse-mode NCX increases mitochondrial Ca^{2+} flux in ATP-stimulated cells. A Inhibition of the mitochondrial Na^+/Ca^{2+}-exchanger with CGP-37157 (20 μM) causes a steady-state increase of $[Ca^{2+}]_{MT}$ in resting cells that is larger in the presence of ATP (**B**). **C**. In an independent series of experiments, the addition of CGP in the presence of ATP caused a smaller increase in $[Ca^{2+}]_{MT}$ in cells pre-treated wuth KB-R7943 (10 μM). Grey dotted traces shows average response in absence of KB-R7943.

3.4 DISCUSSION

Mitochondria interactions with plasmalemmal ion channels have been demonstrated in numerous cell types. In smooth muscle, mitochondrial buffering of $[Ca^{2+}]_{subPM}$ was first indicated using the activity of Ca^{2+}-sensitive K^+- and Cl^--channels as an indirect measure of $[Ca^{2+}]_{subPM}$ (91;261). Rembold and Chen later took advantage of the fact that untargeted aequorin and fura-2 are differentially sensitive to focal changes in $[Ca^{2+}]$ to demonstrate that the superficial buffer barrier creates a standing $[Ca^{2+}]$ gradient between the subplasmalemmal space and the bulk cytosol in VSM (187;235). While untargeted (i.e. cytosolic) aequorin can detect $[Ca^{2+}]$ changes in the subplasmalemmal microdomain, the PM-aequorin provides more accurate and robust measures of $[Ca^{2+}]_{subPM}$ (20). Using an approach similar to Rembold, we find that mitochondria buffer Ca^{2+} entering the sub-plasmalemmal cytoplasm upon NCX reversal.

Traditionally, the Na^+/Ca^{2+}-exchanger is viewed as an extrusion mechanism relying on release of Ca^{2+} from closely associated superficial SR to locally generate the $[Ca^{2+}]$ required to overcome its low Ca^{2+}-affinity (161;220), but this close association also allows that SR to buffer Ca^{2+} influx upon NCX reversal (131). Our current results further illustrate that the superficial SR buffers revNCX-mediated Ca^{2+} entry in competition with the peripherally located mitochondria, and these processes are active during purinergic receptor stimulation.

3.4.1 Functional and localized interaction of NCX, SERCA and Ca^{2+} uniporter: Electron microscopy studies in VMS have revealed sub-plasmalemmal mitochondria neighbouring junctions of the plasmalemma and superficial SR (176). In adrenal chromaffin cells, subplasmalemmal mitochondria mediate specialized Ca^{2+} handling (7); however, little is known of the specific Ca^{2+} handling of these peripheral mitochondria in VMS (reviewed in (177)). However, the NCX is thought to be localized at PM-SR junctions. The current data provide strong evidence that peripheral mitochondria directly communication with the NCX. Furthermore, the co-operative $[Ca^{2+}]_{subPM}$ buffering in stimulated and resting cells illustrates a functional Ca^{2+} signaling complex consisting of the NCX, SERCA and the mitochondrial uniporter. The process of direct Ca^{2+} transfer between organelles, especially mitochondria, is thought to rely on their close spatial association (98;193). In this case the close linkage of the plasmalemmal NCX and the mitochondrial uniporter is supported by the immediate and parallel changes in $[Ca^{2+}]_{MT}$ (Figure 3.1) and $[Ca^{2+}]_{subPM}$ (Figure 3.2) upon extracellular Na^+-removal. The restricted localization of these Ca^{2+} signals to the sub-plasmalemmal cytosol, and thus a sub-population of mitochondria, is further supported by the delayed and modest changes in the fura-2 response to $0Na^+$, which reports predominantly bulk cytosolic $[Ca^{2+}]$ changes (Figure 3.3).

3.4.2 SERCA and the Ca^{2+} uniporter compete for Ca^{2+} entering the cell through reverse-mode NCX: The increased responses in $[Ca^{2+}]_{subPM}$ and $[Ca^{2+}]_{MT}$ Na^+-removal by inhibition of SERCA with CPA indicated that both the peripheral SR and mitochondria take up Ca^{2+} that enters the cell through reverse-mode NCX. Moreover, the fact that CPA enhanced the mitochondrial response (Figure 4) under conditions that deplete releasable SR Ca^{2+} stores indicates that the mitochondrial response to NCX reversal was not due to Ca^{2+}-induced-Ca^{2+}-release (220). Rather, SERCA-mediated Ca^{2+} buffering moderated the $[Ca^{2+}]_{MT}$ elevations upon NCX reversal. The simplest explanation of these findings is that the loss of SR Ca^{2+} buffering of

leads to increased and prolonged elevations of $[Ca^{2+}]_{subPM}$ and consequently $[Ca^{2+}]_{MT}$ indicating competitive or co-operative buffering of $[Ca^{2+}]_{subPM}$ elevations by mitochondria and the superficial SR. This model is in line with reports that mitochondria buffer capacitative Ca^{2+} entry and facilitate refilling of the endoplasmic reticulum {(106;147;169) and reviewed in (176)}.

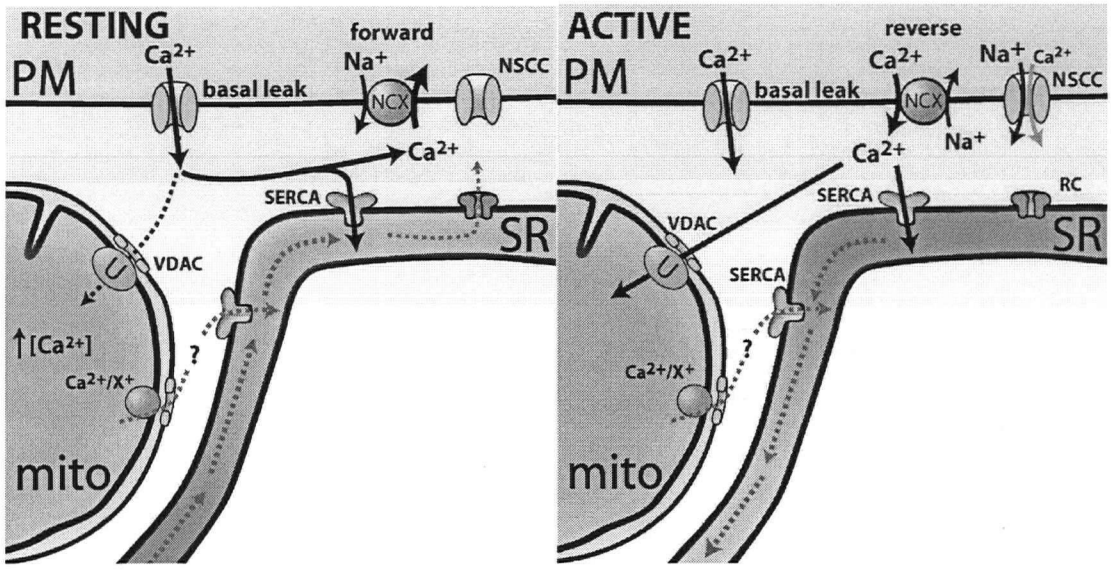

Figure 3.8. Model for interaction of NCX, SERCA and mitochondria in vascular smooth muscle. Left. In resting smooth muscle, SERCA buffers resting Ca^{2+} influx and SR Ca^{2+} release channels deliver this Ca^{2+} to the NCX operating in forward-mode. NCX is also directly activated by the elevated $[Ca^{2+}]_{subPM}$ independent of SR Ca^{2+} release. Mitochondria also take-up basal Ca^{2+} influx, but Ca^{2+} removal from the sub-plasmalemmal space by NCX and SERCA reduces the exposure of mitochondria to this Ca^{2+} entry. **Right.** Stimulation with ATP causes NCX reversal and immediate elevation of $[Ca^{2+}]_{subPM}$. This is due to opening of Na^+-permeable channels in response to receptor activation or SR Ca^{2+}-depletion. The resulting Ca^{2+}-influx is taken up into the SR and mitochondria by SERCA and the Ca^{2+} uniporter, respectively. Abbreviations: RC, Ca^{2+}-release channel; SERCA, sarco-endoplasmic reticulum Ca^{2+}-ATPase; Ca^{2+}/X^+, mitochondria Na^+/Ca^{2+}-exchanger and or H^+/Ca^{2+}-exchanger; U, Ca^{2+} uniporter; VDAC, voltage-dependant anion channel.

Direct inhibition of mitochondrial Ca^{2+} uptake further demonstrate that mitochondria sufficiently buffer revNCX-mediated Ca^{2+} influx to regulate subplasmalemmal Ca^{2+} signaling (Figure 3.4D & E). Indirect evidence has previously pointed to such a role for mitochondria in smooth muscle cells (91), and a recent report by Frieden *et al.* in endothelial cells elegantly demonstrated that mitochondria regulate the local $[Ca^{2+}]_{subPM}$ near Ca^{2+}-activated K^+-channels (76). We used two independent means of inhibiting mitochondrial Ca^{2+} uptake to confirm that mitochondria buffer $[Ca^{2+}]_{subPM}$ as While both FCCP and ruthenium red can have distinct actions other than inhibiting mitochondrial Ca^{2+} uptake, FCCP is commonly used to inhibit mitochondrial Ca^{2+} uptake by depolarizing mitochondria, and previous reports in smooth muscle have provided indirect evidence indicating that FCCP increases $[Ca^{2+}]_{subPM}$ (91;261). While it is

possible that mitochondrial depolarization can cause confounding effects on Ca^{2+} signaling that are not the direct results of the loss of mitochondrial Ca^{2+} uptake (i.e. altered SR Ca^{2+} release, ATP production and membrane potential (41;48;129), the fact that ruthenium red also enhanced the PM-aequorin response to NCX reversal further supports the conclusion that the Ca^{2+} buffering capacity of peripheral mitochondria is sufficient to moderate $[Ca^{2+}]_{subPM}$ fluctuations in smooth muscle cells.

By inducing robust NCX-reversal, we have demonstrated direct Ca^{2+} crosstalk between the NCX, SERCA and the Ca^{2+} uniporter. This crosstalk is likely restricted to a specific population of mitochondria that are exposed to local elevations of $[Ca^{2+}]_{subPM}$ that are not readily translated into the bulk cytosol. Such a subplasmalemmal microdomain was postulated as an essential part of the "superficial buffer barrier" (233), and we hypothesize that peripheral mitochondria constitute a rapidly acting element of the superficial buffer barrier (illustrated in Figure 3.8). Such superficial Ca^{2+} buffering by mitochondrial is highlighted in studies of the regulation of capacitative Ca^{2+} entry by local $[Ca^{2+}]_{subPM}$ (106;147;169). In smooth muscle, store/receptor-operated Ca^{2+} entry likely occurs via the functional linkage of NCX with non-selective cation channels of the TRP family (11;21).

3.4.3 NCX-reversal stimulates mitochondrial Ca^{2+} uptake upon purinergic receptor stimulation: We have shown that reverse-mode NCX is required to sustain the tonic $[Ca^{2+}]_i$ elevation that follows purinergic receptor activation by ATP (Figure 3.6), similar to recent findings in duodenal mucosa (64). Presumably, this NCX reversal is due to the opening of Na^+-permeable store-operated channels (SOC) associated with NCX and the local elevation of $[Na^+]_{subPM}$ causing to reverse the NCX as proposed by Blaustein and co-workers (11). The molecular basis of this model was subsequently supported by functional linkage of NCX and TRPC3 in HEK293 cells (197). We have previously shown that such NCX reversal mediates refilling of SR Ca^{2+} stores in adrenergicaly-stimulated inferior *vena cava* via specialized PM-SR junctions that couple the NCX to SERCA (131;134), and Hellstrand's group found that mitochondrial inhibition alters the frequency and amplitude of adrenergicaly-driven Ca^{2+}-oscillations (217). This regulation of Ca^{2+} oscillations by mitochondria likely reflects the mitochondrial modulation of Ca^{2+}-dependent gating of IP_3R, but it is tempting to speculate that the interaction of mitochondria with NCX described herein also affects the nature of Ca^{2+} oscillations and SR refilling.

In line with a recent report in endothelial cells (147), we propose that peripherally located mitochondria co-operate with the PM and SR ion transporters in the junctional Ca^{2+} signaling complexes thought to facilitate SR refilling during agonist-mediated Ca^{2+} signaling in some VSM (176). Central to this argument, the first detectable effect of KB-R7943 on the down stroke of the agonist-mediated $[Ca^{2+}]_{MT}$ response coincided with the onset of the $[Ca^{2+}]_i$ plateau (Figure 6). While KB-R7943 affected only a small portion of the total mitochondrial response to ATP, this must be considered in context. The transient phase of the mitochondrial response to ATP is mediated primarily by SR Ca^{2+} release (220), which should stimulate mitochondria throughout the cell (Figure 3.5). In contrast, the agonist-induced NCX-reversal that followed SR Ca^{2+} release and coincided with the tail of the $[Ca^{2+}]_{MT}$ elevation (Figure 3.6) should stimulate only peripheral mitochondria. Moreover, it is the trans-mitochondrial flux, rather than Ca^{2+} accumulation, that may be important to allow sustained agonist-induced Ca^{2+} entry (147).

One of the most interesting finds in the current study is the demonstration of agonist-induced up-regulation of mitochondrial NCX-mediated Ca^{2+} extrusion (Figure 3.7). This in part masked the elevated mitochondrial Ca^{2+} flux during purinergic stimulation. Similar elevation of mitochondrial Ca^{2+} flux despite $[Ca^{2+}]_{MT}$ returning to resting levels in the sustained presence of agonist was also observed in endothelial cell (147), and we further demonstrate that Ca^{2+} flux was facilitated by revNCX-mediated Ca^{2+} entry. If in fact the plasmalemmal Na^+/Ca^{2+}-exchanger associates with Na^+-permeable TRPC channels in these cells (expressing TRPC1, 4 and 6 (178)), it is conceivable that elevation of $[Na^+]_{subPM}$ facilitates the increase in mitochondrial Na^+/Ca^{2+}-exchange. In doing so Na^+-influx would mediate both Ca^{2+} influx via NCX reversal support the continuous mitochondrial Ca^{2+} flux that Malli *et al.* find to be required for sustained capacitative Ca^{2+} entry in endothelial cells (147). In light of the literature cited above, our current findings are likely to be of relevance in a number of different cell types.

3.4.4 Conclusion: Investigations of the role of mitochondria in the generation of localized Ca^{2+} gradients near the plasmalemma and SR have offered exciting insights into site-specific Ca^{2+} signaling, and we are only beginning to understand how mitochondria modulate these localized signals in VSM. Here we report the localized interaction of a sub-population of peripheral mitochondria, the Na^+/Ca^{2+}-exchanger and SERCA in VSM. These mitochondria assist the SR in buffering agonist-mediated Ca^{2+} influx before it can diffuse deeper into the

cytosol. The agonist-mediated Ca^{2+} influx is mediated by reversal of the Na^{+}/Ca^{2+} exchanger, which attributed to localization of NCX near Na^{+}-permeable TRPC channels.

CHAPTER IV

IP_3 and ryanodine receptors localize to separate SR sub-compartments that preferentially co-localize near mitochondria[5]

4.1 INTRODUCTION:

The regulation of calcium signaling in vascular smooth muscle (VSM) is highly dependent on the ultra-structural architecture of the cell. Contraction is one of many processes, including secretion, proliferation and apoptosis that are controlled by fluctuations in the cytosolic concentration of free ionic calcium ($[Ca^{2+}]_i$). In order for this single ion to simultaneous control multiple processes, cells have developed highly ordered systems to regulate the spatial and temporal patterns of $[Ca^{2+}]_i$ fluctuations resulting from Ca^{2+} influx across the plasmalemma and release from the sarcoplasmic reticulum (SR) (23;176). While Ca^{2+} influx plays an important role in refilling SR Ca^{2+} stores and modulating $[Ca^{2+}]_i$ signals, in this report we focus on the release of SR Ca^{2+} during agonist mediated $[Ca^{2+}]_i$ elevation in the vascular smooth muscle. Unlike striated muscle, smooth muscle utilizes both inositol-1,4,5-trisphosphate receptors (IP_3R) and ryanodine receptors (RyR) to release Ca^{2+} from the SR and generate the increase in global $[Ca^{2+}]_i$ that stimulates myofilament contraction (32;87;255). The gating of IP_3R and RyR is modulated by Ca^{2+} in addition to inositol 1,4,5-trisphosphate and cyclic-ADP ribose, respectively (244;254), and it is thought that localized Ca^{2+} gradients in the cytosolic microdomains between the SR and closely associated plasmalemma and mitochondria facilitate localized feedback control of IP_3R and RyR (23;176). Because of the localized nature of these interactions, the precise sub-cellular distribution and spatial relationship of IP_3R and RyR with each other, the plasmalemma and mitochondria are highly relevant to the regulation of cytosolic Ca^{2+} signaling and contraction in VSM.

A long-standing question in VSM physiology is whether IP_3R and RyR are expressed on and release Ca^{2+} from separate elements (or sub-compartments) of the SR or whether they are expressed on the same SR elements and share a common store of Ca^{2+}. Fluorescent labeling of the SR of colonic smooth muscle revealed that IP_3R and RyR are largely localized to same elements of SR (255), which is consistent with a recent review concluding that IP_3R and RyR release Ca^{2+} from a common or overlapping pool of SR in most smooth muscle (153). However,

[5] A version of this chapter has been prepared for publication in the Journal of Cell Biology as: IP_3 and ryanodine receptors localize to separate SR sub-compartments that preferentially co-localize near mitochondria in aorta smooth muscle cells. Damon Poburko, Kathryn Potter, Eric Lin, Megan McLarnon, Nicola Fameli, Hubert Walinski, Tania Szado, Cornelis van Breemen

direct imaging of changes in SR [Ca^{2+}] in VSM shows that Ca^{2+} can be differentially released from closely associated but spatially and pharmacologically distinct sub-compartments of the SR (85). This strongly suggests that IP_3R and RyR are expressed on and release Ca^{2+} from separate SR elements in VSM. In portal vein, immuno-labeling has shown IP_3R and RyR to be localized throughout cross sections of myocytes (31), but detailed analysis of their co-localization has yet to be reported in vascular smooth muscle cells.

The subcellular localization of IP_3R and RyR is also directly relevant to the stimulation of mitochondrial Ca^{2+} uptake because almost all mitochondria in smooth muscle cells are found in close association with SR (57;131;210). Release of SR Ca^{2+} into these SR-MT junctions generates the micromolar [Ca^{2+}] required to activate the mitochondrial Ca^{2+} uniporter (160;192;220), which allows mitochondria to take up Ca^{2+} and thereby: 1) assist with SR refilling, 2) modulate the gating of IP_3R and RyR by buffering local Ca^{2+} gradients, and 3) to serve as sensitive reporters of localized SR Ca^{2+} release. While in some types of smooth muscle, mitochondrial Ca^{2+} uptake may not be highly dependent on close mito-SR coupling (151), both the IP_3R and RyR are closely coupled with the mitochondria in aorta myocytes (160;220). Moreover, in conduit artery smooth muscle, mito-SR cross talk is thought to play an important role in regulating the frequency and amplitude of agonist-induced Ca^{2+} oscillations (131;217). However, the relative contributions of IP_3R and RyR to agonist-mediated mitochondrial Ca^{2+} uptake and the relevance of their cross-talk (and therefore sub-cellular localization) is poorly characterized in VMS.

Recently, we reported that distinct SR sub-compartments stimulate mitochondria in cultured aorta SMC (220), and in our present study we have again used aequorin targeted to the mitochondria to detect localized SR Ca^{2+} release (191) in combination with immuno-cytochemistry to demonstrate that IP_3R and RyR are localized to, and release Ca^{2+} from, separate SR sub-compartments. Activation of two phospholipase-C coupled receptors caused increased $[Ca^{2+}]_{MT}$ by similar patterns of SR Ca^{2+} release. Furthermore, comparison of agonist-mediated increases in $[Ca^{2+}]_i$ and $[Ca^{2+}]_{MT}$ with the sub-cellular distribution of IP_3R and RyR has provided novel insights into how IP_3R-RyR cross talk differentially influences cytosolic and mitochondrial Ca^{2+} signaling.

4.2 MATERIALS & METHODS:

4.2.1 Smooth muscle cell culture: Cells were cultured as described previously (220). A proprietary line of cultured rat aortic smooth muscle cells (RASMC), stored in 90% DMEM/10% DMSO in liquid nitrogen, were thawed and used between passages 8–12. Cells were incubated at 37°C in a humidified atmosphere of 5% CO_2.

4.2.2 Expression of mito-aequorin and inverse pericam: Transfection of RASMC with mitochondrial aequorin has been previously described (mito-aequorin) (148;194). Inverse pericam (Riken Institute) was transiently transfected into RASMC on Thermanox™ cover slips coated with 1/30x Matrigel™ (30 min, 37°C) (Nunc, Life Technologies). 24 hours after plating, cells were washed with Ca^{2+}/Mg^{2+}-free PBS and fed with DMEM (10% FCS) before transfection with Effectene® (Qiagen) as per manufacturer's instructions (1 μg DNA per 2.77 μL Effectene). Cells were used for experiments on the following day.

4.2.3 Measurement of mitochondrial [Ca^{2+}]: Changes in mitochondrial [Ca^{2+}] were reported by mito-aequorin. On the day of experiment, mito-aequorin was reconstituted with coelenterazine (5 μmol/L, serum free DMEM) for 2–4 hrs. Experiments were performed in thermostated perfusion chambers (37°C) that were positioned ~5 mm below photon detectors. Cells were superfused (1 mL/min) with physiological salt solution (PSS, in mmol/L: NaCl 145, KCl 5, $MgCl_2$ 1, HEPES 5, glucose 10, and $CaCl_2$ 1.2, pH 7.4). Luminescence was detected by photomultiplier tubes (B2F-RFI/9789A and P25232, Electron Tubes Inc, USA), and photon emission was sampled at 1 Hz with EM6 photo-counting software (Electron Tubes Inc, USA). Off-line calibration of photon emission to [Ca^{2+}] has been previously described (148;220).

4.2.4 Measurement of cytosolic [Ca^{2+}]: Cover slips with pericam-expressing cells were mounted in a thermostated (35-37°C) perfusion chamber and perfused with PSS (~ 1.5 ml/min). Pericam fluorescence was imaged on an Olympus BX50WI microscope (10x UMPlanFl objective, 0.30 NA) with an Ultraview Nipkow disc (Perkin Elmer). Image acquisition and analysis was performed with Ultraview 4.0 software (Perkin Elmer). Cells were excited at 488 nm (Argon/Krypton laser, Melles Griot), and fluorescence emission was collected at 525/530 nm. Fluorescence intensity was corrected for linear decay before data was inverted and expressed in the form of $(F-F_o)/(F_{max}-F_o)$ where F_o is the baseline fluorescence prior to stimulation and F_{max}

is the maximal change in fluorescence after permeabilizing cells with digitonin (100μM) in the presence of 2.5mM Ca^{2+}.

4.2.5 Immuno-cytochemistry: Cells grown on cover slips were washed with Ca^{2+}/Mg^{2+}-containing phosphate buffered solution (2 x 5min) followed by $0Ca^{2+}/0Mg^{2+}$-PBS (PBS, GIBCO) immediately prior to fixation with paraformaldehyde (PFA, 4%, 10min). Subsequent solutions were made with PBS (pH 7.4). After fixation, cells were washed 3 times for 5 min with PBS, followed by 5 min in 0.2 M glycine and two more PBS washes. Cells were permeabilized with Triton X-100 (0.1%, 10 min) and washed 3 x 5 min with PBS. Cell were incubated for 1 hr in blocking solution-step (PBS, 1% goat serum, 1% bovine serum albumin) before incubation with primary antibodies (1:100 mouse anti-RyR (PA3-925) and 1:200 rabbit anti-IP3R-1 (PA3-901), Affinity Bioreagents) over-night at 4°C. Excess primary antibody was removed with three 20 min washes in blocking solution prior to a 1 hr incubation at room temperature with fluorescent labels, which included goat anti-mouse $F(ab_2)$' Alexa-fluor 488 or 546 (1:100), goat anti-rabbit highly cross-adsorbed Alexa-fluor 594 (1:100) and Alex-fluor 488 conjugated phalloydin (1:200) (Molecular Probes, Oregon) as described. Cover slips were then mounted on slides with Prolong Gold (Molecular Probes) and cured overnight before acquiring images. For each set of labeled cells, images were taken with the same acquisition parameters from control cells that were treated identically but were not exposed to primary antibody.

4.2.6 Confocal image acquisition & deconvolution: Images were acquired on a Leica SP2 inverted confocal microscope with an 63x HCX PL APO objective (1.4 NA). In order to maximize image resolution several key factors were taken into account. Images were super-sampled at a pixel size of 71nm by 71nm and an z-interval of 150nm to ensure anti-aliasing and to supersede the Nyquist Sampling criteria (i.e. pixels size was than one-half of the theoretical limit of diffraction limited optical resolution). Images were sampled using 8 line-averaging to increase the signal to noise ratio. Dual labeled cells were illuminated at 488 nm and 594 nm simultaneously, and emission was collected on separate photomultiplier tubes at 495-580 nm and 605-720 nm. For triple labeled cells, excitation was switched from 488/594 nm to 543 nm between scan lines, and emission bands were collected on three separate photomultiplier tubes at 495-550, 555-605 and 620-720 nm. Due to the resolution dependencies of co-localization analysis, our images were processed offline to maximize image resolution. Images were deconvolved with a Maximum Likelihood Estimation algorithm using Huygens Professional

(Version 2.18 Scientific Volume Imaging) (see (203)). This algorithm takes into account the following imaging parameters: NA of the microscope objective (1.4); refractive index of medium (1.515); refractive index of sample (1.43); excitation wavelength (488/543/594); emission wavelength (525/585/625); confocal pinhole radius (212/237/258); pixel size (71 nm); *z*-axis interval (150 nm); microscope type (confocal); and number of excitation photons (1).

4.2.7 Co-localization analysis: Co-localization analysis, 3D visualization and reconstruction of 3D models were performed with Imaris (Bitplane, Switzerland). The intensity threshold values for co-localization analysis were determined in a two-step process. A minimal background was determined as the mean plus 2 standard deviations of intensity level that eliminated all but the brightest random-shot noise (not greater than 2 x 2 x2 voxels) from 4-5 controls images. Due to the dense packing of the IP_3R and RyR labels and the limits of axial resolution, we determined an additional threshold to limit the contribution of out of focus light, which blurs binarized images of the IP_3R and RyR labels. In each cell, 10 instances of what appeared to be SR elements labeled for each of IP_3R and RyR were sampled independently in 3-dimensions to determine the threshold required to limit the width of the SR label in the x-y plane to 3-4 pixels (~200-300nm). The mean intensity value of the 10 samples was used as the threshold for co-localization analysis. Since the GFP-labeled mitochondria are expected to have a width of 300-400 nm, GFP-images were subject to a median filter (3x3x1) and thresholded as above using 3-dimensional visualization to limit the size of binarized mitochondria to ~400 nm. Co-localization was calculated as the percentage of pixels (i.e., volume) of one label that were also occupied by the other label being analyzed. Co-localization was treated as a binary event, thus all mito-IP_3R and mito-RyR co-localization events were used to calculate the co-localization of IP_3R and RyR that were also associated with the mitochondria.

The 3-dimensional models were generated using the Surpass module of Imaris. The spatial relationship of the IP_3R and RyR are depicted as space filling iso-surfaces (Figure 4.6G-I). The relationships of IP_3R and RyR with mitochondria are depicted by maximal intensity projections of the mitochondria merged with the mito-IP3R, mito-RyR and mito-IP3R-RyR co-localization events (Figure 4.7D-F).

4.2.8 Modeling the effect of voxel clustering on random co-localization: For this analysis custom routines were written in IDL (IDL 5.6, RSI Inc.). Two 3-dimensional binary arrays were generated containing 115,000 elements, representing the average number of mito-GFP labeled

voxels per cell after thresholding for co-localization analysis. 41% and 34% of the elements in the two arrays (i.e. the mean co-localization of IP_3R and RyR with mitochondria, respectively) were set to a value of 1 and randomly distributed. The extent of random co-localization was calculated as the number of elements retaining a value of 1 when the two arrays were multiplied. Co-localization was then assessed when the random distribution of voxels (or elements) was constrained by grouping voxels into 7-element star-shaped kernels or 27-element cube shaped kernels to loosely mimic the reticular clustering of IP_3R and RyR labeled voxels in the deconvolved images.

4.2.9 Statistical Analysis: Values are expressed as mean ± standard error (SE) with the number of replicates indicated for each experiment. Means were compared with the most robust test appropriate to each experimental design subject to validation of statistical assumptions. For comparison of greater than two means ANOVA was used with pair-wise comparisons made by Bonferroni planned comparisons (i.e., p-values use Bonferroni corrected error). Data was compiled and analyzed using GraphPad Prism 4.0 in coordination with Microsoft Excel. NCSS was used to perform statistical tests. Significance was determined by an α-value of 0.05.

4.3 RESULTS:

4.3.1 Mitochondria detect activation of IP_3R and RyR by purinergic stimulation. To investigate the contributions of IP_3R and RyR to ATP-mediated SR Ca^{2+} release, we measured $[Ca^{2+}]_{MT}$ responses to ATP following pharmacological blockade of IP_3R or RyR. Under our experimental conditions, Ca^{2+} release from IP_3R is selectively blocked by 2-APB (220) and Ca^{2+} release from RyR is blocked by procaine (108;110) (for control experiments see Figure 4.9). Pre-incubation with 2-APB (75μM) reduced the peak ATP-mediated $[Ca^{2+}]_{MT}$ elevation to 67 ± 4% of controls values, and procaine (10mM) reduced the $[Ca^{2+}]_{MT}$ response to 57 ± 6% (Figure 4.1). Together these two blockers reduced the mitochondrial response to 14 ± 6% of controls. These mean values of inhibition suggested that this effect was additive, but careful analysis showed the inhibitory effect of 2-APB and procaine together to be slightly greater than the sum of their individual effects indicating a subtle synergism ($p = 0.049$, 2-sample t-test). We have previously shown that incubation of these cells in Ca^{2+}-free media ($0Ca^{2+}$) selectively depletes a superficial element of the SR that is preferentially associated with the NCX (220). We now find that incubation in $0Ca^{2+}$ had an additive effect with 2-APB, reducing the ATP-mediated responses

from 67 ± 4% to 51 ± 5% of controls. In contrast, the effect of $0Ca^{2+}$ was not additive with the effect of procaine, as procaine and $0Ca^{2+}$ together reduced the ATP-mediated responses to 51 ± 7%. This effect was not statistically different from the inhibition seen with procaine alone (Figure 4.1D), which suggested that $0Ca^{2+}$ caused the depletion of a superficial sub-compartment of the SR that was distinct from the sub-compartment released by the IP_3R and indistinguishable from the sub-compartment released by RyR.

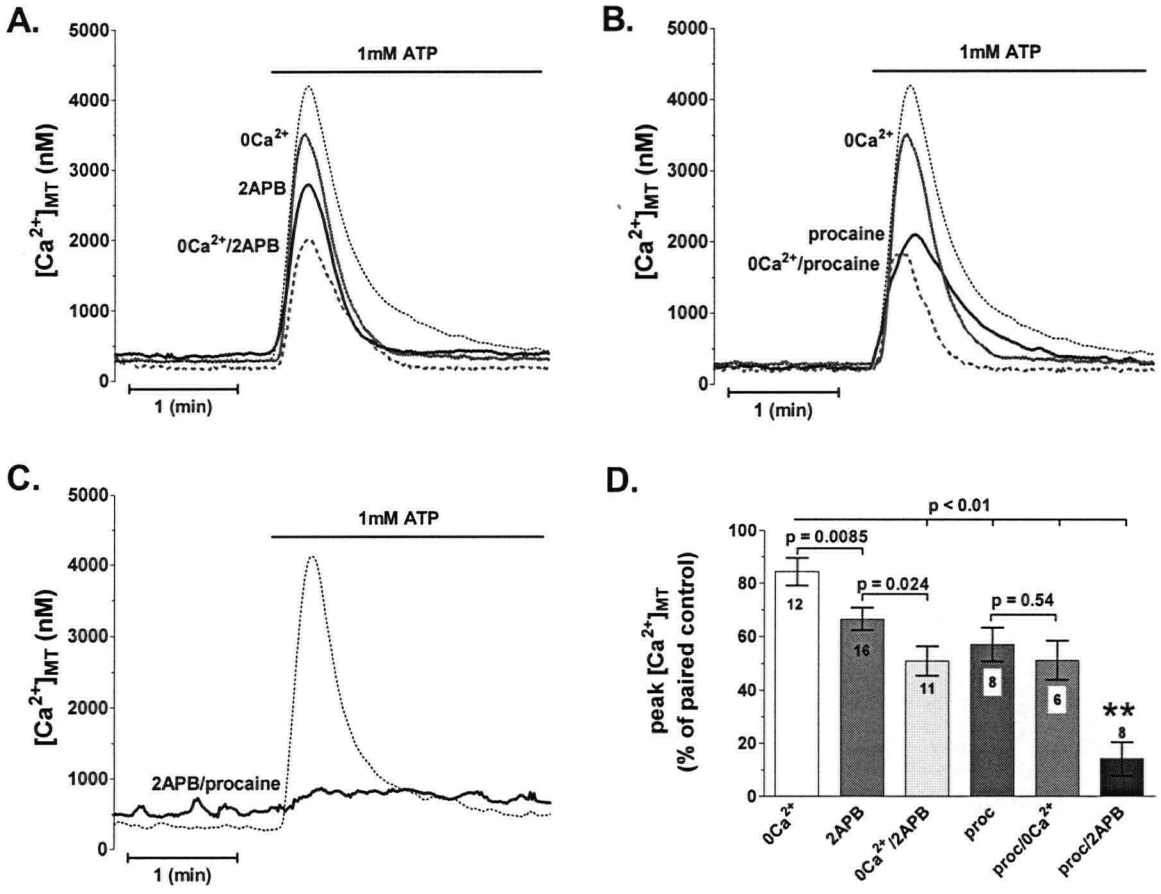

Figure 4.1. Purinergic stimulation increases $[Ca^{2+}]_{MT}$ by activation both IP_3R and RyR. A-C. Average $[Ca^{2+}]_{MT}$ responses to ATP show the individual and combined effects of IP_3R inhibition with 2-APB (75 μM), RyR inhibition with procaine (10 mM) and depletion of peripheral SR Ca^{2+} stores in Ca^{2+}-free solution ($0Ca^{2+}$, 0.1 mM EGTA). The average control response to ATP is shown as the faint dotted trace. D. The effects of each treatment were compared to paired control responses with only ATP, and means of normalized responses were compared by ANOVA. P-values from planned Bonferroni comparison are show between specific treatments.

4.3.2 Cytosolic detection of Ca^{2+}-release from IP_3R and RyR during purinergic stimulation.

Changes in $[Ca^{2+}]_i$ were measured under conditions parallel to those used to measure $[Ca^{2+}]_{MT}$. 2-APB inhibited the cytosolic response to 69 ± 7% of matched controls, similar to its inhibitory effect on the mitochondrial responses (Figure 4.2A). Procaine, however, only reduced the cytosolic response to 80 ± 5% of control responses, much less inhibition than was observed for the mitochondrial response (Figure 4.2B). In contrast to the effects observed on the mitochondrial responses, the inhibition of the $[Ca^{2+}]_i$ response to ATP by 2-APB and procaine

together was highly synergistic (Figure 4.2C). This synergism was consistent with reports that cross-talk between IP_3R and RyR is an important factor in the generation of physiological cytosolic Ca^{2+} signals (30;87;114).

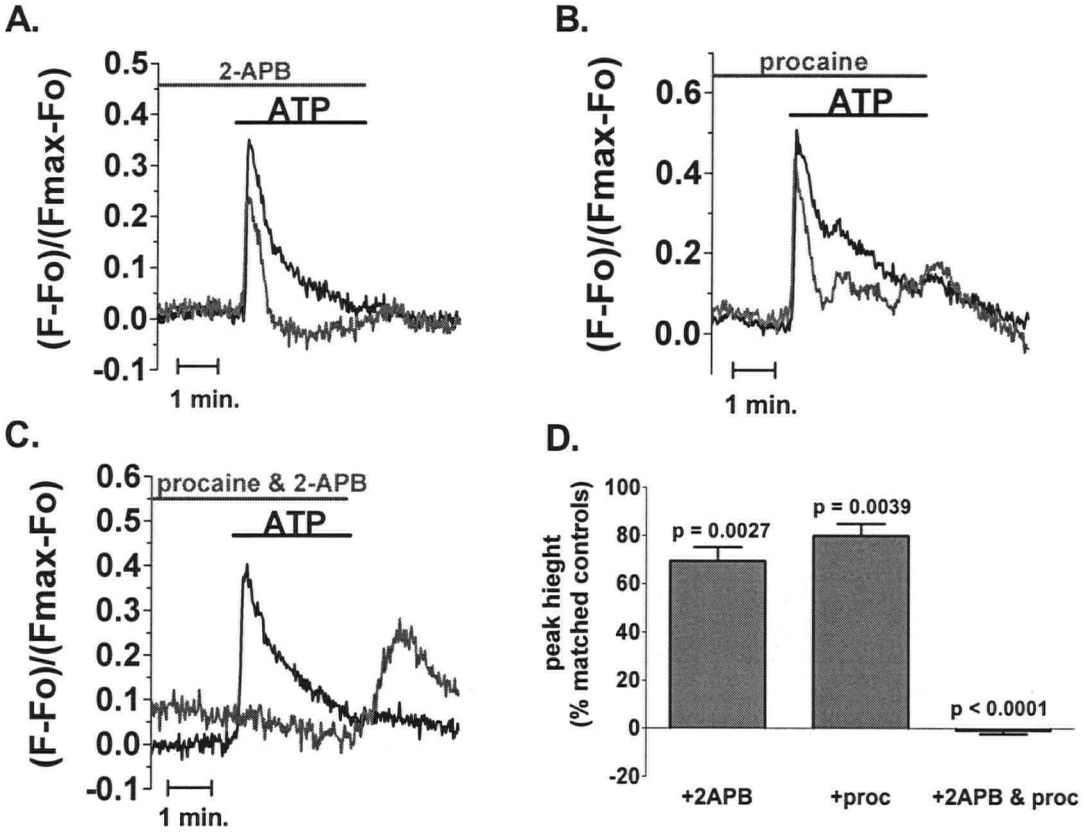

Figure 4.2. Both IP_3R and RyR contribute to the ATP-mediated elevation of cytosolic Ca^{2+}. A-C. Changes in $[Ca^{2+}]_i$ in response to ATP (1 mM) were reported by transiently expressed inverse-pericams in the absence (black traces) or presence of 2-APB (75 μM) and/or procaine (10 mM) (grey traces) as indicated. On average, 2-APB and procaine reduced responses to 71% and 79% of their respective controls. **D.** Quantification of the effects of 2-APB and procaine by two sample t-tests. 2-APB (n = 25) reduced responses to 71% of respective controls (n = 32). Procaine (n = 36) reduced responses to 79% of respective controls (n = 49). 2-APB and procaine together (26) reduced responses to -0.5% of controls (31). Data show as mean ± SE. n equals number of cells analyzed from at least 3 independent experiments.

4.3.3 Mitochondrial stimulation by IP_3R and RyR as a common response to vasopressor agonists. The above results obtained with ATP led us to test whether stimulation of mitochondria by IP_3R and RyR is a general phenomenon common to phospholipase lipase C-coupled vasopressor agonists in VSM. [ARG^8]-vasopressin (AVP) was used to stimulate SR Ca^{2+} release and the contributions of IP_3R and RyR to $[Ca^{2+}]_{MT}$ elevations were dissected as for ATP-mediated stimulations. AVP stimulated Ca^{2+} release from both channel types (Figure 4.3A&B), but the 2-APB/procaine synergy was more obvious in the mitochondrial response to AVP (Figure 4.3C). Statistical analysis showed that $0Ca^{2+}$ had an additive effect with 2-APB but not procaine (Figure 4.3D). Given the similarities in the mitochondrial responses to ATP- and

AVP-mediated SR Ca^{2+} release, we further investigated whether the two PLC-coupled receptors stimulated the same population of mitochondria by analyzing their cross-consumption of aequorin (156). Aequorin luminescence generated in response to AVP or ATP was reduced if cells were first stimulated with the other agonist (Figure 4.4A). Comparison of the raw aequorin luminescence with the calibrated $[Ca^{2+}]_{MT}$ elevations (Figure 4.4B) confirmed that vasopressin could reduce the amount of aequorin available for ATP to activate, without changing the amplitude of the $[Ca^{2+}]_{MT}$. This indicated that in addition to stimulating similar patterns of IP_3R and RyR activation, the two agonists stimulated overlapping populations of mitochondria.

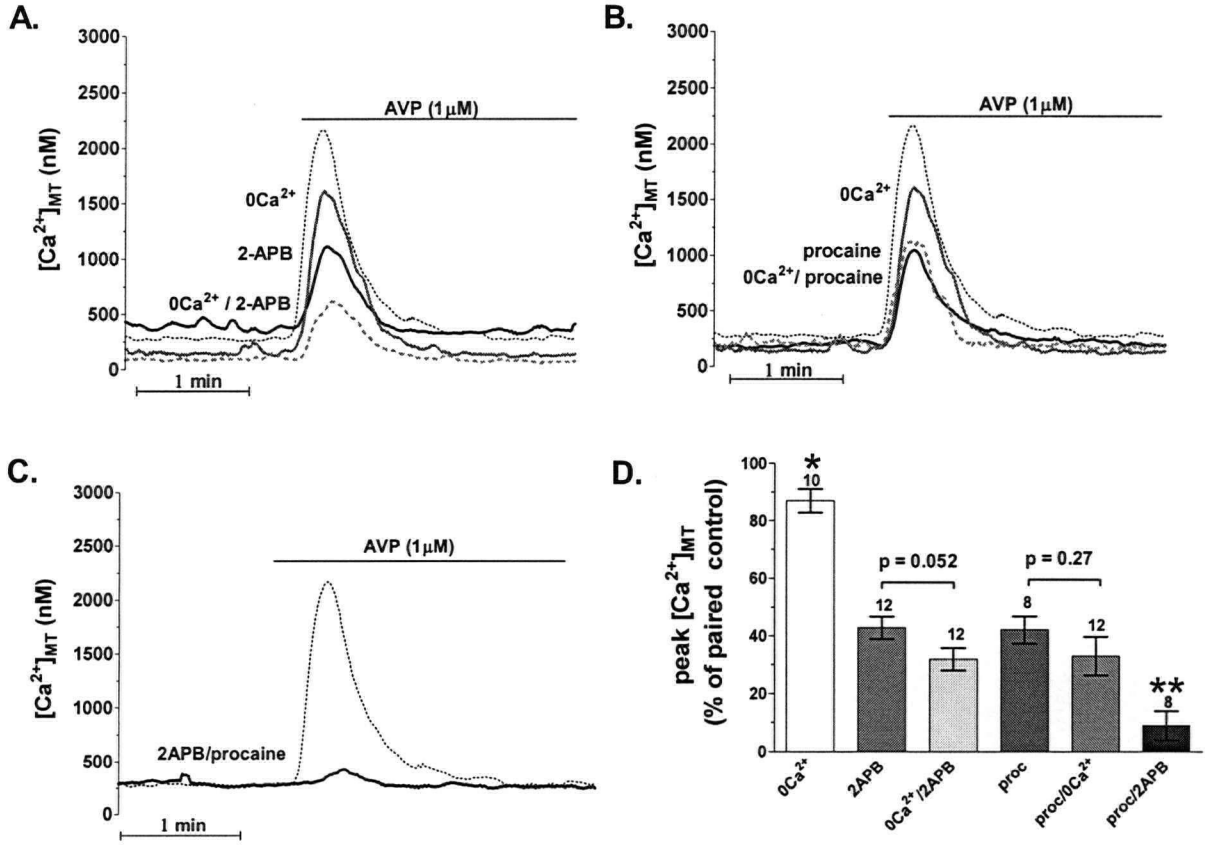

Figure 4.3. Activation of V_1 vasopressin receptors increases $[Ca^{2+}]_{MT}$ by activation both IP_3R and RyR. A-C. Average $[Ca^{2+}]_{MT}$ responses to AVP show the individual and combined effects of IP_3R inhibition with 2-APB (75 μM), RyR inhibition with procaine (10 mM) and depletion of peripheral SR Ca^{2+} stores in Ca^{2+}-free solution ($0Ca^{2+}$, 0.1 mM EGTA). The average control response to AVP is shown as the faint dotted trace. D. The effects of each treatment were normalized against paired control responses with only AVP, and means of normalized responses were compared by ANOVA. P-values from planned Bonferroni comparison are show between specific treatments.

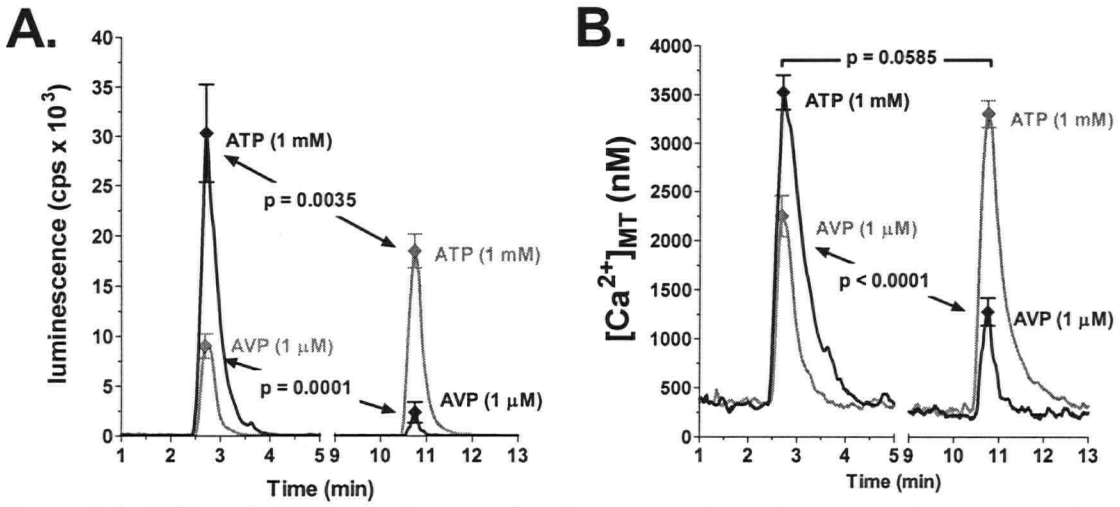

Figure 4.4. ATP and AVP stimulate overlapping populations of mitochondria. Averaged mitochondrial responses are shown from cells that were consecutively stimulated with ATP and then AVP (black traces, n = 4) or AVP followed by ATP (grey traces, n = 6). **A.** Analysis of aequorin luminescence by two sample t tests. **B.** Analysis of calibrated changes in $[Ca^{2+}]_{MT}$ by two sample t tests. In both cases, average traces are shown with mean ± SE at peaks.

4.3.4 Imaging IP_3R and RyR distribution in RASMC. In cells dual-labeled for IP_3R and RyR, both release channels were widely expressed throughout the cell (Figure 4.5A&B), but direct comparison of the two labels indicated several consistent differences in their subcellular distribution. Ryanodine receptors were diffusely expressed throughout the cell with some degree of peri-nuclear accumulation (Figure 4.5B), while high concentrations of IP_3R were observed at the cell periphery and in striations running across the cell (Figure 4.5A). These striations were reminiscent of actin stress fibers, which we subsequently labeled with fluorescently-conjugated phalloidin (Figure 4.5C). In merged images of IP_3R, RyR and phalloidin, the IP_3R, but not RyR, were preferentially distributed with actin filaments (Figure 4.5D). This gross difference in the distribution of IP_3R and RyR at the level of the whole cell provided direct evidence for the localization of IP_3R and RyR to different SR elements in VMSC.

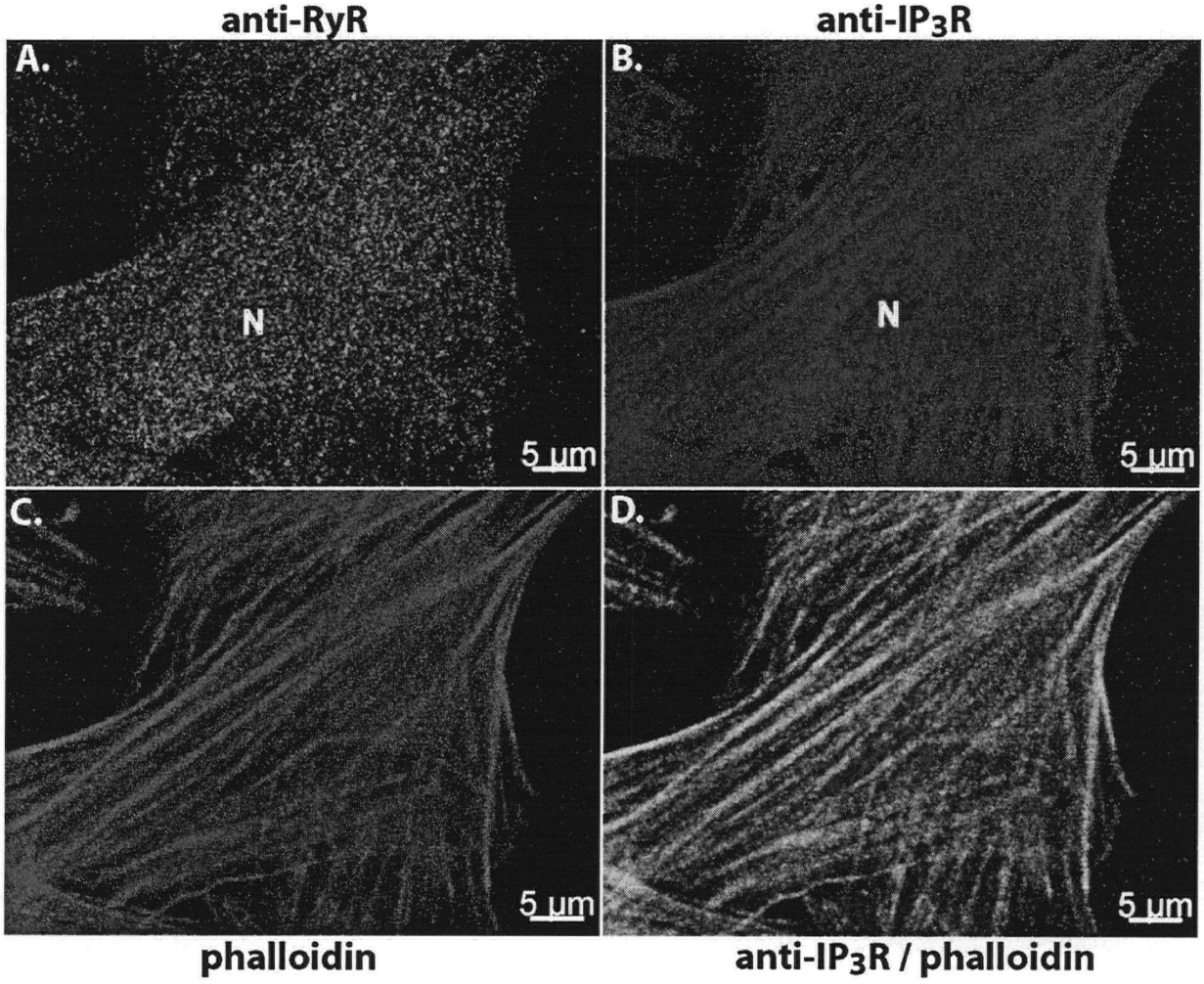

Figure 4.5. Subcellular distribution of IP_3R, RyR and actin in RASMC. A representative cell is shown in which (A) RyR-1/2 and (B) IP_3R were immuno-fluorescently labeled and (C) F-actin was labeled with phalloidin. (D) Merging the IP_3R (red) and actin images (green) confirmed that IP_3R are extensively associated with actin filaments (yellow). Images representative of 9 cells imaged from >3 independent experiments. IP_3R striations were also seen in the absence of phalloidin. N - nucleus.

4.3.5 Localization of IP_3R and RyR to separate SR elements. With the assistance of digital deconvolution and 3D-reconstruction, analysis of the image volumes at higher magnification revealed that IP_3R and RyR were largely localized to separate reticular structures (Figure 4.6A-F). The two SR labels were highly interlaced but often separated by 300 - 400 nm, and analysis of their co-localization showed that the IP_3R and RyR were not extensively co-localized (Table 4.1, see methods). Moreover, co-localization events often occurred between perpendicular strands of IP_3R and RyR label (Figure 4.6F), which were likely due to separate elements of the SR passing over and under each other. The IP_3R- and RyR-labeled reticular networks and their minimal overlap are more clearly illustrated in 3D reconstructions (Figure 4.6G-I). This distribution of IP_3R and RyR provided direct evidence to support the hypothesis that the two types of release channels are physically localized to separate SR elements, which raised the

question of why procaine inhibited the mitochondrial responses to a greater extent than cytosolic responses when 2-APB had a very similar effect on the two responses. To rule out the possibility that this was due to a preferentially localization of RyR with mitochondria, we analyzed mito-RyR and mito-IP_3R co-localization.

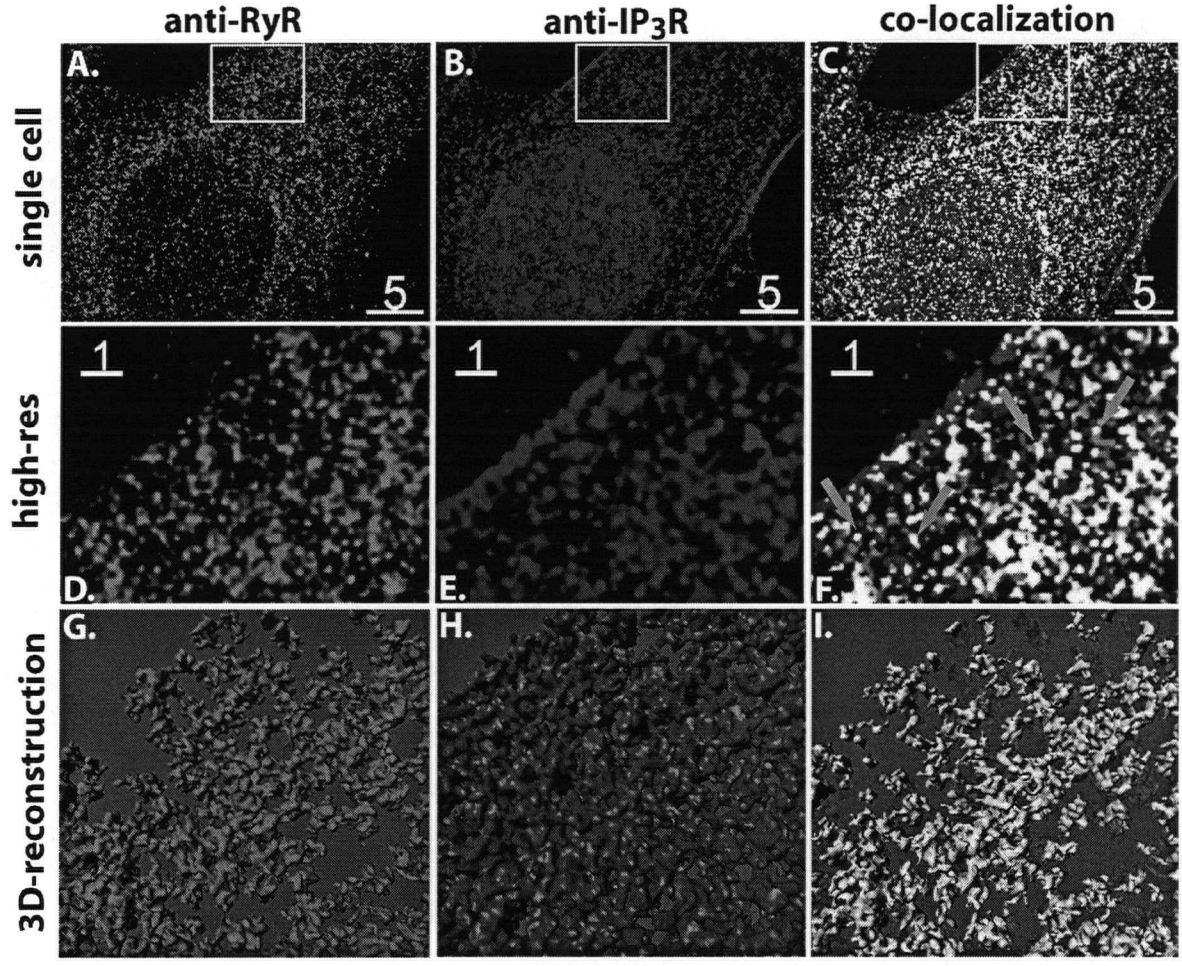

Figure 4.6. Co-localization analysis of IP_3R & RyR. (A-C) Single deconvolved images at the middle of a representative cell are shown for RyR (A, green), IP_3R (B, red) and their co-localization (C, white). The nucleus is prominently labeled by the IP_3R anti-body. Scale bar is 5 μm. (D-F) Higher magnification of the boxed region from A-C reveals the distinct separation of RyR (green) and IP_3R (red) labeled elements on separate reticular networks. (F) Co-localization events (white) often occurred at orthogonal intersections (blue arrows) of RyR andIP_3R. The closely inter-twined reticular RyR (G, green) and IP_3R (H, red) networks are more evident in 3-D reconstructions. (I) 3-D reconstruction of c-localization events (white) is shown relative to the RyR (transparent green).

Table 4.1. Co-localization statistics of IP_3R and RyR in dual-labeled cells.

I.		% co-localization	
Label A	Label B	A with B	B with A
IP_3R-1	RyR-1/2	19 ± 1	34 ± 3

4.3.6 Visualizing the relationship of IP_3R and RyR with mitochondria. We investigated the spatial relationships between the two release channels and mitochondria by dual-labeling the RyR and IP_3R in cells expressing mito-targeted GFP. These images revealed extensive association of the mitochondria with IP_3R and RyR, but they did not indicate a preferential association of mitochondria with RyR (Figure 4.7A-C). Co-localization analysis confirmed that similar portions of the RyR and IP_3R labeled SR were associated with the mitochondria (14 ± 1% and 17 ± 2% respectively, n = 17 cells). To better understand the spatial relationship of the RyR and IP_3R with the mitochondria, we generated 3D-models of the mitochondria in each cell and used the co-localization results to paint the portions of the mitochondria that were closely associated with either IP_3R (Red), RyR (yellow) or both (white) (Figure 4.7D-F). This method provides a more detailed visualization than can obtained from single images and allowed us to observe that most of the mitochondria labeled voxels were associated with an IP_3R or RyR label (41 ± 2% and 34 ± 3% of mitochondrial surface, respectively). In fact, many mitochondria appeared to be associated with both SR labels.

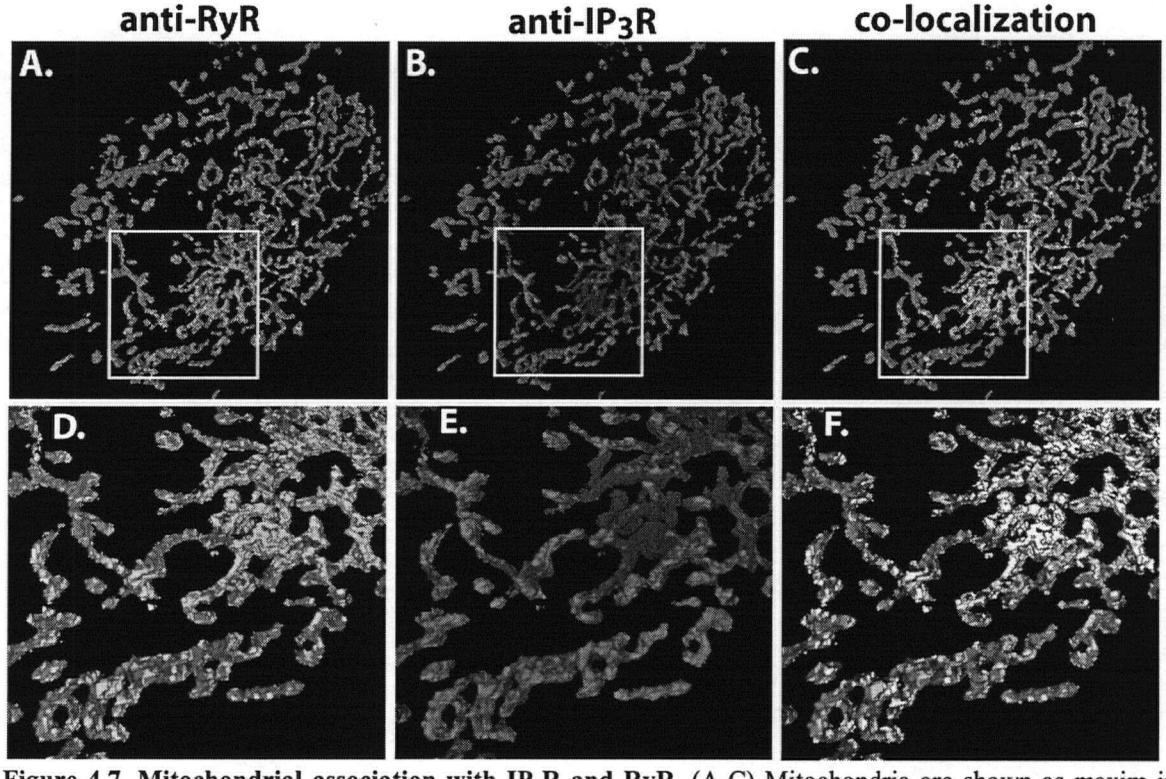

Figure 4.7. Mitochondrial association with IP_3R and RyR. (A-C) Mitochondria are shown as maxim intensity projections (green), upon which the co-localization of RyR (yellow), IP_3R (red) or both (white) is painted. (D-F) At higher magnification the association it can be seen that most mitochondria associate with RyR (D, yellow) and or IP_3R (E, ref). (F) For mitochondria associated with both RyR (yellow) and IP_3R (red), co-localization (white) of the two SR labels is common.

4.3.7 Preferential co-localization of IP_3R and RyR near mitochondria. Based on these observations and previous reports that IP_3R and RyR can be found in high concentrations near mitochondria, we hypothesized that IP_3R-RyR co-localization occurs more frequently for SR elements neighbouring the mitochondrial surface than in the bulk cytosol. On a cell by cell basis, we statistically analyzed the co-localization between the IP_3R, RyR and mitochondria (see Table 4.2). The IP_3R- and RyR-labeled voxels that were co-localized with the mitochondria were then analyzed for co-localization with each other to isolate the IP_3R-RyR co-localization events associated with the mitochondria (Figure 4.7C&F). This analysis revealed that co-localization was significantly more frequent (1.4-fold) for IP_3R and RyR specifically associated with the mitochondria than the average IP_3R-RyR co-localization across the entire cell.

Table 4.2. Co-localization statistics of IP_3R and RyR with mitochondria.

I.		% co-localization	
Label A	Label B	A with B	B with A
mitochondria	IP_3R-1	41 ± 2 (IP_3R_{mito})	14 ± 1
mitochondria	RyR-1/2	33 ± 3 (RyR_{mito})	17 ± 2
IP_3R-1	RyR-1/2	33 ± 3 [a]	45 ± 2 [b]
IP_3R_{mito}. [c]	RyR_{mito}. [c]	45 ± 3 [a]	56 ± 3 [b]
II.			
% of mitochondrial voxels with IP_3R-RyR co-localization			19 ± 2 [d]

a & b For values with matched superscripts paired t-test gives $p < 0.0001$, n = 16-18 pairs.
c mito-IP_3R & mito-RyR co-localization events were co-localized with each other.
d = (IP_3R_{mito}) x (IP_3R_{mito} with RyR_{mito}) = (RyR_{mito}) x (RyR_{mito} with IP_3R_{mito})

This mitochondria-associated IP_3R-RyR co-localization was compared with that which might be expected by random co-incidence of the two labels given the total number of mitochondrial voxels and percent of those voxels that were also labeled for the IP_3R or RyR. If the IP_3R and RyR voxels were distributed across the mitochondria completely randomly, then the product of the percent of mitochondrial voxels that co-localized with IP_3R (41 ± 2%) and RyR (33 ± 3%) should *predict* the percent of the mitochondrial voxels in which IP_3R-RyR co-localize (14 ± 2%, mean of 16 cells). However, the mitochondria associated IP_3R-RyR co-localization measured from the images was 19 ± 2% (mean of same 16 cells), which was significantly (1.35 times) more frequent than would predicted for a purely randomly con-incidence of a similar number of voxels (paired t-test, $p < 0.0001$, n = 16 cells). However, fluorescently labeled voxels do not distribute purely randomly. Rather, they cluster into the shape of the labeled structure or into small kernels in the case of sub-resolution structures such as ion channels. We created an algorithm to generate 3D-arrays (representing the mitochondrial volume) and calculate the co-localization of randomly placed "IP_3R" and "RyR" voxels (see methods). When individual IP_3R

and RyR voxels (41% and 33% of the model volume, respectively) were randomly distribute, the predicted co-localization was simply the product of the percent of IP_3R- and RyR-labeled voxels (~14%) (Figure 4.8A). However, when voxels were clustered into simple 7-voxel star-shaped kernels or 27-voxel cube-shaped kernels, the extent of "random" co-localization increased dramatically, with the actual shape of the kernel having little effect (Figure 4.8A&C). The extent of random co-localization was also sensitive to the cross-sectional area of the modeled volume. When this cross-section approximated the size of imaged mitochondria, the random co-localization of clustered voxels closely matched the mitochondria-associated IP_3R-RyR co-localization measured from our images (1.35 - 1.45-fold greater than for individually distributed voxels). Thus the IP_3R-RyR co-localization associated with the mitochondria was likely no greater than could be expected by random co-incidence given the density of the two labels within the mitochondrial volume. We must stress however, that this issue is distinct from the observation that the incidence of IP_3R-RyR co-localization near the mitochondria was greater than the average incidence across the entire cell.

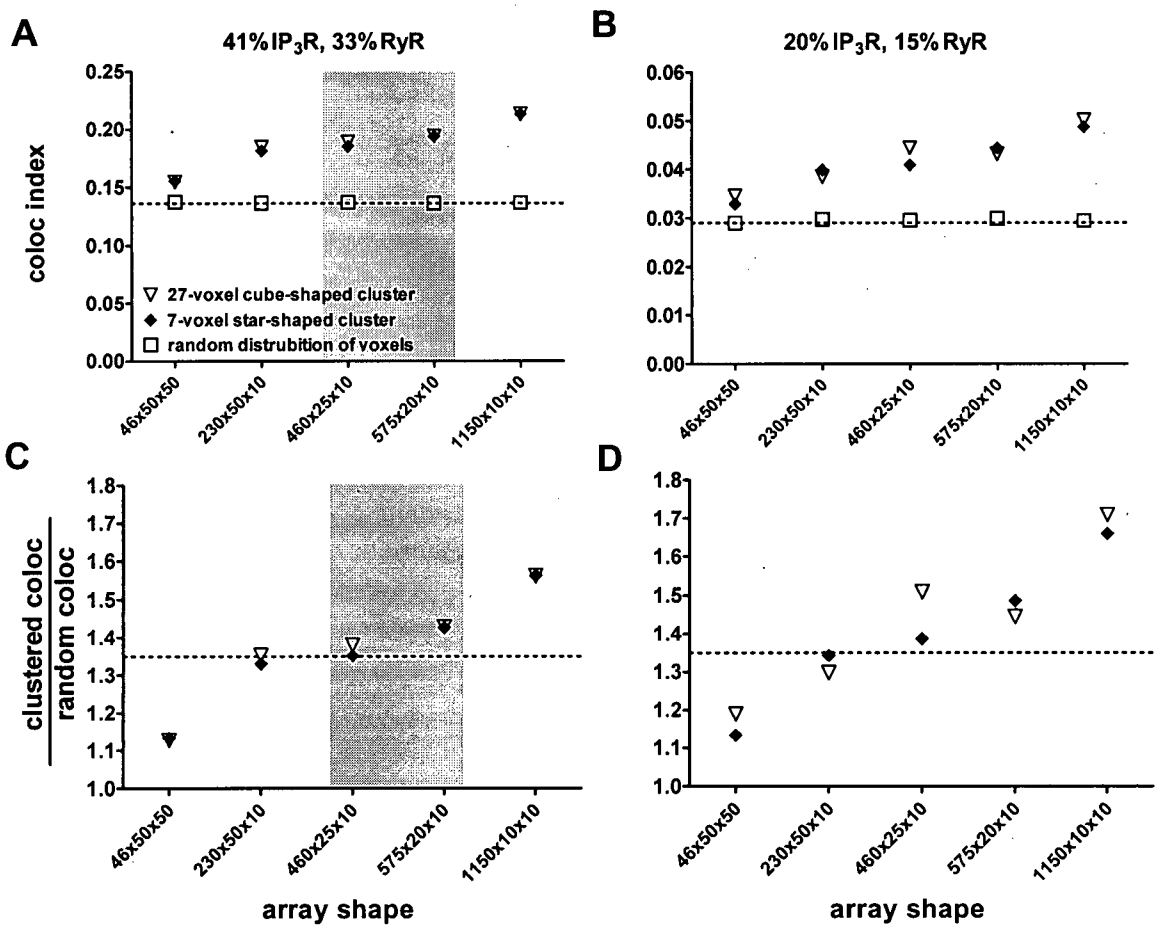

Figure 4.8. Modeling the effect of voxel clustering on random co-localization of mitochondria associated IP_3R and RyR. Co-localization was assessed after randomly filling two computer-generated 3D arrays of 115,00 voxels (i.e., mean mitochondrial volume analyzed) with IP_3R and RyR at densities equal to (A,C) or half of that which was measured during image analysis (B, D). (A, B) Co-localization was assessed when "IP_3R" and "RyR" voxels were randomly distributed as individual voxels, 7-voxel star-shaped clusters or 27-voxel cubic clusters. The dotted line shows the "random" co-localization predicted by multiplying the fraction of voxels labeled for IP_3R and RyR. (C, D) Co-localization of clustered voxels was normalized against co-localization of individually distributed voxels. Error associated with repeated simulations is less than 0.1%.

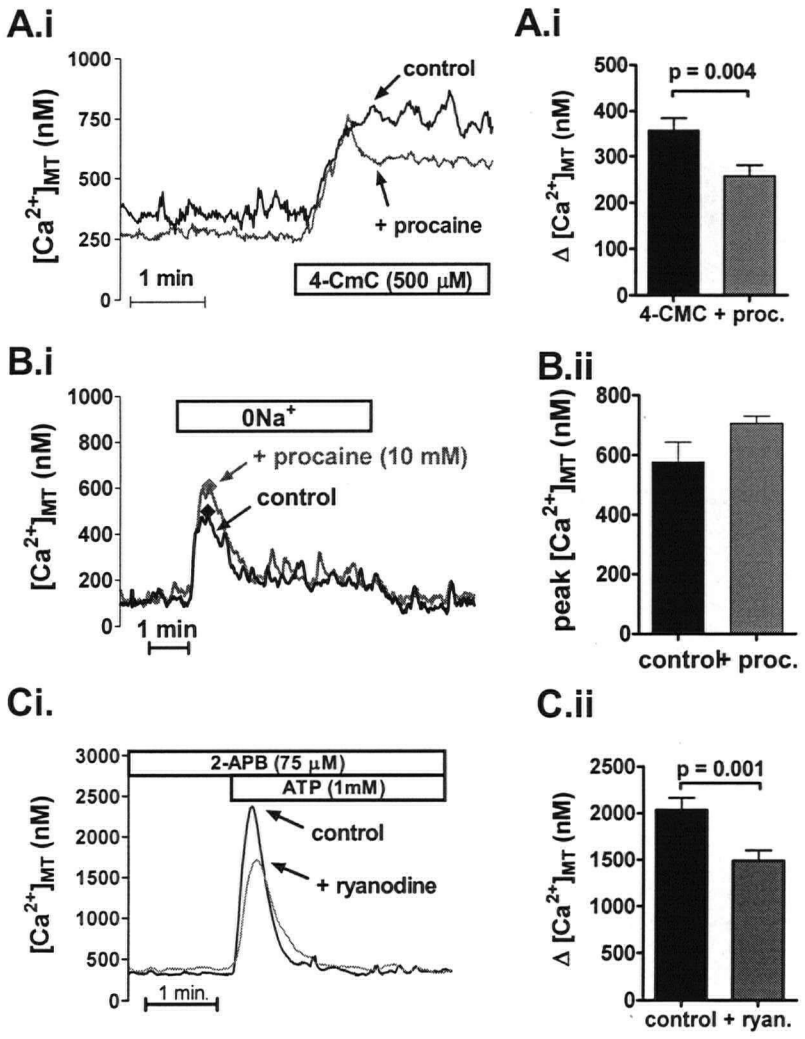

Figure 4.9. Assessing the selectivity of procaine for RYR versus mitochondria. A) Representative traces showing procaine-mediated inhibition of the $[Ca^{2+}]_{MT}$ elevation upon activation of RyR with 4-chloro-*m*-cresol (4-CmC). Aii) The effect of procaine was significant as determined by a two-sample t-test (n = 4 control, 6 procaine). B) Iso-osmotic replacement of extracellular Na^+ with n-methyl-D-glucamine (145 mM) causes Ca^{2+} influx via the Na^+/Ca^{2+}-exchanger which is taken up by mitochondria. Procaine did not inhibit the mitochondrial Ca^{2+} uptake in response to $0Na^+$ (n = 3 control, 3 procaine). C) When IP_3R are inhibited by 2-APB, ryanodine (100μM, 30 min) further reduces the mitochondrial response to ATP-mediated SR Ca^{2+} release. Bii) The effect of ryanodine was assessed by a paired t-test (n = 9 pairs).

4.4 DISCUSSION:

Ca^{2+} signaling in smooth muscle is highly dependent on the SR, which is composed of membrane bound elements exhibiting heterogeneous expression of Ca^{2+} pumps, channels and buffer proteins (136;157;164;181). In this investigation we address a long standing question in smooth muscle physiology, which is whether RyR and IP_3R are functionally and structurally localized to the same or separate elements of the SR. In vascular smooth muscle this issue is complicated in 1) that the relative contribution of RyR and IP_3R to Ca^{2+} signaling varies between different blood vessels (176) and 2) that the fundamental principles governing the interaction of IP_3R and RyR in VSM are not completely elucidated. Here we present functional and imaging data indicating that IP_3R and RyR are localized to separate elements of the SR in RASMC. Moreover, we propose that the extensive mitochondrial association with the SR locally increases the juxtaposition of IP_3R and RyR on separate SR elements such the IP_3R-RyR cross-talk differentially influences cytosolic and mitochondrial Ca^{2+} signaling.

4.4.1 Functional Localization of IP_3R and RyR in VSM. Despite the fact that RyR can be widely distributed through VSM (30;31), they are best known for their peripheral juxtaposition near and modulation of Ca^{2+}-sensitive Cl^-- and K^+-channels on the adjacent plasmalemma (254). In some VSM the peripheral SR also interacts with the NCX to mediate preferential Ca^{2+} extrusion by the NCX over the plasmalemmal Ca^{2+} ATPase (3;162). We have previously shown this SR-NCX coupling to cause the NCX to extrude Ca^{2+} released from a specific sub-compartment of the SR in the absence of extracellular Ca^{2+} (220), and our current data indicate that this SR sub-compartment releases Ca^{2+} via RyR, rather than IP_3R (also see (138)). This conclusion is based on the observation that 2-APB and $0Ca^{2+}$ treatment additively reduced the $[Ca^{2+}]_{MT}$ elevation in response to ATP and AVP. In contrast, removal of extracellular Ca^{2+} did not have an additive effect with procaine and caused much less inhibition of the $[Ca^{2+}]_{MT}$ elevations than did procaine. This indicated that mitochondria took-up Ca^{2+} released from RyR-associated SR throughout the cell, while only a peripheral portion of the RyR-associated SR was directly coupled to the NCX. This latter point is corroborated by direct observation of widespread RyR distribution throughout the cell, consistent with previous investigations in VSM (30;49;136). Further more, this underscores an important principle that the SR is composed of functionally distinct sub-domains (85).

The IP_3R can also be found throughout the cell. Immuno-gold labeling of the IP_3R in aortic smooth muscle revealed gold particles localized to both central and peripheral SR (164). Immunocytochemistry has revealed a uniform distribution of IP_3R in a fine network of deep and peripheral SR in portal vein myocytes (31), with some evidence for isoform specific patterns of localization (77;164;224;244). We also observed that IP_3R were localized to a fine network in both the peripheral and central SR, and we found that IP_3R were highly concentrated along actin stress fibers traversing the cell, which was consistent with previous reports (90;216). In terms of structure-function relationships, this pattern of IP_3R distribution suggests that IP_3R may be strategically localized to regulate myofilament contraction. Furthermore, despite extensive localization of IP_3R to the sub-plasmalemmal SR, the aequorin data suggests that IP_3R do not interact with the NCX, which emphasizes the notion that functional coupling of the SR and NCX requires highly localized interactions (23;176). This observation and the strikingly different patterns of IP_3R and RyR distribution at the level of gross subcellular organization (figure 4.5) strongly indicate that the IP_3R and RyR are localized to separate elements of the SR.

To pursue this issue in greater detail, we have provided a detailed co-localization analysis of IP_3R and RyR in vascular SMC. At high magnification, the distribution of IP_3R and RyR in fine reticular networks was consistent with previous reports (30;31;88). By examining the IP_3R and RyR in 3-D volumes of digitally deconvolved images at high magnification, we found that the IP_3R and RyR labels were largely distributed on separated but interlaced reticular networks that run throughout the cell. Statistical analysis confirmed that IP_3R and RyR were not highly co-localized throughout the cytosol (see table 4.1), but without a reliable marker of the cell membrane it is difficult to estimate the density of the two labels within the cell volume and therefore to mathematically assess whether the extent of co-localization was greater than would be expected by chance given the density and clustering of the two SR labels. We can however assume the co-localization analysis likely overestimates the incidence of co-localization since the width of the SR (~50-100 nm in diameter) would be exaggerated by the limited resolution of optical microscopy (full-width half-max: ~300 nm x-y, ~700 nm axial). Moreover, co-localization often occurred at orthogonal intersections of the IP_3R/RyR labels indicating that some co-localization events were due to separate elements of the SR passing over and under each other at distances below the axial resolution of the deconvolved volumes. Overall the evidence strongly argues in favour of IP_3R and RyR being localized to closely neighbouring but separate SR elements with distinct Ca^{2+} stores. While we cannot exclude the possibility that IP_3R and RyR labeled SR elements might be joined by unlabeled sections of SR, our current evidence is consistent with functional studies from a variety of VSM, which are considered below in the context of functional interactions between IP_3R and RyR observed in this study.

4.4.2 Functional interaction of IP_3R and RyR. Three basic models have been presented for the functional interaction of IP_3R and RyR in smooth muscle (153). The two channels could communicate 1) through a shared SR lumen, 2) through an interaction of SR membrane proteins, and or 3) through diffusible cytosolic factors (such as Ca^{2+}). If we were to consider only the changes in $[Ca^{2+}]_i$ and the synergistic effect of 2APB and procaine, we might conclude that the IP_3R and RyR release Ca^{2+} from a single store such that inhibition of either type of release channel would increase the Ca^{2+} that was available for the other channel to release. Indeed, this model is consistent with the existing data from most types of smooth muscle (153). However, when we also consider the distinct patterns of IP_3R and RyR localization discussed above and the near lack of synergy between 2APB and procaine on SR-dependent changes in $[Ca^{2+}]_{MT}$ reported here, then we would conclude that IP_3R and RyR in these cultured rat aortic smooth muscle cells

release Ca^{2+} from separate SR sub-compartments and interact via allosteric modulation of channel gating by locally generated $[Ca^{2+}]_i$ gradients.

The open probability of IP_3R and RyR are regulated by the $[Ca^{2+}]$ in the neighbouring cytosol and the SR lumen. Type 1 IP_3R (the predominant VSM isoform) have an EC_{50} of ~300 nM Ca^{2+}, and Ca^{2+} exerts an inhibitory effect at concentrations greater than ~1μM (26;183). In contrast, Ca^{2+}-induced activation of RyR *in situ* is triggered by $[Ca^{2+}] \geq$ ~1μM and plays an important role in the stimulation of rapid elevations of $[Ca^{2+}]_{MT}$ (108;160). This threshold is reduced experimentally by 4-chloro-*m*-cresol or caffeine and endogenously by cyclic-ADP ribose, which likely accounts for the elevation of $[Ca^{2+}]_{MT}$ elicited by both ATP and AVP in the presence of 2-APB. In rat portal vein, photolysis of caged-IP_3 activates IP_3R at global $[Ca^{2+}]_i <$ 200 nM, suggesting that the micromolar $[Ca^{2+}]_i$ threshold to activate RyR is restricted to cytosolic microdomains between neighbouring IP_3R and RyR (9;30;31;114;160). This local cross-talk is required for the initiation of both agonist-induced and spontaneous cytosolic Ca^{2+} waves, in which IP_3R provide the trigger Ca^{2+} to stimulate RyR and convert Ca^{2+} sparks into waves (87;134;199). Along the Ca^{2+} wave front, propagating activation of Ca^{2+} release units has been resolved at ~1-2 μm separation, but the trigger Ca^{2+} released from IP_3R has yet be resolved from the initiating Ca^{2+} spark (87). Here we found that IP_3R and RyR in deconvolved images of fixed cells were often separated by less than 400 nm, which provides a structural basis for the technical difficulty of imaging the local IP_3R-mediated $[Ca^{2+}]_i$ elevation that is thought to convert Ca^{2+} sparks (averaging 1.5–2 μm in width) into Ca^{2+} waves (9;88;114).

Mitochondrial aequorin provides an alternative and sensitive, if indirect, indicator of localized SR Ca^{2+} release (191;192), and it has previously been used in aorta smooth muscle cells to demonstrate that IP_3R and RyR are functionally coupled with mitochondria (160;220). In one of these studies it was concluded that mitochondria did not detect IP_3R-RyR cross-talk in RASMC because $[Ca^{2+}]_{MT}$ responses to IP_3 and caffeine persisted in the presence of ryanodine and heparin, respectively (160). However, in similar rat aorta SMCs we find that mitochondria do detect IP_3R-RyR cross-talk based on: 1) the synergistic inhibition of ATP-mediated elevations of $[Ca^{2+}]_{MT}$ and 2) the preferential co-localization of IP_3R and RyR near mitochondria. Moreover, novel insights into localized IP_3R-RyR crosstalk can be drawn from the differences in the extent of 2-APB/procaine synergy on the mitochondrial versus cytosolic responses. Upon Ca^{2+} release into the cytosolic microdomain between the SR and closely apposed mitochondria

the local $[Ca^{2+}]_i$ is thought to exceed 10 μM (55), which facilitates activation of the mitochondrial Ca^{2+} uniporter and mitochondrial Ca^{2+} buffering (98;192). This same local elevation of $[Ca^{2+}]_i$ will also cause IP_3R facing the mito-SR junctional space to be more rapidly inactivated relative to IP_3R localized elsewhere on the SR. Consistent with this model, we found that IP_3R alone (i.e., in the presence of procaine) generated ~80% of the parallel ATP-mediated $[Ca^{2+}]_i$ elevations, and only ~55% of the normal mitochondrial response. In contrast, the elevation of $[Ca^{2+}]_i$ by RyR alone (i.e., in the presence of 2APB) was well correlated with the parallel elevation in $[Ca^{2+}]_{MT}$ (both ~65% of respective controls), which is consistent with reports that inactivation of RyR in VSM is governed by time-dependent inactivation more than by local $[Ca^{2+}]_i$ elevations or decreases in $[Ca^{2+}]_{SR}$ (9;88). Thus, the pronounced 2-APB/procaine synergy on $[Ca^{2+}]_i$ elevations likely indicates that Ca^{2+} release from IP_3R normally activates neighbouring RyR, from which Ca^{2+} release causes feedback inhibition of the IP_3R (30;31;114). This provides a simple explanation as to why IP_3Rs alone (in the presence of procaine) were able to generate of ~80% of normal cytosolic Ca^{2+} elevations. At the Mito-SR junctions, however, impaired diffusion of Ca^{2+} released from IP_3R likely causes sufficient auto-inhibition such that RyR do not cause detectable inhibition of IP_3R. However, IP_3R-RyR co-localization is significantly (1.4-times) more likely near mitochondria, and IP_3R alone were only capable of generating ~65% of normal $[Ca^{2+}]_{MT}$ responses to ATP or AVP. Thus, we propose that IP_3R-mediated activation of RyR plays a critical role in generating physiological $[Ca^{2+}]_{MT}$ signals in vascular smooth muscle cells, which is currently under further investigation (160).

The model described above is based on the comparison of aequorin and pericam responses and the selectivity of the pharmacological agents used, which warrants consideration. Since aequorin and the inverse pericam have different mathematical relationships to changes in $[Ca^{2+}]$, the effects of 2-APB and procaine were normalized against control responses. 2-APB inhibited the cytosolic and mitochondrial responses to similar extents suggesting that the relative response of the two reporters can be reliably compared. Since the transient phase of ATP- and AVP-mediated responses is primarily due to SR Ca^{2+} release (220) and 2-APB and $0Ca^{2+}$ additively reduced the mitochondrial responses, the action of 2-APB as used here was likely on IP_3R rather than store-operated Ca^{2+} channels (34). While procaine is commonly used as a Na^+-channel blocker in non-excitable cells it has been used to inhibit RyR in muscle (108). Procaine did not directly impair mitochondrial Ca^{2+} uptake as the $[Ca^{2+}]_{MT}$ elevation in response to NCX-

mediated Ca^{2+} influx was not affected by procaine (Figure 4.9), and the mitochondrial effects of procaine were mimicked by ryanodine (100 μM) (Figure 4.9).

4.4.3 Spatial association of IP_3R and RyR near mitochondria. Important and unresolved physiological questions regarding rapid Ca^{2+} transfer between the SR/ER and mitochondria are whether SR/ER-mitochondria associations occur at specific sites on the opposing membranes and whether the Ca^{2+} handling machinery is localized to these sites. Immuno-labeled electron micrographs show IP_3R and RyR on SR/ER elements neighbouring mitochondria in VMS consistent with our current imaging data (136;164), but whether the concentration of IP_3R and RyR is higher at the SR-mito junctions relative to the rest of the SR remains to be quantified in VSM (see (201)). Since the co-localization analysis used here disregards intensity information after the images are thresholded, we cannot draw inferences on the local concentrations of IP_3R or RyR on the SR, but we can draw inferences on localized concentrations of IP_3R or RyR expressing SR. Specifically, co-localization of IP_3R (~17%) and RyR (14%) voxels associated with the mitochondria was 1.4-times more frequent than the average IP_3R-RyR co-localization throughout the cell. This could be explained by two probable mechanisms: 1) both SR Ca^{2+} release channels could be preferentially associated with common sites on the mitochondria, or 2) an increased density of SR near the mitochondria could increase the random co-incidence of the two labels.

In smooth muscle (vascular and other), mitochondria are often found wrapped in SR (63;176). Quantification of this phenomenon from electron micrographs revealed that 82% of mitochondria are completely enwrapped in SR and that 48% of the average OMM is within 30 nm of the SR in resting tracheal SMC (57). Given the limits of optical resolution, this enwrapping of the mitochondria with SR would be manifest as an increased density or concentration of IP_3R and RyR labeled SR neighbouring the mitochondria. This provides an ultra-structural basis for the increased co-localization of IP_3R and RyR near the mitochondria assuming that overlap of IP_3R and RyR labeled elements of the SR would be more likely where the concentration of SR is increased. However, evidence from a number of cell types indicates that SR/ER-mitochondria associations occur at specific sites on the SR and outer mitochondrial membranes (OMM). In MDK cells a sub-compartment of the ER containing the autocrine-motility factor receptor (AMF-R) preferentially associates with mitochondria in a Ca^{2+}-dependent manner (250), while voltage-dependent anion channels (VDAC), the primary route for

Ca^{2+} permeation across the OMM, appear to be preferentially distributed at close contacts with the ER in HeLa cells (185). Thus it was necessary to determine in our aortic smooth muscle cells whether IP_3R-RyR co-localization events associated with the mitochondria occurred more frequently than might be expected by chance. We developed a simple, but robust, algorithm that randomly distributes two labels within a specified volume and calculates their co-localization. This algorithm indicated that co-localization of two labels that were "randomly" distributed as clusters (9 or 27 voxels in size) was much higher than when the labels were distributed as individual voxels. When the minor cross section of the model mitochondria approximated that of the GFP-labeled mitochondria, the random co-localization closely matched the measured incidence of mito-associated IP_3R-RyR co-localization, which indicated that the incidence of IP_3R-RyR co-localization near mitochondria was not greater than could be expected by chance. Thus the preferential co-localization of IP_3R and RyR neighbouring the mitochondria was not a direct indication of an association with common loci on the mitochondria, but was likely due to an increased concentration of SR near the mitochondria.

4.4.4 Conclusion: In summary, the work presented herein demonstrates a method to assess the localization of IP_3R and RyR to separate SR sub-compartments, which takes into account both structural and functional evidence. Our results further support the functional relevance of localized interactions between mitochondria, IP_3R and RyR, and demonstrate differential roles of IP_3R-RyR crosstalk in the generation of mitochondrial and global Ca^{2+} signals in vascular smooth muscle cells. While the separation of IP_3R and RyR should be further assessed with immuno-electron microscopy, our current findings provide as starting point for functional and electron microscopy studies to further investigate the dynamic nature mito-SR interactions during stimulation of smooth muscle.

CHAPTER V

GENERAL CONCLUSIONS & RECOMMENDATIONS FOR FUTURE WORK

Vascular smooth muscle is essential to the regulation of blood pressure and responds to the neuro-humoural signals that control regional blood flow. It must be able to respond rapidly to the moment-to-moment metabolic demands of specific tissues, while maintaining global vascular tone, which requires constant and exquisite control of cytosolic $[Ca^{2+}]_i$. This thesis focuses on the notion that intracellular Ca^{2+} signals are spatially and temporally partitioned, such that Ca^{2+} can simultaneously modulate contraction and processes such as gene transcription and oxidative metabolism. Great effort has been devoted to understanding how the subcellular architecture of the SR contributes to this partitioning of cytosolic Ca^{2+} gradients. By comparison, mitochondria have received much less attention than the PM and SR regarding the establishment and maintenance of local Ca^{2+} gradients and feedback mechanisms in VSM, despite the fact that mitochondria are able to rapidly sequester Ca^{2+}. This thesis presents novel information regarding the nature of agonist-mediated mitochondrial $[Ca^{2+}]$ elevations specifically in VSM and exploits mitochondria as indicators of localized cytosolic Ca^{2+} elevations.

5.1 IMPLICATIONS OF BASAL Ca^{2+} ENTRY

In recent years basal Ca^{2+} influx into VSMC was attributed to the basal flicker of at last two distinct Ca^{2+} permeable channels. The pharmacological dissection of the leak reported herein suggests that these channels are likely the same channels that are activated by SR Ca^{2+}-depletion and or PLC-coupled receptor activation. Moreover, we provide numerous indirect lines of evidence that this basal Ca^{2+} influx may result from basal SR Ca^{2+} release (from both RyR and IP_3R) and or basal activity of PLC.

Based on our estimate of the basal rate of Ca^{2+} influx, it appears as though VSMC are capable of maintaining low $[Ca^{2+}]_i$ despite considerable Ca^{2+} influx at rest. Given that $[Ca^{2+}]_{subPM}$ was higher than most estimates of bulk $[Ca^{2+}]_i$ at rest, our current findings further support the notion that the superficial SR and mitochondria are able to establish a standing Ca^{2+} gradient at the periphery of the cell.

Two important implications of such a standing gradient are that: 1) basal Ca^{2+} influx is taken up by mitochondria and is a critical determinant of basal $[Ca^{2+}]_{MT}$, and 2) that studies of store-operated Ca^{2+}-entry (SOCE) induced by SERCA inhibition must take into consideration

that loss of SR-mediated Ca^{2+} buffering will greatly confound potential increases in $[Ca^{2+}]_i$ due to SOCE.

5.2 MITOCHONDRIA AND LOCAL Ca^{2+} EVENTS

5.2.1 Mitochondria and plasmalemma Na^+/Ca^{2+}-exchange. We have utilized mitochondria and other targeted Ca^{2+} indicators to examine the interaction of the mitochondria, SR and NCX. We found that rapid buffering of Ca^{2+} entering the cytosol from the extracellular space by the SR and mitochondria can limit the detection of such Ca^{2+} influx by fluorescent cytosolic Ca^{2+} indicators. We observed that mitochondria readily buffer Ca^{2+} entry due to reversal of the plasmalemmal NCX, and that reverse-mode NCX mediates considerable Ca^{2+}-entry during stimulation of VSMC with PLC-coupled agonists. These observations were consistent with the hypothesis that reverse-mode NCX is functionally coupled with the agonist-induced opening non-selective cation channels (likely TRPs).

This represents an important paradigm shift in the study of agonist-induced Ca^{2+}-influx and has met with considerable resistance. Not only do our current results support the physiological existence of such a mechanism, but they suggest that the activation of non-selective cation channels may provide an important source of Na^+ to permit the up-regulation of mitochondrial Na^+/Ca^{2+}-exchange during agonist stimulation (else where suggest to occur in endothelial cells).

Concrete demonstration of such a mechanism will benefit from; 1) detailed characterization of changes in intracellular Na^+, and 2) in situ characterization of TRPC proteins as constituents of Ca^{2+} channels or non-selective cation channels.

5.2.2 Agonist-mediated stimulation of mitochondria by IP_3R & RyR. Mitochondria have proven to be excellent indicators of localized Ca^{2+} events in a number of cells. Here, pharmacological dissection of agonist-induced $[Ca^{2+}]_{MT}$ elevations revealed that PLC-coupled agonists evoke Ca^{2+} release from and mitochondrial stimulation by both IP_3R and RyR, which appear to release Ca^{2+} from separate sub-compartments of the SR. 3-Dimensional analysis of cells in which the mitochondria, IP_3R and RyR were fluorescently labeled suggested that the extensive association of mitochondria and SR influenced the stimulation of mitochondria by IP_3R and RyR.

Previous studies of mitochondrial Ca^{2+} signaling in VSM have largely relied on mitochondrial accumulation of the cationic, Ca^{2+}-sensitive dye Rhod-2 and have suggested that

SR Ca^{2+} release results in prolonged elevations of $[Ca^{2+}]_{MT}$. In contrast, our studies with mito-aequorin indicate that agonist-induced elevations of $[Ca^{2+}]_{MT}$ are transient and completely return to resting levels due to up-regulation of mitochondria Ca^{2+}extrusion. Given that the kinetics of the $[Ca^{2+}]_{MT}$ elevation reported with aequorin closely resembled those of the $[Ca^{2+}]_i$ elevations (reported with fura-2, fluo-3 and cytosolic pericams), it is unlikely that the transient nature of the $[Ca^{2+}]_{MT}$ was due to excessive consumption of aequorin. Rather, this is likely because 1) only sub-population of MT are exposed to the localized supra-micromolar $[Ca^{2+}]$ elevations caused by Ca^{2+} influx, and 2) mitochondrial Ca^{2+} extrusion is up-regulated to compensate for the increased Ca^{2+} uptake. Thus we would conclude that transient elevations of $[Ca^{2+}]_{MT}$ likely represent the physiological mode of mitochondrial stimulation in VSM.

5.3 CLOSING COMMENTS

The impetus behind these studies is ultimately to gain a comprehensive understanding of Ca^{2+} signaling in smooth muscle of blood vessels; healthy and diseased, young and old. The contributions made in this thesis to further defining the nature of $[Ca^{2+}]_{MT}$ elevations resulting from "physiological" stimulation of VSM bring us that much closer to being able to identify the nature of the $[Ca^{2+}]_{MT}$ elevations that lead to activation of apoptotic cell death when Ca^{2+} homeostasis is compromised. With the proliferation of targeted indicators and the development of technologies to deliver intact proteins into living tissue, our ability to address this issue is primarily limited by: 1) our creativity in designing new probes and 2) our ability to extract meaning full data from the images that we are now readily able to capture. While cultured cells provide a ready means to develop principles, lessons from previous studies underscore the heterogeneity exhibited in the behaviour of mitochondria in different blood vessels and tissues. Thus in closing, we emphasize the importance of characterizing the detailed behaviour and role of mitochondria in the context of the specific tissue under investigation. Such studies should culminate in the unraveling of the relationship between mitochondrial Ca^{2+} transport and smooth muscle heterogeneity.

BIBLIOGRAPHY

1. (1995) *Handbook of Biological Confocal Microscopy*, 2nd Ed., Plenum Press, New York
2. Aalkaer C and Nilsson H (2005) Vasomotion: cellular background for the oscillator and for the synchronization of smooth muscle cells. Br. J Pharmacol. 144 (5), 605-616
3. Aaronson P and van Breemen C (1981) Effects of sodium gradient manipulation upon cellular calcium, 45Ca fluxes and cellular sodium in the guinea-pig taenia coli. J. Physiol 319, 443-461
4. Adams DJ, Barakeh J, Laskey R, and van Breemen C (1989) Ion channels and regulation of intracellular calcium in vascular endothelial cells. FASEB J. 3 (12), 2389-2400
5. Alderton JM and Steinhardt RA (2000) Calcium influx through calcium leak channels is responsible for the elevated levels of calcium-dependent proteolysis in dystrophic myotubes. J. Biol. Chem. 275 (13), 9452-9460
6. Allen BG and Walsh MP (1994) The biochemical basis of the regulation of smooth-muscle contraction. Trends Biochem. Sci. 19 (9), 362-368
7. Alonso MT, Montero M, Carnicero E, Garcia-Sancho J, and Alvarez J (2002) Subcellular Ca(2+) dynamics measured with targeted aequorin in chromaffin cells. Ann. N. Y. Acad. Sci. 971:634-40., 634-640
8. Archer SL, Weir EK, Reeve HL, and Michelakis E (2000) Molecular identification of O2 sensors and O2-sensitive potassium channels in the pulmonary circulation. Adv. Exp. Med. Biol. 475:219-40., 219-240
9. Arnaudeau S, Boittin FX, Macrez N, Lavie JL, Mironneau C, and Mironneau J (1997) L-type and Ca2+ release channel-dependent hierarchical Ca2+ signalling in rat portal vein myocytes. Cell Calcium 22 (5), 399-411
10. Arnaudeau S, Kelley WL, Walsh JV, Jr., and Demaurex N (2001) Mitochondria recycle Ca(2+) to the endoplasmic reticulum and prevent the depletion of neighboring endoplasmic reticulum regions. J Biol. Chem. 276 (31), 29430-29439
11. Arnon A, Hamlyn JM, and Blaustein MP (2000) Na+ entry via store-operated channels modulates Ca2+ signaling in arterial myocytes. Am. J. Physiol Cell Physiol 278 (1), C163-C173
12. Arnon A, Hamlyn JM, and Blaustein MP (2000) Ouabain augments Ca2+ transients in arterial smooth muscle without raising cytosolic Na+. Am J Physiol Heart Circ Physiol 279 (2), H679-H691
13. Babcock DF and Hille B (1998) Mitochondrial oversight of cellular Ca2+ signaling. Curr. Opin. Neurobiol. 8 (3), 398-404
14. Babiychuk VS, Draeger A, and Babiychuk EB (2000) Smooth muscle actomyosin promotes Ca2+-dependent interactions between annexin VI and detergent-insoluble glycosphingolipid-enriched membrane domains. Acta Biochim. Pol. 47 (3), 579-589
15. Bai N, Lee HC, and Laher I (2005) Emerging role of cyclic ADP-ribose (cADPR) in smooth muscle. Pharmacol. Ther. 105 (2), 189-207
16. Balaban RS, Bose S, French SA, and Territo PR (2003) Role of calcium in metabolic signaling between cardiac sarcoplasmic reticulum and mitochondria in vitro. Am J Physiol Cell Physiol 284 (2), C285-C293
17. Barrett-Jolley R and Davies NW (1997) Kinetic analysis of the inhibitory effect of glibenclamide on KATP channels of mammalian skeletal muscle. J Membr. Biol. 155 (3), 257-262
18. Barron JT, Gu L, and Parrillo JE (1999) Relation of NADH/NAD to contraction in vascular smooth muscle. Mol Cell Biochem. 194 (1-2), 283-290
19. Barron JT, Gu L, and Parrillo JE (1998) Malate-Aspartate Shuttle, Cytoplasmic NADH Redox Potential, and Energetics in Vascular Smooth Muscle*1. Journal of Molecular and Cellular Cardiology 30 (8), 1571-1579
20. Basset O, Boittin FX, Dorchies OM, Chatton JY, van BC, and Ruegg UT (2004) Involvement of inositol 1,4,5-trisphosphate in nicotinic calcium responses in dystrophic myotubes assessed by near-plasma membrane calcium measurement. J Biol. Chem. 279 (45), 47092-47100
21. Beech DJ, Muraki K, and Flemming R (2004) Non-selective cationic channels of smooth muscle and the mammalian homologues of Drosophila TRP. J. Physiol 559 (Pt 3), 685-706
22. Bernardi P (1999) Mitochondrial Transport of Cations: Channels, Exchangers, and Permeability Transition. Physiol. Rev. 79 (4), 1127-1155
23. Berridge MJ, Bootman MD, and Roderick HL (2003) Calcium signalling: dynamics, homeostasis and remodelling. Nat. Rev. Mol Cell Biol. 4 (7), 517-529

24. Bers, D. M. (2001) *Exitation-Contraction Coupling and Cardiac Contractile Force*, 2nd Ed., Kluwer Academic Publishers,
25. Bezprozvanny I and Ehrlich BE (1995) The inositol 1,4,5-trisphosphate (InsP3) receptor. J Membr. Biol. 145 (3), 205-216
26. Bezprozvanny I, Watras J, and Ehrlich BE (1991) Bell-shaped calcium-response curves of Ins(1,4,5)P3- and calcium-gated channels from endoplasmic reticulum of cerebellum. Nature 351 (6329), 751-754
27. Blaustein MP (1977) Sodium ions, calcium ions, blood pressure regulation, and hypertension: a reassessment and a hypothesis. Am J Physiol 232 (5), C165-C173
28. Blaustein MP (1993) Physiological effects of endogenous ouabain: control of intracellular Ca2+ stores and cell responsiveness. Am. J Physiol 264 (6 Pt 1), C1367-C1387
29. Boitier E, Rea R, and Duchen MR (1999) Mitochondria exert a negative feedback on the propagation of intracellular Ca2+ waves in rat cortical astrocytes. J Cell Biol. 145 (4), 795-808
30. Boittin FX, Coussin F, Macrez N, Mironneau C, and Mironneau J (1998) Inositol 1,4,5-trisphosphate- and ryanodine-sensitive Ca2+ release channel-dependent Ca2+ signalling in rat portal vein myocytes. Cell Calcium 23 (5), 303-311
31. Boittin FX, Macrez N, Halet G, and Mironneau J (1999) Norepinephrine-induced Ca(2+) waves depend on InsP(3) and ryanodine receptor activation in vascular myocytes. Am. J Physiol 277 (1 Pt 1), C139-C151
32. Bolton TB, Gordienko DV, Pucovsky V, Parsons S, and Povstyan O (2002) Calcium release events in excitation-contraction coupling in smooth muscle. Novartis. Found. Symp. 246, 154-168
33. Bolton TB, Prestwich SA, Zholos AV, and Gordienko DV (1999) Excitation-contraction coupling in gastrointestinal and other smooth muscles. Annu. Rev. Physiol 61, 85-115
34. Bootman MD, Collins TJ, Mackenzie L, Roderick HL, Berridge MJ, and Peppiatt CM (2002) 2-aminoethoxydiphenyl borate (2-APB) is a reliable blocker of store-operated Ca2+ entry but an inconsistent inhibitor of InsP3-induced Ca2+ release. FASEB J 16 (10), 1145-1150
35. Boulay G, Zhu X, Peyton M, Jiang M, Hurst R, Stefani E, and Birnbaumer L (1997) Cloning and expression of a novel mammalian homolog of Drosophila transient receptor potential (Trp) involved in calcium entry secondary to activation of receptors coupled by the Gq class of G protein. J. Biol. Chem. 272 (47), 29672-29680
36. Bowser DN, Petrou S, Panchal RG, Smart ML, and Williams DA (2002) Release of mitochondrial Ca2+ via the permeability transition activates endoplasmic reticulum Ca2+ uptake. FASEB J 16 (9), 1105-1107
37. Brini M (2003) Ca2+ signalling in mitochondria: mechanism and role in physiology and pathology. Cell Calcium 34 (4-5), 399-405
38. Brown GC (1992) Control of respiration and ATP synthesis in mammalian mitochondria and cells. Biochem. J 284 (Pt 1), 1-13
39. Busselberg D, Platt B, Michael D, Carpenter DO, and Haas HL (1994) Mammalian voltage-activated calcium channel currents are blocked by Pb2+, Zn2+, and Al3+. J. Neurophysiol. 71 (4), 1491-1497
40. Camello C, Lomax R, Petersen OH, and Tepikin AV (2002) Calcium leak from intracellular stores--the enigma of calcium signalling. Cell Calcium 32 (5-6), 355-361
41. Campbell JD and Paul RJ (1992) The nature of fuel provision for the Na+,K(+)-ATPase in porcine vascular smooth muscle. J. Physiol 447, 67-82
42. Casteels R and Droogmans G (1981) Exchange characteristics of the noradrenaline-sensitive calcium store in vascular smooth muscle cells or rabbit ear artery. J Physiol 317, 263-279
43. Chakraborti T, Das S, Mondal M, Roychoudhury S, and Chakraborti S (1999) Oxidant, Mitochondria and Calcium: An Overview. Cellular Signalling 11 (2), 77-85
44. Charuk JH, Pirraglia CA, and Reithmeier RA (1990) Interaction of ruthenium red with Ca2(+)-binding proteins. Anal. Biochem. 188 (1), 123-131
45. Chen Q, Vazquez EJ, Moghaddas S, Hoppel CL, and Lesnefsky EJ (2003) Production of reactive oxygen species by mitochondria: central role of complex III. J Biol. Chem. %19;278 (38), 36027-36031
46. Clark JF, Matsumoto T, and Nakayama S (2000) Intact smooth muscle metabolism: its responses to cyanide poisoning and pyruvate stimulation. Front Biosci. 5:A18-23., A18-A23
47. Collins TJ, Lipp P, Berridge MJ, and Bootman MD (2001) Mitochondrial Ca(2+) uptake depends on the spatial and temporal profile of cytosolic Ca(2+) signals. J Biol. Chem. 276 (28), 26411-26420
48. Collins TJ, Lipp P, Berridge MJ, Li W, and Bootman MD (2000) Inositol 1,4,5-trisphosphate-induced Ca2+ release is inhibited by mitochondrial depolarization. Biochem. J 347 (Pt 2), 593-600

49. Coussin F, Macrez N, Morel JL, and Mironneau J (2000) Requirement of ryanodine receptor subtypes 1 and 2 for Ca(2+)-induced Ca(2+) release in vascular myocytes. J Biol. Chem. 275 (13), 9596-9603
50. Cox DA, Conforti L, Sperelakis N, and Matlib MA (1993) Selectivity of inhibition of Na(+)-Ca2+ exchange of heart mitochondria by benzothiazepine CGP-37157. J Cardiovasc. Pharmacol. 21 (4), 595-599
51. Crimmins D, Morris JG, Walker GL, Sue CM, Byrne E, Stevens S, Jean-Francis B, Yiannikas C, and Pamphlett R (1993) Mitochondrial encephalomyopathy: variable clinical expression within a single kindred. J Neurol. Neurosurg. Psychiatry 56 (8), 900-905
52. Crompton M, Barksby E, Johnson N, and Capano M (2002) Mitochondrial intermembrane junctional complexes and their involvement in cell death. Biochimie 84 (2-3), 143-152
53. Crompton M, Moser R, Ludi H, and Carafoli E (1978) The interrelations between the transport of sodium and calcium in mitochondria of various mammalian tissues. Eur. J Biochem. 82 (1), 25-31
54. Csordas G, Thomas AP, and Hajnoczky G (2001) Calcium signal transmission between ryanodine receptors and mitochondria in cardiac muscle. Trends Cardiovasc. Med. 11 (7), 269-275
55. Csordas G, Thomas AP, and Hajnoczky G (1999) Quasi-synaptic calcium signal transmission between endoplasmic reticulum and mitochondria. EMBO J 18 (1), 96-108
56. Csordas G and Hajnoczky G (2003) Plasticity of Mitochondrial Calcium Signaling. J. Biol. Chem. 278 (43), 42273-42282
57. Dai J, Kuo KH, Leo JM, van BC, and Lee CH (2005) Rearrangement of the close contact between the mitochondria and the sarcoplasmic reticulum in airway smooth muscle. Cell Calcium 37 (4), 333-340
58. Darby PJ, Kwan CY, and Daniel EE (2000) Caveolae from canine airway smooth muscle contain the necessary components for a role in Ca(2+) handling. Am J Physiol Lung Cell Mol Physiol 279 (6), L1226-L1235
59. Dedov VN, Mandadi S, Armati PJ, and Verkhratsky A (2001) Capsaicin-induced depolarisation of mitochondria in dorsal root ganglion neurons is enhanced by vanilloid receptors. Neuroscience 103 (1), 219-226
60. Demaurex N and Distelhorst C (2003) Cell biology. Apoptosis--the calcium connection. Science 300 (5616), 65-67
61. Denton RM, McCormack JG, and Edgell NJ (1980) Role of calcium ions in the regulation of intramitochondrial metabolism. Effects of Na+, Mg2+ and ruthenium red on the Ca2+-stimulated oxidation of oxoglutarate and on pyruvate dehydrogenase activity in intact rat heart mitochondria. Biochem. J 190 (1), 107-117
62. Deth R and van Breemen C (1974) Relative contributions of Ca2+ influx and cellular Ca2+ release during drug induced activation of the rabbit aorta. Pflugers Arch. 348 (1), 13-22
63. Devine CE, Somlyo AV, and Somlyo AP (1972) Sarcoplasmic reticulum and excitation-contraction coupling in mammalian smooth muscles. J Cell Biol. 52 (3), 690-718
64. Dong H, Sellers ZM, Smith A, Chow JY, and Barrett KE (2005) Na(+)/Ca(2+) exchange regulates Ca(2+)-dependent duodenal mucosal ion transport and HCO(3)(-) secretion in mice. Am. J Physiol Gastrointest. Liver Physiol 288 (3), G457-G465
65. Drummond RM and Fay FS (1996) Mitochondria contribute to Ca2+ removal in smooth muscle cells. Pflugers Arch. 431 (4), 473-482
66. Drummond RM and Tuft RA (1999) Release of Ca2+ from the sarcoplasmic reticulum increases mitochondrial [Ca2+] in rat pulmonary artery smooth muscle cells. J Physiol 516 (Pt 1), 139-147
67. Duchen MR (1999) Contributions of mitochondria to animal physiology: from homeostatic sensor to calcium signalling and cell death. J Physiol 516 (Pt 1), 1-17
68. Duchen MR, Surin A, and Jacobson J (2003) Imaging mitochondrial function in intact cells. Methods Enzymol. 361:353-89., 353-389
69. EL-Mezgueldi M (1996) Calponin. Int. J Biochem. Cell Biol. 28 (11), 1185-1189
70. Evans JH and Sanderson MJ (1999) Intracellular calcium oscillations induced by ATP in airway epithelial cells. Am J Physiol 277 (1 Pt 1), L30-L41
71. Fayazi AH, Lapidot SA, Huang BK, Tucker RW, and Phair RD (1996) Resolution of the basal plasma membrane calcium flux in vascular smooth muscle cells. Am J Physiol Heart Circ Physiol 270 (6), H1972-H1978
72. Feng W, Tu J, Yang T, Vernon PS, Allen PD, Worley PF, and Pessah IN (2002) Homer Regulates Gain of Ryanodine Receptor Type 1 Channel Complex. J. Biol. Chem. 277 (47), 44722-44730
73. Fiekers JF, Gelbspan D, and Heppner TJ (2001) Calcium homeostasis in a clonal pituitary cell line of mouse corticotropes. Can. J Physiol Pharmacol. 79 (6), 502-511

74. Filippin L, Magalhaes PJ, Di Benedetto G, Colella M, and Pozzan T (2003) Stable interactions between mitochondria and endoplasmic reticulum allow rapid accumulation of calcium in a subpopulation of mitochondria. J Biol. Chem. .
75. Fontaine E and Bernardi P (1999) Progress on the mitochondrial permeability transition pore: regulation by complex I and ubiquinone analogs. J Bioenerg. Biomembr. 31 (4), 335-345
76. Frieden M, Malli R, Samardzija M, Demaurex N, and Graier WF (2002) Subplasmalemmal endoplasmic reticulum controls K(Ca) channel activity upon stimulation with a moderate histamine concentration in a human umbilical vein endothelial cell line. J Physiol 540 (Pt 1), 73-84
77. Fujimoto T, Miyawaki A, and Mikoshiba K (1995) Inositol 1,4,5-trisphosphate receptor-like protein in plasmalemmal caveolae is linked to actin filaments. J Cell Sci. 108 (Pt 1), 7-15
78. Fukuta H, Kito Y, and Suzuki H (2002) Spontaneous electrical activity and associated changes in calcium concentration in guinea-pig gastric smooth muscle. J Physiol 540 (Pt 1), 249-260
79. Gamberucci A, Innocenti B, Fulceri R, Banhegyi G, Giunti R, Pozzan T, and Benedetti A (1994) Modulation of Ca2+ influx dependent on store depletion by intracellular adenine-guanine nucleotide levels. J. Biol. Chem. 269 (38), 23597-23602
80. Ganitkevich VY (1996) The amount of acetylcholine mobilisable Ca2+ in single smooth muscle cells measured with the exogenous cytoplasmic Ca2+ buffer, Indo-1. Cell Calcium 20 (6), 483-492
81. Garlid KD, Paucek P, Yarov-Yarovoy V, Sun X, and Schindler PA (1996) The Mitochondrial K[IMAGE] Channel as a Receptor for Potassium Channel Openers. J. Biol. Chem. 271 (15), 8796-8799
82. Genova ML, Pich MM, Biondi A, Bernacchia A, Falasca A, Bovina C, Formiggini G, Castelli GP, and Lenaz G (2003) Mitochondrial production of oxygen radical species and the role of Coenzyme Q as an antioxidant. Exp. Biol Med. (Maywood.) 228 (5), 506-513
83. Goel M, Sinkins WG, and Schilling WP (2002) Selective association of TRPC channel subunits in rat brain synaptosomes. J Biol. Chem. 277 (50), 48303-48310
84. Gollasch M, Hescheler J, Quayle JM, Patlak JB, and Nelson MT (1992) Single calcium channel currents of arterial smooth muscle at physiological calcium concentrations. Am J Physiol 263 (5 Pt 1), C948-C952
85. Golovina VA and Blaustein MP (1997) Spatially and functionally distinct Ca2+ stores in sarcoplasmic and endoplasmic reticulum. Science 275 (5306), 1643-1648
86. Gonzalez-Pacheco FR, Caramelo C, Castilla MA, Deudero JJ, Arias J, Yague S, Jimenez S, Bragado R, and Alvarez-Arroyo MV (2002) Mechanism of vascular smooth muscle cells activation by hydrogen peroxide: role of phospholipase C gamma. Nephrol. Dial. Transplant. 17 (3), 392-398
87. Gordienko DV and Bolton TB (2002) Crosstalk between ryanodine receptors and IP(3) receptors as a factor shaping spontaneous Ca(2+)-release events in rabbit portal vein myocytes. J Physiol 542 (Pt 3), 743-762
88. Gordienko DV, Greenwood IA, and Bolton TB (2001) Direct visualization of sarcoplasmic reticulum regions discharging Ca(2+)sparks in vascular myocytes. Cell Calcium 29 (1), 13-28
89. Grasso P, Santa-Coloma TA, and Reichert LE, Jr. (1992) Correlation of follicle-stimulating hormone (FSH)-receptor complex internalization with the sustained phase of FSH-induced calcium uptake by cultured rat Sertoli cells. Endocrinology 131 (6), 2622-2628
90. Grayson TH, Haddock RE, Murray TP, Wojcikiewicz RJ, and Hill CE (2004) Inositol 1,4,5-trisphosphate receptor subtypes are differentially distributed between smooth muscle and endothelial layers of rat arteries. Cell Calcium 36 (6), 447-458
91. Greenwood IA, Helliwell RM, and Large WA (1997) Modulation of Ca(2+)-activated Cl- currents in rabbit portal vein smooth muscle by an inhibitor of mitochondrial Ca2+ uptake. J Physiol 505 (Pt 1), 53-64
92. Greenwood IA, Miller LJ, Ohya S, and Horowitz B (2002) The large conductance potassium channel beta-subunit can interact with and modulate the functional properties of a calcium-activated chloride channel, CLCA1. J Biol. Chem. 277 (25), 22119-22122
93. Gunter TE and Gunter KK (2001) Uptake of calcium by mitochondria: transport and possible function. IUBMB. Life 52 (3-5), 197-204
94. Gunter TE, Gunter KK, Sheu SS, and Gavin CE (1994) Mitochondrial calcium transport: physiological and pathological relevance. Am J Physiol 267 (2 Pt 1), C313-C339
95. Gurney AM, Drummond RM, and Fay FS (2000) Calcium signalling in sarcoplasmic reticulum, cytoplasm and mitochondria during activation of rabbit aorta myocytes. Cell Calcium 27 (6), 339-351
96. Hai CM and Kim HR (2005) An expanded latch-bridge model of protein kinase C-mediated smooth muscle contraction. J Appl. Physiol 98 (4), 1356-1365

97. Hai CM and Murphy RA (1988) Cross-bridge phosphorylation and regulation of latch state in smooth muscle. Am. J Physiol 254 (1 Pt 1), C99-106
98. Hajnoczky G, Csordas G, Madesh M, and Pacher P (2000) The machinery of local Ca2+ signalling between sarco-endoplasmic reticulum and mitochondria. J. Physiol 529 Pt 1, 69-81
99. Hajnoczky G, Hager R, and Thomas AP (1999) Mitochondria suppress local feedback activation of inositol 1,4, 5- trisphosphate receptors by Ca2+. J Biol. Chem. 274 (20), 14157-14162
100. Hardin CD, Raeymaekers L, and Paul RJ (1992) Comparison of endogenous and exogenous sources of ATP in fueling Ca2+ uptake in smooth muscle plasma membrane vesicles. J Gen. Physiol 99 (1), 21-40
101. He FJ and MacGregor GA (2004) Effect of longer-term modest salt reduction on blood pressure. The Cochrane Database of Systematic Reviews (1)
102. Herrera GM and Nelson MT (2002) Sarcoplasmic reticulum and membrane currents. Novartis. Found. Symp. 246, 189-203
103. Himpens B, De Smedt H, Droogmans G, and Casteels R (1992) Differences in regulation between nuclear and cytoplasmic Ca2+ in cultured smooth muscle cells. Am J Physiol 263 (1 Pt 1), C95-105
104. Ho SH, Das GU, and Rieske JS (1985) Detection of antimycin-binding subunits of complex III by photoaffinity-labeling with an azido derivative of antimycin. J Bioenerg. Biomembr. 17 (5), 269-282
105. Hopf FW, Reddy P, Hong J, and Steinhardt RA (1996) A capacitative calcium current in cultured skeletal muscle cells is mediated by the calcium-specific leak channel and inhibited by dihydropyridine compounds. J. Biol. Chem. 271 (37), 22358-22367
106. Hoth M, Fanger CM, and Lewis RS (1997) Mitochondrial regulation of store-operated calcium signaling in T lymphocytes. J. Cell Biol. 137 (3), 633-648
107. Humbert JP, Matter N, Artault JC, Koppler P, and Malviya AN (1996) Inositol 1,4,5-trisphosphate receptor is located to the inner nuclear membrane vindicating regulation of nuclear calcium signaling by inositol 1,4,5-trisphosphate. Discrete distribution of inositol phosphate receptors to inner and outer nuclear membranes. J Biol. Chem. 271 (1), 478-485
108. Iino M (1989) Calcium-induced calcium release mechanism in guinea pig taenia caeci. J Gen. Physiol 94 (2), 363-383
109. Iino M (2002) Molecular basis and physiological functions of dynamic Ca2+ signalling in smooth muscle cells. Novartis. Found. Symp. 246, 142-146
110. Iizuka K, Yoshii A, Dobashi K, Horie T, Mori M, and Nakazawa T (1998) InsP3, but not novel Ca2+ releasers, contributes to agonist-initiated contraction in rabbit airway smooth muscle. J Physiol 511 (Pt 3), 915-933
111. Jaburek M, Yarov-Yarovoy V, Paucek P, and Garlid KD (1998) State-dependent inhibition of the mitochondrial KATP channel by glyburide and 5-hydroxydecanoate. J Biol. Chem. 273 (22), 13578-13582
112. Jaggar JH and Nelson MT (2000) Differential regulation of Ca(2+) sparks and Ca(2+) waves by UTP in rat cerebral artery smooth muscle cells. Am J Physiol Cell Physiol 279 (5), C1528-C1539
113. Jaggar JH, Porter VA, Lederer WJ, and Nelson MT (2000) Calcium sparks in smooth muscle. Am J Physiol Cell Physiol 278 (2), C235-C256
114. Janiak R, Wilson SM, Montague S, and Hume JR (2001) Heterogeneity of calcium stores and elementary release events in canine pulmonary arterial smooth muscle cells. Am. J Physiol Cell Physiol 280 (1), C22-C33
115. Janssen LJ, Betti PA, Netherton SJ, and Walters DK (1999) Superficial buffer barrier and preferentially directed release of Ca2+ in canine airway smooth muscle. Am J Physiol 276 (5 Pt 1), L744-L753
116. Juhaszova M and Blaustein MP (1997) Distinct distribution of different Na+ pump alpha subunit isoforms in plasmalemma. Physiological implications. Ann. N. Y. Acad. Sci. 834, 524-536
117. Jung S, Strotmann R, Schultz G, and Plant TD (2002) TRPC6 is a candidate channel involved in receptor-stimulated cation currents in A7r5 smooth muscle cells. Am J Physiol Cell Physiol 282 (2), C347-C359
118. Kamishima T, Davies NW, and Standen NB (2000) Mechanisms that regulate [Ca2+]i following depolarization in rat systemic arterial smooth muscle cells. J Physiol 522 Pt 2:285-95., 285-295
119. Kamishima T and McCarron JG (1998) Ca2+ removal mechanisms in rat cerebral resistance size arteries. Biophys. J. 75 (4), 1767-1773
120. Kamishima T and Quayle JM (2002) Mitochondrial Ca2+ uptake is important over low [Ca2+]i range in arterial smooth muscle. Am J Physiol Heart Circ Physiol 283 (6), H2431-H2439

121. Kang TM, Park MK, and Uhm DY (2003) Effects of hypoxia and mitochondrial inhibition on the capacitative calcium entry in rabbit pulmonary arterial smooth muscle cells. Life Sci. 72 (13), 1467-1479
122. Kennedy CH, Winston GW, Church DF, and Pryor WA (1989) Benzoyl peroxide interaction with mitochondria: inhibition of respiration and induction of rapid, large-amplitude swelling. Arch. Biochem. Biophys. 271 (2), 456-470
123. Knot HJ, de Ree MM, Gahwiler BH, and Ruegg UT (1991) Modulation of electrical activity and of intracellular calcium oscillations of smooth muscle cells by calcium antagonists, agonists, and vasopressin. J. Cardiovasc. Pharmacol. 18 Suppl 10, S7-14
124. Kotlikoff ML, Wang YX, Xin HB, and Ji G (2002) Calcium release by ryanodine receptors in smooth muscle. Novartis. Found. Symp. 246, 108-119
125. Kotlyar AB and Gutman M (1992) The effect of delta mu H+ on the interaction of rotenone with complex I of submitochondrial particles. Biochim. Biophys. Acta 1140 (2), 169-174
126. Krick S, Platoshyn O, Sweeney M, Kim H, and Yuan JX (2001) Activation of K+ channels induces apoptosis in vascular smooth muscle cells. Am J Physiol Cell Physiol 280 (4), C970-C979
127. Kubota Y, Hashitani H, Fukuta H, Kubota H, Kohri K, and Suzuki H (2003) Role of mitochondria in the generation of spontaneous activity in detrusor smooth muscles of the Guinea pig bladder. J Urol. 170 (2 Pt 1), 628-633
128. Kuge O and Nishijima M (2003) Biosynthetic regulation and intracellular transport of phosphatidylserine in mammalian cells. J Biochem. (Tokyo) 133 (4), 397-403
129. Landolfi B, Curci S, Debellis L, Pozzan T, and Hofer AM (1998) Ca2+ homeostasis in the agonist-sensitive internal store: functional interactions between mitochondria and the ER measured In situ in intact cells. J. Cell Biol. 142 (5), 1235-1243
130. Leach RM, Hill HM, Snetkov VA, Robertson TP, and Ward JP (2001) Divergent roles of glycolysis and the mitochondrial electron transport chain in hypoxic pulmonary vasoconstriction of the rat: identity of the hypoxic sensor. J Physiol 536 (Pt 1), 211-224
131. Lee CH, Kuo KH, Dai J, Leo JM, Seow CY, and Breemen C (2005) Calyculin-A disrupts subplasmalemmal junction and recurring Ca2+ waves in vascular smooth muscle. Cell Calcium 37 (1), 9-16
132. Lee CH, Poburko D, Kuo KH, Seow C, and van Breemen C (2002) Relationship between the sarcoplasmic reticulum and the plasma membrane. Novartis. Found. Symp. 246:26-41; discussion 41-7, 48-51., 26-41
133. Lee CH, Poburko D, Kuo KH, Seow CY, and van Breemen C (2002) Ca(2+) oscillations, gradients, and homeostasis in vascular smooth muscle. Am J Physiol Heart Circ Physiol 282 (5), H1571-H1583
134. Lee CH, Poburko D, Sahota P, Sandhu J, Ruehlmann DO, and van Breemen C (2001) The mechanism of phenylephrine-mediated [Ca(2+)](i) oscillations underlying tonic contraction in the rabbit inferior vena cava. J Physiol 534 (Pt 3), 641-650
135. Lee CH, Rahimian R, Szado T, Sandhu J, Poburko D, Behra T, Chan L, and van Breemen C (2002) Sequential opening of IP(3)-sensitive Ca(2+) channels and SOC during alpha-adrenergic activation of rabbit vena cava. Am J Physiol Heart Circ Physiol 282 (5), H1768-H1777
136. Lesh RE, Nixon GF, Fleischer S, Airey JA, Somlyo AP, and Somlyo AV (1998) Localization of ryanodine receptors in smooth muscle. Circ. Res. 82 (2), 175-185
137. Li SW, Westwick J, and Poll CT (2002) Receptor-operated Ca2+ influx channels in leukocytes: a therapeutic target? Trends Pharmacol. Sci. 23 (2), 63-70
138. Liang W, Buluc M, van BC, and Wang X (2004) Vectorial Ca2+ release via ryanodine receptors contributes to Ca2+ extrusion from freshly isolated rabbit aortic endothelial cells. Cell Calcium 36 (5), 431-443
139. Liu Y, Zhao H, Li H, Kalyanaraman B, Nicolosi AC, and Gutterman DD (2003) Mitochondrial sources of H2O2 generation play a key role in flow-mediated dilation in human coronary resistance arteries. Circ Res. %19;93 (6), 573-580
140. Lo Russo A., Passaquin AC, Andre P, Skutella M, and Ruegg UT (1996) Effect of cyclosporin A and analogues on cytosolic calcium and vasoconstriction: possible lack of relationship to immunosuppressive activity. Br. J. Pharmacol. 118 (4), 885-892
141. Loew LM, Carrington W, Tuft RA, and Fay FS (1994) Physiological cytosolic Ca2+ transients evoke concurrent mitochondrial depolarizations. Proc. Natl. Acad. Sci. U. S. A %20;91 (26), 12579-12583
142. Loew LM, Tuft RA, Carrington W, and Fay FS (1993) Imaging in five dimensions: time-dependent membrane potentials in individual mitochondria. Biophys. J 65 (6), 2396-2407

143. Lounsbury KM, Hu Q, and Ziegelstein RC (2000) Calcium signaling and oxidant stress in the vasculature. Free Radic. Biol. Med. 28 (9), 1362-1369
144. Luttun A and Carmeliet P (2003) De novo vasculogenesis in the heart. Cardiovasc. Res. 58 (2), 378-389
145. Ma HT, Patterson RL, van Rossum DB, Birnbaumer L, Mikoshiba K, and Gill DL (2000) Requirement of the inositol trisphosphate receptor for activation of store-operated Ca2+ channels. Science 287 (5458), 1647-1651
146. Malli R, Frieden M, Osibow K, and Graier WF (2003) Mitochondria efficiently buffer subplasmalemmal Ca2+ elevation during agonist stimulation. J Biol. Chem. 278 (12), 10807-10815
147. Malli R, Frieden M, Osibow K, Zoratti C, Mayer M, Demaurex N, and Graier WF (2003) Sustained Ca2+ transfer across mitochondria is Essential for mitochondrial Ca2+ buffering, sore-operated Ca2+ entry, and Ca2+ store refilling. J Biol. Chem. 278 (45), 44769-44779
148. Marsault R, Murgia M, Pozzan T, and Rizzuto R (1997) Domains of high Ca2+ beneath the plasma membrane of living A7r5 cells. EMBO J. 16 (7), 1575-1581
149. Marshall C, Elias C, Xue XH, Le HD, Omelchenko A, Hryshko LV, and Tibbits GF (2002) Determinants of cardiac Na+/Ca2+ exchanger temperature dependence: NH2-terminal transmembrane segments. Am. J. Physiol Cell Physiol 283 (2), C512-C520
150. Matlib MA, Zhou Z, Knight S, Ahmed S, Choi KM, Krause-Bauer J, Phillips R, Altschuld R, Katsube Y, Sperelakis N, and Bers DM (1998) Oxygen-bridged dinuclear ruthenium amine complex specifically inhibits Ca2+ uptake into mitochondria in vitro and in situ in single cardiac myocytes. J Biol. Chem. 273 (17), 10223-10231
151. McCarron JG and Muir TC (1999) Mitochondrial regulation of the cytosolic Ca2+ concentration and the InsP3-sensitive Ca2+ store in guinea-pig colonic smooth muscle. J Physiol 516 (Pt 1), 149-161
152. McDaniel SS, Platoshyn O, Wang J, Yu Y, Sweeney M, Krick S, Rubin LJ, and Yuan JX (2001) Capacitative Ca(2+) entry in agonist-induced pulmonary vasoconstriction. Am. J. Physiol Lung Cell Mol. Physiol 280 (5), L870-L880
153. McGeown JG (2004) Interactions between inositol 1,4,5-trisphosphate receptors and ryanodine receptors in smooth muscle: one store or two? Cell Calcium 35 (6), 613-619
154. Michelakis ED, Hampl V, Nsair A, Wu X, Harry G, Haromy A, Gurtu R, and Archer SL (2002) Diversity in mitochondrial function explains differences in vascular oxygen sensing. Circ Res. 90 (12), 1307-1315
155. Montero M, Alonso MT, Albillos A, Garcia-Sancho J, and Alvarez J (2001) Mitochondrial Ca(2+)-induced Ca(2+) release mediated by the Ca(2+) uniporter. Mol. Biol. Cell 12 (1), 63-71
156. Montero M, Alonso MT, Carnicero E, Cuchillo-Ibanez I, Albillos A, Garcia AG, Garcia-Sancho J, and Alvarez J (2000) Chromaffin-cell stimulation triggers fast millimolar mitochondrial Ca2+ transients that modulate secretion. Nat. Cell Biol. 2 (2), 57-61
157. Moore ED, Etter EF, Philipson KD, Carrington WA, Fogarty KE, Lifshitz LM, and Fay FS (1993) Coupling of the Na+/Ca2+ exchanger, Na+/K+ pump and sarcoplasmic reticulum in smooth muscle. Nature 365 (6447), 657-660
158. Moore RA, Nguyen H, Galceran J, Pessah IN, and Allen PD (1998) A transgenic myogenic cell line lacking ryanodine receptor protein for homologous expression studies: reconstitution of Ry1R protein and function. J Cell Biol. 140 (4), 843-851
159. Nadler MJ, Hermosura MC, Inabe K, Perraud AL, Zhu Q, Stokes AJ, Kurosaki T, Kinet JP, Penner R, Scharenberg AM, and Fleig A (2001) LTRPC7 is a Mg.ATP-regulated divalent cation channel required for cell viability. Nature 411 (6837), 590-595
160. Nassar A and Simpson AW (2000) Elevation of mitochondrial calcium by ryanodine-sensitive calcium-induced calcium release. J Biol. Chem. 275 (31), 23661-23665
161. Nazer MA and van Breemen C (1998) A role for the sarcoplasmic reticulum in Ca2+ extrusion from rabbit inferior vena cava smooth muscle. Am. J. Physiol 274 (1 Pt 2), H123-H131
162. Nazer MA and van Breemen C (1998) Functional linkage of Na(+)-Ca2+ exchange and sarcoplasmic reticulum Ca2+ release mediates Ca2+ cycling in vascular smooth muscle. Cell Calcium 24 (4), 275-283
163. Nilius B (2003) From TRPs to SOCs, CCEs, and CRACs: consensus and controversies. Cell Calcium 33 (5-6), 293-298
164. Nixon GF, Mignery GA, and Somlyo AV (1994) Immunogold localization of inositol 1,4,5-trisphosphate receptors and characterization of ultrastructural features of the sarcoplasmic reticulum in phasic and tonic smooth muscle. J Muscle Res. Cell Motil. 15 (6), 682-700

165. Nowycky MC, Fox AP, and Tsien RW (1985) Long-opening mode of gating of neuronal calcium channels and its promotion by the dihydropyridine calcium agonist Bay K 8644. Proc. Natl. Acad. Sci. U. S. A 82 (7), 2178-2182
166. Obejero-Paz CA, Jones SW, and Scarpa A (1998) Multiple channels mediate calcium leakage in the A7r5 smooth muscle- derived cell line. Biophys. J. 75 (3), 1271-1286
167. Obukhov AG and Nowycky MC (2002) TRPC4 can be activated by G-protein-coupled receptors and provides sufficient Ca(2+) to trigger exocytosis in neuroendocrine cells. J Biol. Chem. 277 (18), 16172-16178
168. Pacher P, Thomas AP, and Hajnoczky G (2002) Ca2+ marks: miniature calcium signals in single mitochondria driven by ryanodine receptors. Proc. Natl. Acad. Sci. U. S. A 99 (4), 2380-2385
169. Parekh AB (2003) Store-operated Ca2+ entry: dynamic interplay between endoplasmic reticulum, mitochondria and plasma membrane. J Physiol 547 (Pt 2), 333-348
170. Park MK, Ashby MC, Erdemli G, Petersen OH, and Tepikin AV (2001) Perinuclear, perigranular and sub-plasmalemmal mitochondria have distinct functions in the regulation of cellular calcium transport. EMBO J. 20 (8), 1863-1874
171. Paul RJ (1990) Smooth muscle energetics and theories of cross-bridge regulation. Am. J Physiol 258 (2 Pt 1), C369-C375
172. Peng H, Matchkov V, Ivarsen A, Aalkjaer C, and Nilsson H (2001) Hypothesis for the initiation of vasomotion. Circ Res. 88 (8), 810-815
173. Perez-Vizcaino F, Tamargo J, Hof RP, and Ruegg UT (1993) Vascular selectivity of seven prototype calcium antagonists: a study at the single cell level. J. Cardiovasc. Pharmacol. 22 (5), 768-775
174. Pfeiffer DR, Gunter TE, Eliseev R, Broekemeier KM, and Gunter KK (2001) Release of Ca2+ from mitochondria via the saturable mechanisms and the permeability transition. IUBMB. Life 52 (3-5), 205-212
175. Plant TD and Schaefer M (2003) TRPC4 and TRPC5: receptor-operated Ca2+-permeable nonselective cation channels. Cell Calcium 33 (5-6), 441-450
176. Poburko D, Kuo KH, Dai J, Lee CH, and van Breemen C (2004) Organellar junctions promote targeted Ca2+ signaling in smooth muscle: why two membranes are better than one. Trends Pharmacol. Sci. 25 (1), 8-15
177. Poburko D, Lee CH, and van Breemen C (2004) Vascular smooth muscle mitochondria at the cross roads of Ca2+ signaling. Cell Calcium 35 (6), 509-521
178. Poburko D, Lhote P, Szado T, Behra T, Rahimian R, McManus B, van Breemen C, and Ruegg UT (2004) Basal calcium entry in vascular smooth muscle. European Journal of Pharmacology 505 (1-3), 19-29
179. Pozzan T, Rizzuto R, Volpe P, and Meldolesi J (1994) Molecular and cellular physiology of intracellular calcium stores. Physiol Rev. 74 (3), 595-636
180. Radi R, Cassina A, Hodara R, Quijano C, and Castro L (2002) Peroxynitrite reactions and formation in mitochondria. Free Radic. Biol. Med. 33 (11), 1451-1464
181. Raeymaekers L, Verbist J, Wuytack F, Plessers L, and Casteels R (1993) Expression of Ca2+ binding proteins of the sarcoplasmic reticulum of striated muscle in the endoplasmic reticulum of pig smooth muscles. Cell Calcium 14 (8), 581-589
182. Ragan CI and Bloxham DP (1977) Specific labelling of a constituent polypeptide of bovine heart mitochondrial reduced nicotinamide-adenine dinucleotide-ubiquinone reductase by the inhibitor diphenyleneiodonium. Biochem. J 163 (3), 605-615
183. Ramos-Franco J, Fill M, and Mignery GA (1998) Isoform-specific function of single inositol 1,4,5-trisphosphate receptor channels. Biophys. J 75 (2), 834-839
184. Ramsay RR, Ackrell BA, Coles CJ, Singer TP, White GA, and Thorn GD (1981) Reaction site of carboxanilides and of thenoyltrifluoroacetone in complex II. Proc. Natl. Acad. Sci. U. S. A 78 (2), 825-828
185. Rapizzi E, Pinton P, Szabadkai G, Wieckowski MR, Vandecasteele G, Baird G, Tuft RA, Fogarty KE, and Rizzuto R (2002) Recombinant expression of the voltage-dependent anion channel enhances the transfer of Ca2+ microdomains to mitochondria. J Cell Biol. 159 (4), 613-624
186. Rathaus M and Bernheim J (2002) Oxygen species in the microvascular environment: regulation of vascular tone and the development of hypertension. Nephrol. Dial. Transplant. 17 (2), 216-221
187. Rembold CM and Chen XL (1998) The buffer barrier hypothesis, [Ca2+]i homogeneity, and sarcoplasmic reticulum function in swine carotid artery. J Physiol 513 (Pt 2), 477-492
188. Rembold CM and Murphy RA (1990) Latch-bridge model in smooth muscle: [Ca2+]i can quantitatively predict stress. Am. J Physiol 259 (2 Pt 1), C251-C257

189. Rich PR, Jeal AE, Madgwick SA, and Moody AJ (1990) Inhibitor effects on redox-linked protonations of the b haems of the mitochondrial bc1 complex. Biochim. Biophys. Acta 1018 (1), 29-40
190. Rizzuto R, Bernardi P, and Pozzan T (2000) Mitochondria as all-round players of the calcium game. J Physiol 529 Pt 1, 37-47
191. Rizzuto R, Brini M, and Pozzan T (1993) Intracellular targeting of the photoprotein aequorin: a new approach for measuring, in living cells, Ca2+ concentrations in defined cellular compartments. Cytotechnology 11 Suppl 1, S44-S46
192. Rizzuto R, Duchen MR, and Pozzan T (2004) Flirting in little space: the ER/mitochondria Ca2+ liaison. Sci. STKE. 2004 (215), re1
193. Rizzuto R, Pinton P, Carrington W, Fay FS, Fogarty KE, Lifshitz LM, Tuft RA, and Pozzan T (1998) Close contacts with the endoplasmic reticulum as determinants of mitochondrial Ca2+ responses. Science 280 (5370), 1763-1766
194. Rizzuto R, Simpson AW, Brini M, and Pozzan T (1992) Rapid changes of mitochondrial Ca2+ revealed by specifically targeted recombinant aequorin. Nature 358 (6384), 325-327
195. Robb-Gaspers LD, Rutter GA, Burnett P, Hajnoczky G, Denton RM, and Thomas AP (1998) Coupling between cytosolic and mitochondrial calcium oscillations: role in the regulation of hepatic metabolism. Biochim. Biophys. Acta 1366 (1-2), 17-32
196. Robert V, Gurlini P, Tosello V, Nagai T, Miyawaki A, Di Lisa F, and Pozzan T (2001) Beat-to-beat oscillations of mitochondrial [Ca2+] in cardiac cells. EMBO J. 20 (17), 4998-5007
197. Rosker C, Graziani A, Lukas M, Eder P, Zhu MX, Romanin C, and Groschner K (2004) Ca2+ Signaling by TRPC3 Involves Na+ Entry and Local Coupling to the Na+/Ca2+ Exchanger. J. Biol. Chem. 279 (14), 13696-13704
198. Rudolf R, Mongillo M, Rizzuto R, and Pozzan T (2003) Looking forward to seeing calcium. Nat. Rev. Mol Cell Biol. 4 (7), 579-586
199. Ruehlmann DO, Lee CH, Poburko D, and van Breemen C (2000) Asynchronous Ca(2+) waves in intact venous smooth muscle. Circ Res. 86 (4), E72-E79
200. Salomon AR, Voehringer DW, Herzenberg LA, and Khosla C (2001) Apoptolidin, a selective cytotoxic agent, is an inhibitor of F0F1-ATPase. Chem. Biol. 8 (1), 71-80
201. Satoh T, Ross CA, Villa A, Supattapone S, Pozzan T, Snyder SH, and Meldolesi J (1990) The inositol 1,4,5,-trisphosphate receptor in cerebellar Purkinje cells: quantitative immunogold labeling reveals concentration in an ER subcompartment. J. Cell Biol. 111 (2), 615-624
202. Schumacher C, Konigs B, Sigmund M, Kohne B, Schondube F, Vob M, Stein B, Weil J, and Hanrath P (1995) The ryanodine binding sarcoplasmic reticulum calcium release channel in nonfailing and in failing human myocardium. Naunyn Schmiedebergs Arch. Pharmacol. 353 (1), 80-85
203. Sedarat F, Lin E, Moore ED, and Tibbits GF (2004) Deconvolution of confocal images of dihydropyridine and ryanodine receptors in developing cardiomyocytes. J Appl. Physiol 97 (3), 1098-1103
204. Seguchi H, Ritter M, Shizukuishi M, Ishida H, Chokoh G, Nakazawa H, Spitzer KW, and Barry WH (2005) Propagation of Ca(2+) release in cardiac myocytes: Role of mitochondria. Cell Calcium 38 (1), 1-9
205. Sensi SL, Ton-That D, and Weiss JH (2002) Mitochondrial sequestration and Ca(2+)-dependent release of cytosolic Zn(2+) loads in cortical neurons. Neurobiol. Dis. 10 (2), 100-108
206. Setoguchi M, Ohya Y, Abe I, and Fujishima M (1997) Stretch-activated whole-cell currents in smooth muscle cells from mesenteric resistance artery of guinea-pig. J Physiol 501 (Pt 2), 343-353
207. Shmigol AV, Eisner DA, and Wray S (2001) Simultaneous measurements of changes in sarcoplasmic reticulum and cytosolic. J Physiol 531 (Pt 3), 707-713
208. Sitsapesan R, McGarry SJ, and Williams AJ (1995) Cyclic ADP-ribose, the ryanodine receptor and Ca2+ release. Trends Pharmacol. Sci. 16 (11), 386-391
209. Skutella M and Ruegg UT (1996) Increase of empty pool-activated Ca2+ influx using an intracellular Ca2+ chelating agent. Biochem. Biophys. Res. Commun. 218 (3), 837-841
210. Somlyo AP (1985) Excitation-contraction coupling and the ultrastructure of smooth muscle. Circ. Res. 57 (4), 497-507
211. Sotnikova R (1998) Investigation of the mechanisms underlying H2O2-evoked contraction in the isolated rat aorta. Gen. Pharmacol. 31 (1), 115-119
212. Sparagna GC, Gunter KK, Sheu SS, and Gunter TE (1995) Mitochondrial calcium uptake from physiological-type pulses of calcium. A description of the rapid uptake mode. J Biol. Chem. 270 (46), 27510-27515

213. Steenbergen JM and Fay FS (1996) The quantal nature of calcium release to caffeine in single smooth muscle cells results from activation of the sarcoplasmic reticulum Ca(2+)-ATPase. J Biol. Chem. 271 (4), 1821-1824
214. Sturek M, Kunda K, and Hu Q (1992) Sarcoplasmic reticulum buffering of myoplasmic calcium in bovine coronary artery smooth muscle. J Physiol 451, 25-48
215. Su Z, Barker DS, Csutora P, Chang T, Shoemaker RL, Marchase RB, and Blalock JE (2003) Regulation of Ca2+ release-activated Ca2+ channels by INAD and Ca2+ influx factor. Am J Physiol Cell Physiol 284 (2), C497-C505
216. Sugiyama T, Matsuda Y, and Mikoshiba K (2000) Inositol 1,4,5-trisphosphate receptor associated with focal contact cytoskeletal proteins. FEBS Lett. 466 (1), 29-34
217. Sward K, Dreja K, Lindqvist A, Persson E, and Hellstrand P (2002) Influence of mitochondrial inhibition on global and local [Ca(2+)](I) in rat tail artery. Circ Res. %19;90 (7), 792-799
218. Sward K, Mita M, Wilson DP, Deng JT, Susnjar M, and Walsh MP (2003) The role of RhoA and Rho-associated kinase in vascular smooth muscle contraction. Curr. Hypertens. Rep. 5 (1), 66-72
219. Szabadkai G, Pitter JG, and Spat A (2001) Cytoplasmic Ca2+ at low submicromolar concentration stimulates mitochondrial metabolism in rat luteal cells. Pflugers Arch. 441 (5), 678-685
220. Szado T, Kuo KH, Bernard-Helary K, Poburko D, Lee CH, Seow C, Ruegg UT, and van Breemen C (2003) Agonist-induced mitochondrial Ca2+ transients in smooth muscle. FASEB J 17 (1), 28-37
221. Szado T, McLarnon M, Wang X, and van Breemen C (2001) Role of sarcoplasmic reticulum in regulation of tonic contraction of rabbit basilar artery. Am J Physiol Heart Circ Physiol 281 (4), H1481-H1489
222. Taggart MJ and Wray S (1997) Agonist mobilization of sarcoplasmic reticular calcium in smooth muscle: functional coupling to the plasmalemmal Na+/Ca2+ exchanger? Cell Calcium 22 (5), 333-341
223. Takeshima H, Komazaki S, Nishi M, Iino M, and Kangawa K (2000) Junctophilins: a novel family of junctional membrane complex proteins. Mol Cell 6 (1), 11-22
224. Tasker PN, Taylor CW, and Nixon GF (2000) Expression and distribution of InsP(3) receptor subtypes in proliferating vascular smooth muscle cells. Biochem. Biophys. Res. Commun. 273 (3), 907-912
225. Thebault S, Zholos A, Enfissi A, Slomianny C, Dewailly E, Roudbaraki M, Parys J, and Prevarskaya N (2005) Receptor-operated Ca(2+) entry mediated by TRPC3/TRPC6 proteins in rat prostate smooth muscle (PS1) cell line. J Cell Physiol .
226. Thyagarajan B, Poteser M, Romanin C, Kahr H, Zhu MX, and Groschner K (2001) Expression of Trp3 Determines Sensitivity of Capacitative Ca2+ Entry to Nitric Oxide and Mitochondrial Ca2+ Handling. EVIDENCE FOR A ROLE OF Trp3 AS A SUBUNIT OF CAPACITATIVE Ca2+ ENTRY CHANNELS. J. Biol. Chem. 276 (51), 48149-48158
227. Tiruppathi C, Freichel M, Vogel SM, Paria BC, Mehta D, Flockerzi V, and Malik AB (2002) Impairment of store-operated Ca2+ entry in TRPC4(-/-) mice interferes with increase in lung microvascular permeability. Circ Res. 91 (1), 70-76
228. Tokunaga H, Hollenberg NK, and Graves SW (2000) Sodium-dependent calcium release from vascular smooth muscle mitochondria. Hypertens. Res. 23 (1), 39-45
229. Trebak M, Bird GS, McKay RR, and Putney JW, Jr. (2002) Comparison of human TRPC3 channels in receptor-activated and store- operated modes. Differential sensitivity to channel blockers suggests fundamental differences in channel composition. J Biol. Chem. 277 (24), 21617-21623
230. Trebak M, Vazquez G, Bird GS, and Putney JW, Jr. (2003) The TRPC3/6/7 subfamily of cation channels. Cell Calcium 33 (5-6), 451-461
231. Vallot O, Combettes L, and Lompre AM (2001) Functional coupling between the caffeine/ryanodine-sensitive Ca2+ store and mitochondria in rat aortic smooth muscle cells. Biochem. J 357 (Pt 2), 363-371
232. van Breemen C (1968) Permselectivity of a porous phospholipid-cholesterol artificial membrane. Calcium and lanthanum effects. Biochem. Biophys. Res. Commun. 32 (6), 977-983
233. van Breemen C (1977) Calcium requirement for activation of intact aortic smooth muscle. J. Physiol 272 (2), 317-329
234. van Breemen C, Cauvin C, Johns A, Leijten P, and Yamamoto H (1986) Ca2+ regulation of vascular smooth muscle. Fed. Proc. 45 (12), 2746-2751
235. van Breemen C, Chen Q, and Laher I (1995) Superficial buffer barrier function of smooth muscle sarcoplasmic reticulum. Trends Pharmacol. Sci. 16 (3), 98-105
236. van Breemen C, Farinas BR, Casteels R, Gerba P, Wuytack F, and Deth R (1973) Factors controlling cytoplasmic Ca 2+ concentration. Philos. Trans. R. Soc. Lond B Biol. Sci. 265 (867), 57-71

237. van Breemen C, Lukeman S, Leijten P, Yamamoto H, and Loutzenhiser R (1986) The role of superficial SR in modulating force development induced by Ca entry into arterial smooth muscle. J. Cardiovasc. Pharmacol. 8 Suppl 8, S111-S116
238. Van Breemen D and van Breemen C (1969) Calcium exchange diffusion in a porous phospholipid ion-exchange membrane. Nature 223 (209), 898-900
239. Van Dyke RW, Scharschmidt BF, and Steer CJ (1985) ATP-dependent proton transport by isolated brain clathrin-coated vesicles. Role of clathrin and other determinants of acidification. Biochim. Biophys. Acta 812 (2), 423-436
240. Vandebrouck C, Martin D, Schoor MC-V, Debaix H, and Gailly P (2002) Involvement of TRPC in the abnormal calcium influx observed in dystrophic (mdx) mouse skeletal muscle fibers. J. Cell Biol. 158 (6), 1089
241. Vandecasteele G, Szabadkai G, and Rizzuto R (2001) Mitochondrial calcium homeostasis: mechanisms and molecules. IUBMB. Life 52 (3-5), 213-219
242. Vasilyeva EA, Minkov IB, Fitin AF, and Vinogradov AD (1982) Kinetic mechanism of mitochondrial adenosine triphosphatase. Inhibition by azide and activation by sulphite. Biochem. J 202 (1), 15-23
243. Vennekens R, Voets T, Bindels RJM, Droogmans G, and Nilius B (2002) Current understanding of mammalian TRP homologues. Cell Calcium 31 (6), 253-264
244. Vermassen E, Parys JB, and Mauger JP (2004) Subcellular distribution of the inositol 1,4,5-trisphosphate receptors: functional relevance and molecular determinants. Biol. Cell 96 (1), 3-17
245. Voronina S, Sukhomlin T, Johnson PR, Erdemli G, Petersen OH, and Tepikin A (2002) Correlation of NADH and Ca2+ signals in mouse pancreatic acinar cells. J Physiol 539 (Pt 1), 41-52
246. Wada AM, Smith TK, Osler ME, Reese DE, and Bader DM (2003) Epicardial/Mesothelial cell line retains vasculogenic potential of embryonic epicardium. Circ Res. 92 (5), 525-531
247. Walker RL, Hume JR, and Horowitz B (2001) Differential expression and alternative splicing of TRP channel genes in smooth muscles. Am. J. Physiol Cell Physiol 280 (5), C1184-C1192
248. Wallnofer A, Cauvin C, Lategan TW, and Ruegg UT (1989) Differential blockade of ago. Am. J. Physiol 257 (4 Pt 1), C607-C611
249. Wamhoff BR, Bowles DK, Dietz NJ, Hu Q, and Sturek M (2002) Exercise training attenuates coronary smooth muscle phenotypic modulation and nuclear Ca2+ signaling. Am J Physiol Heart Circ Physiol 283 (6), H2397-H2410
250. Wang HJ, Guay G, Pogan L, Sauve R, and Nabi IR (2000) Calcium regulates the association between mitochondria and a smooth subdomain of the endoplasmic reticulum. J Cell Biol. 150 (6), 1489-1498
251. Wang YX, Zheng YM, Abdullaev I, and Kotlikoff MI (2003) Metabolic inhibition with cyanide induces calcium release in pulmonary artery myocytes and Xenopus oocytes. Am J Physiol Cell Physiol 284 (2), C378-C388
252. Waypa GB, Marks JD, Mack MM, Boriboun C, Mungai PT, and Schumacker PT (2002) Mitochondrial reactive oxygen species trigger calcium increases during hypoxia in pulmonary arterial myocytes. Circ Res. 91 (8), 719-726
253. Weir EK, Hong Z, Porter VA, and Reeve HL (2002) Redox signaling in oxygen sensing by vessels. Respir. Physiol Neurobiol. 132 (1), 121-130
254. Wellman GC and Nelson MT (2003) Signaling between SR and plasmalemma in smooth muscle: sparks and the activation of Ca(2+)-sensitive ion channels. Cell Calcium 34 (3), 211-229
255. White C and McGeown JG (2002) Carbachol triggers RyR-dependent Ca(2+) release via activation of IP(3) receptors in isolated rat gastric myocytes. J Physiol 542 (Pt 3), 725-733
256. Wilson DP, Sutherland C, and Walsh MP (2002) Ca2+ activation of smooth muscle contraction: evidence for the involvement of calmodulin that is bound to the triton insoluble fraction even in the absence of Ca2+. J Biol. Chem. 277 (3), 2186-2192
257. Wilson HL, Dipp M, Thomas JM, Lad C, Galione A, and Evans AM (2001) Adp-ribosyl cyclase and cyclic ADP-ribose hydrolase act as a redox sensor. a primary role for cyclic ADP-ribose in hypoxic pulmonary vasoconstriction. J Biol. Chem. 276 (14), 11180-11188
258. Wolin MS (2000) Interactions of oxidants with vascular signaling systems. Arterioscler Thromb Vasc Biol 20 (6), 1430-1442
259. Wolin MS, Gupte SA, and Oeckler RA (2002) Superoxide in the vascular system. J Vasc Res. 39 (3), 191-207
260. Wood JN, Winter J, James IF, Rang HP, Yeats J, and Bevan S (1988) Capsaicin-induced ion fluxes in dorsal root ganglion cells in culture. J Neurosci. 8 (9), 3208-3220

261. Yamamura H, Sakamoto K, Ohya S, Muraki K, and Imaizumi Y (2002) Mechanisms underlying the activation of large conductance Ca2+-activated K+ channels by nordihydroguaiaretic acid. Jpn. J Pharmacol. 89 (1), 53-63
262. Yi M, Weaver D, and Hajnoczky G (2004) Control of mitochondrial motility and distribution by the calcium signal: a homeostatic circuit. J Cell Biol. 167 (4), 661-672
263. Zakharov SI, Mongayt DA, Cohen RA, and Bolotina VM (1999) Monovalent cation and L-type Ca2+ channels participate in calcium paradox-like phenomenon in rabbit aortic smooth muscle cells. J. Physiol 514 (Pt 1), 71-81
264. Zazueta C, Sosa-Torres ME, Correa F, and Garza-Ortiz A (1999) Inhibitory properties of ruthenium amine complexes on mitochondrial calcium uptake. J Bioenerg. Biomembr. 31 (6), 551-557
265. Zhang JG and Fariss MW (2002) Thenoyltrifluoroacetone, a potent inhibitor of carboxylesterase activity. Biochem. Pharmacol. 63 (4), 751-754
266. Zhong H and Minneman KP (1999) Alpha1-adrenoceptor subtypes. Eur. J Pharmacol. 375 (1-3), 261-276
267. Zhou Z and Bers DM (2002) Time course of action of antagonists of mitochondrial Ca uptake in intact ventricular myocytes. Pflugers Arch. 445 (1), 132-138
268. Zhu X, Jiang M, and Birnbaumer L (1998) Receptor-activated Ca2+ influx via human Trp3 stably expressed in human embryonic kidney (HEK)293 cells. Evidence for a non-capacitative Ca2+ entry. J. Biol. Chem. 273 (1), 133-142
269. Zimmermann B (2000) Control of InsP3-induced Ca2+ oscillations in permeabilized blowfly salivary gland cells: contribution of mitochondria. J Physiol 525 Pt 3:707-19., 707-719